AD_____

Award Number: DAMD17-00-1-0249

TITLE: FCCC Institutional Breast Cancer Training Program (FCCC-IBCTP)

PRINCIPAL INVESTIGATOR: Jose Russo, M.D.

CONTRACTING ORGANIZATION: Fox Chase Cancer Center
Philadelphia, Pennsylvania 19111-2497

REPORT DATE: January 2005

TYPE OF REPORT: Annual Summary

PREPARED FOR: U.S. Army Medical Research and Materiel Command
Fort Detrick, Maryland 21702-5012

DISTRIBUTION STATEMENT: Approved for Public Release;
Distribution Unlimited

REPORT DOCUMENTATION PAGE

Form Approved
OMB No. 074-0188

1. AGENCY USE ONLY (Leave blank)	2. REPORT DATE	3. REPORT TYPE AND DATES COVERED
	January 2005	Annual Summary (1 Jul 00 - 31 Dec 04)

4. TITLE AND SUBTITLE
FCCC Institutional Breast Cancer Training Program (FCCC-IBCTP)

5. FUNDING NUMBERS
DAMD17-00-1-0249

6. AUTHOR(S)
Jose Russo, M.D.

7. PERFORMING ORGANIZATION NAME(S) AND ADDRESS(ES)
Fox Chase Cancer Center
Philadelphia, Pennsylvania 19111-2497

E-Mail: Jose.Russo@fccc.edu

8. PERFORMING ORGANIZATION REPORT NUMBER

9. SPONSORING / MONITORING AGENCY NAME(S) AND ADDRESS(ES)
U.S. Army Medical Research and Materiel Command
Fort Detrick, Maryland 21702-5012

10. SPONSORING / MONITORING AGENCY REPORT NUMBER

11. SUPPLEMENTARY NOTES
Original contains color plates. All DTIC reproductions will be in black and white.

12a. DISTRIBUTION / AVAILABILITY STATEMENT
Approved for Public Release; Distribution Unlimited

12b. DISTRIBUTION CODE

13. ABSTRACT (Maximum 200 Words)

The focus of the FCCC Institutional Breast Cancer Training Program (IBCTP) is to integrate the unique talents and interests of the Center's basic scientists, clinical investigators and behavioral scientists to create a comprehensive effort to approach the problems of breast cancer. The IBCTP offers to the postdoctoral trainees' practical experience in the fields of cellular and molecular biology, drug resistance and targeted immunotherapy, genetic epidemiology and control, psychosocial and behavioral medicine, as well as breast cancer prevention, diagnosis, and treatment.

During the fourth year of the grant we have been implementing the training phase of the program by monitoring each of the individual projects. The trainees have been attending at least one general lecture a week from those offered by the FCCC and a special seminar targeted to the formation of the trainees addressing critical subjects in breast cancer. We have established a half-day seminar twice a year in which the trainees present their work in front of the Faculty and the Advisory Panel. In this last year of the program, that ended December 31, 2004, Drs E. Pugacheva, X. Li and H. You, that started in January 1, 2003, have completed the training. The present report reflects their work.

14. SUBJECT TERMS
Genomic Instability, Proline 47 Polymorphism, p53, Appl Gene, Mammary Gland

15. NUMBER OF PAGES
98

16. PRICE CODE

17. SECURITY CLASSIFICATION OF REPORT	18. SECURITY CLASSIFICATION OF THIS PAGE	19. SECURITY CLASSIFICATION OF ABSTRACT	20. LIMITATION OF ABSTRACT
Unclassified	Unclassified	Unclassified	Unlimited

Table of Contents

A-INTRODUCTION

The focus of the FCCC Institutional Breast Cancer Training Program (IBCTP) has been to integrate the unique talents and interests of the Center's basic scientists, clinical investigators and behavioral scientists to create a comprehensive effort to approach the problems of breast cancer. The rich scientific and intellectual environment of FCCC is nurtured by a cohesive interdisciplinary program that is based on expertise in areas of high relevance to breast cancer. The Institutional Breast Cancer Training Program has offered to the postdoctoral trainees practical experience in the fields of cellular and molecular biology, drug resistance and targeted immunotherapy, genetic epidemiology and control, psychosocial and behavioral medicine, as well as breast cancer prevention, diagnosis, and treatment.

B-BODY

B-i. Organization of the FCCC-Institutional Breast Cancer Training Program. Following our statement of work we have accomplished the following tasks:

Tasks4-7. During the fourth year of the grant awarded we have been implementing the training phase of the program by monitoring each of the individual projects. The trainees have been attending at least one general lecture a week from those offered by the Fox Chase Cancer Center and a special seminar targeted to the formation of the trainees addressing critical subjects in breast cancer. We have established a half-day seminar twice a year in which the trainees present their work in front of the Faculty and the Advisory Panel.

Task 8. **In this last year of the program that has ended on December 31st 2004 the last three trainees Drs E. Pugacheva, X. Li and H. You have successfully completed the cycle. As a reminder the Training Program started on July 1st 2000 for ending in June 30 of 2004. The only trainee that ended in June 30, 2004 was Dr. S. Fernandez. We have requested and additional six months extension, until December 31st 2004, for allowing the completion of the program for Drs E. Pugacheva, X. Li and H. You), which have started in January 1, 2003. During the last six months the main emphasis has been data collection, analysis and preparation of abstracts and manuscripts. Therefore this report reflects the completion of the training program of Drs E. Pugacheva, X. Li and H. You and therefore will be some overlapping in information with the one submitted in June 30, 2004.**

B-ii- . Predisposition to genomic instability in breast cancer: analysis of molecular mechanisms.

Trainee: Elena Pugacheva, PhD
Mentor: Erica Golemis, Ph.D.
Period reported: August 1, 2003 – to December 31st, 2004

Introduction:

The goal of this research is to better understand intrinsic genetic factors leading to genome instability, with the intent of improving diagnosis and treatment for breast cancer. Based on our data, which define CAS family of focal adhesion signaling molecules as novel factors controlling centrosomal dynamics and spindle formation, we are exploring CAS proteins status as contributing factors to acquisition of a malignant phenotype and drug resistance in breast cancer.

Background.

The **HEF1** scaffolding protein has a well-defined role in mediating integrin-dependent attachment signaling at focal adhesions. We are trying to explore the function of HEF1 in mitosis, as phosphorylation of HEF1 became an important part of controlling mechanism governing HEF1 localization and interaction with target proteins. We have identified potential phosphorylation sites on HEF1 for Aurora A kinase that play pivotal role in mitotic progression. We are currently investigating the significance of HEF1 interaction with AurA for the observed phenotypes induced by HEF1 manipulations on the spindle and centrosome dynamic. We show that HEF1 controls the activation of Aurora A kinase at the centrosome, in an interaction involving association with the AurA activation partner Ajuba. In sum, these results provide a novel mechanism for the coordination of cell attachment status with cell division which is misaligned in tumor cell

Aims of our study are: **1**- To delineate the HEF1 sequence motif responsible for interaction with Aurora A kinase. **2**- To identify the domain of HEF1 responsible for interacting with Aurora A and investigate the influence of this interaction on AurA kinase activity. **3**- To investigate how phosphorylation of HEF1 by Aurora A kinase, is important for localization of the HEF1 protein to the mitotic apparatus, and interaction with Aurora A.

Results

i. Identification of HEF1 as new Aurora A kinase substrate.

We have reported in our previous report that by *in vitro* kinase assay HEF1 (1-363aa) bears a phosphorylation site for AuroraA kinase. Using various deletion mutants (Fig.1a) of HEF1, phosphorylated *in vitro* by active AurA, and mass spectrometry analysis we have identified the potential site for AuroraA kinase (Fig.1b) and have shown this site (Ser 296) was phosphorylated by active Aurora A in vitro (Fig.1c). We made the following mutations at that site and in some cases at an adjacent Ser (Ser298): Ser296/Ala296, Ser296, 298/Ala296, 298 and Ser296/Glu296, Ser296, 298/Glu296, 298. All mutant variants of HEF1 lost the ability to be phosphorylated by Aurora A kinase in vitro (Fig.1d). We are now studying the phosphorylation of HEF1 by Aurora A in vivo and the importance of this phosphorylation for cell cycle progression.

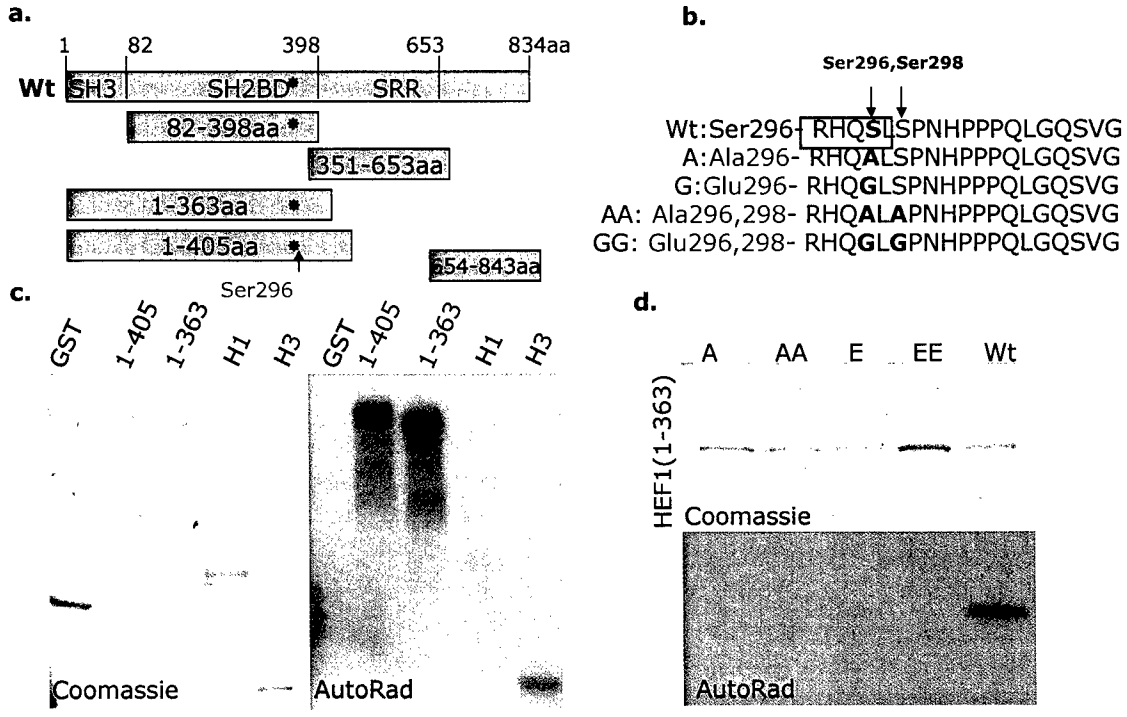

Figure 1. ***HEF1 is an Aurora-A (AurA) phosphorylation target.***
1a. Schematic representation of HEF1 mutants used for the experiments. Red star represents the site of AurA phosphorylation, the blue star a potential second site (not yet confirmed). ***1.b.*** Sequence of the AurA motif in the HEF1. Mutated serines are marked by red arrows. AurA consensuses marked in blue box. ***1c.*** *In vitro* kinase assay with AurA kinase and γ-P-32-ATP. As the substrate, we used HEF1 variants presented in Fig.1a. Coomassie staining indicates the equal loading of protein in the assay. ***1d.*** *In vitro* kinase assay with AurA kinase and γ-P-32-ATP. As the substrate we used the HEF1 (1-363) variant, with mutations represented in panel Fig.1b. Coomassie staining represents the equal loading of protein in the assay.

ii. HEF1 directly interacts with Aurora A kinase in vitro and in vivo.

Using the set of deletion mutants of the HEF1 protein (Fig.1a.) we have delineated the exact region of HEF1 responsible for the interaction with AurA. GST fusion HEF1 deletion mutants were used in *in vitro* GST-pull-down assay to IP in vitro translated human Aurora A (Fig.2a.). The N terminal 1-363aa fragment of HEF1 was sufficient to pull down recombinant AurA kinase. But, *in vivo*, upon transfection of GFP-HEF1 (1-363) and (1-405) into 293 cells, only the 1-405 fragment of HEF1 was able to precipitate AurA from cell lysate (Fig.2b). As we have shown in the previous report, this additional 31 amino acid fragment of HEF1 encompasses 18 Ser/Thr residues that are highly phosphorylated during mitosis, and serves as a centrosomal targeting sequence for HEF1. This suggests that the 1-363aa fragment contains the interaction domain, but cannot be efficiently delivered in vivo to the centrosome, where Aurora A is localized; thus limiting *in vivo* interaction.

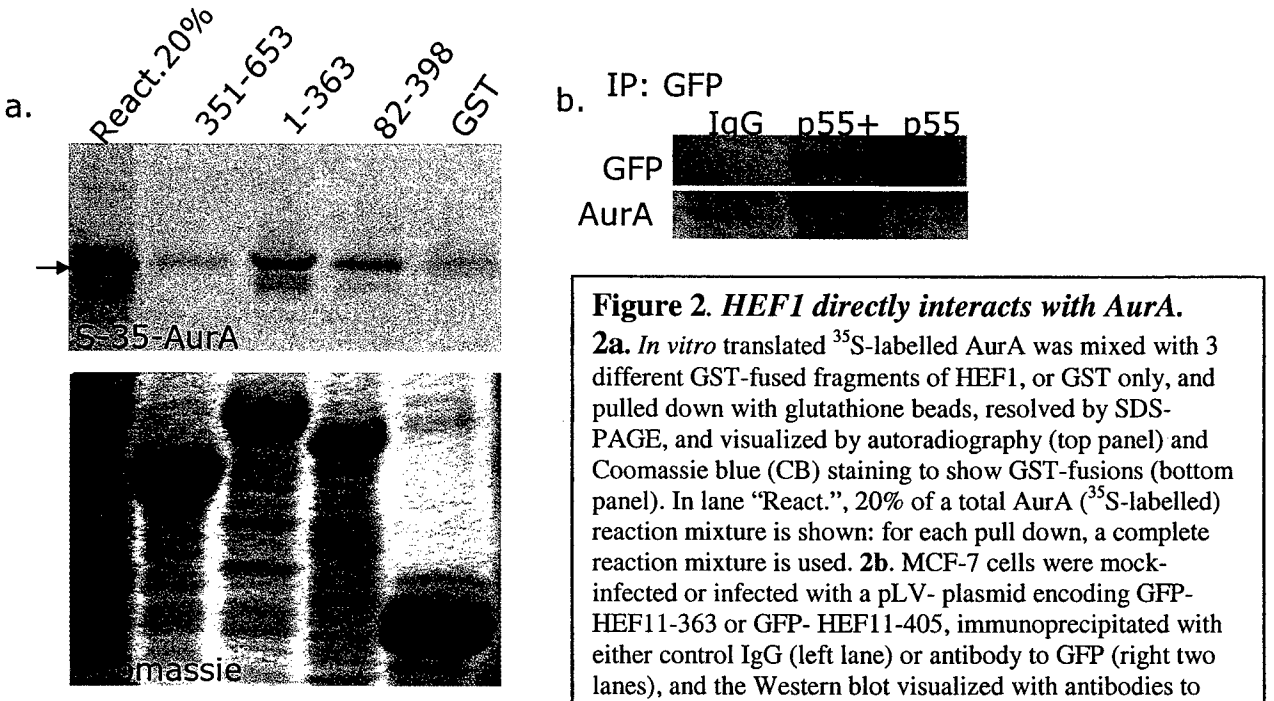

Figure 2. ***HEF1 directly interacts with AurA.*** **2a.** *In vitro* translated ^{35}S-labelled AurA was mixed with 3 different GST-fused fragments of HEF1, or GST only, and pulled down with glutathione beads, resolved by SDS-PAGE, and visualized by autoradiography (top panel) and Coomassie blue (CB) staining to show GST-fusions (bottom panel). In lane "React.", 20% of a total AurA (^{35}S-labelled) reaction mixture is shown: for each pull down, a complete reaction mixture is used. **2b.** MCF-7 cells were mock-infected or infected with a pLV- plasmid encoding GFP-HEF11-363 or GFP- HEF11-405, immunoprecipitated with either control IgG (left lane) or antibody to GFP (right two lanes), and the Western blot visualized with antibodies to GFP or AurA, as indicated.

In *in vitro* kinase assay we have shown that HEF1 (1-363aa) is phosphorylated by Aurora A (Fig.1c). Further, we have investigated how this phosphorylation event may regulate the interaction between Aurora A and HEF1. To address this question, we immunoprecipitated recombinant Aurora A from an *in vitro* kinase reaction in the presence of different GST-fusion HEF1 mutants, and analyzed the amount of co-immunoprecipitated GST HEF1 in the presence or absence of γ-P-32-ATP (Fig.3a, b).

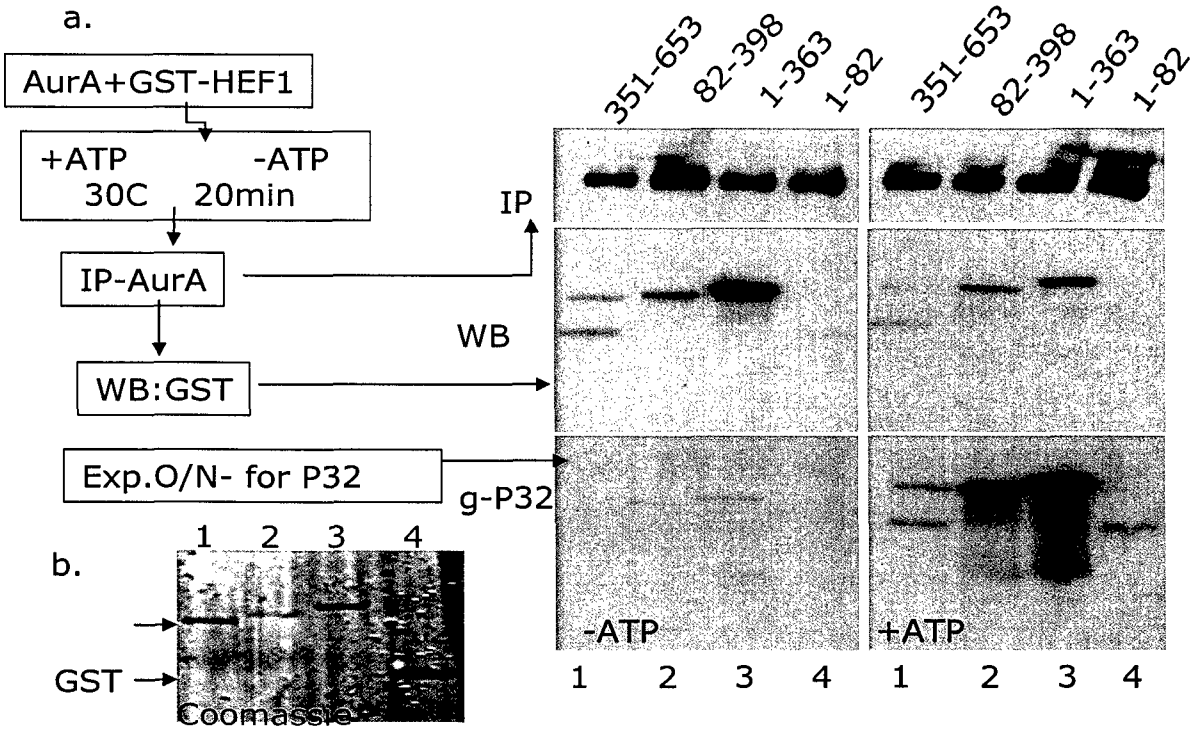

Figure 3. ***HEF1 directly interacts with AurA.***
2a. Schematic representation of experiment is on the left side. An *in vitro* kinase assay was set up using comparable levels of GST-fused HEF1 truncation proteins and recombinant AurA, in the presence (right panel +ATP) or absence (left -ATP) of γ-32-P-ATP. This was followed by immunoprecipitation of AurA (top panel "IP" western blot, with antibody against total AurA), and analysis of GST (by Western blot, "WB", middle panel) and by direct autoradiography (γ-32P) to demonstrate the phosphorylation status of GST-HEF1 fragments (bottom panel). ***2b.*** Coomassie stain of the HEF1 samples used in **2a.**

The non-phosphorylated form of HEF1 was much more efficiently precipitated by Aurora A kinase then phosphorylated HEF1. As we have reported, HEF1 co-immunoprecipitates with Aurora A from cell lysates, and reciprocally, HEF1 is detected in the AurA precipitated complex. Upon determination of a potential Aurora A phosphorylation site in HEF1 molecule, we investigated the influence of this site on the interaction between Aurora A and HEF1. Mutation of this Ser296 to Glu296, which mimics phosphorylated status of this site, completely abolished interaction of of HEF1 with Aurora A in vivo, in comparison with the wild type and alanine substitution mutant (Fig.4).

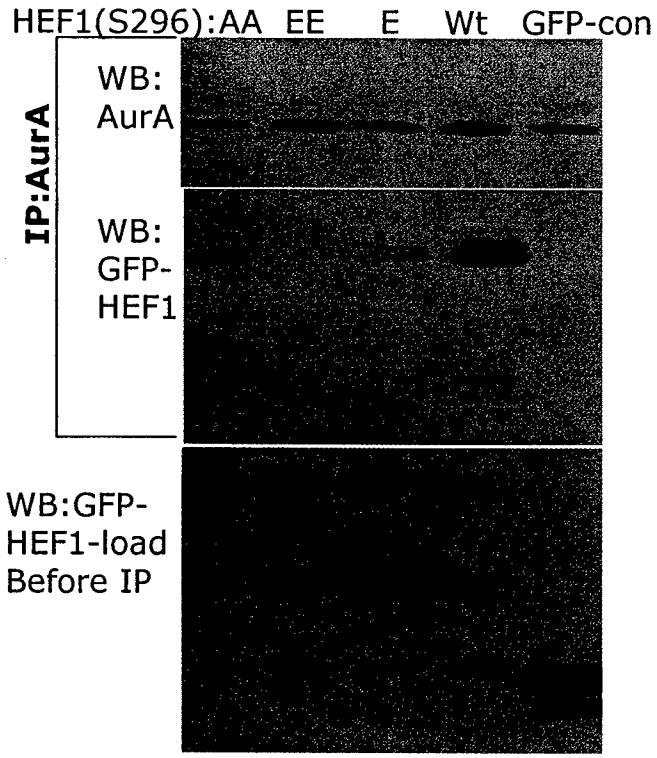

Figure 4. ***HEF1 directly interacts with AurA.***
GFP-fused HEF1, or GFP-HEF1 with mutations at the AurA phosphorylation site as noted, expressed in human embryonic kidney 293 cells (HEK293). Immunoprecipitation of total AurA protein, followed by Western blot (WB) analysis of AurA and GFP-fused HEF1 was performed 24h post-transfection. The total amount of GFP-protein in the AurA lysate is presented in the bottom panel.

iii. HEF1 is required for the activation of AuroraA kinase in vitro and in vivo.

As we have previously reported HEF1 depletion dramatically decreases the amount of active Aurora A protein (T288 phosphorylated) (Fig.5a). To investigate the role of HEF1 in the Aurora A activation signaling pathway, we have used *in vitro* translated Aurora A and recombinant HEF1 protein. An *in vitro* kinase assay was performed on the well-characterized Aurora A substrate, H3 histone. Addition of HEF1 to the kinase reaction causes a significant increase in Aurora A kinase activity in a dose dependent manner (Fig.5b). Further, we analyzed the Aurora A activation potential of different deletion mutants of HEF1, and have found that the same domain which is involved in interaction with Aurora A is important for activation of the kinase (Fig.5c).

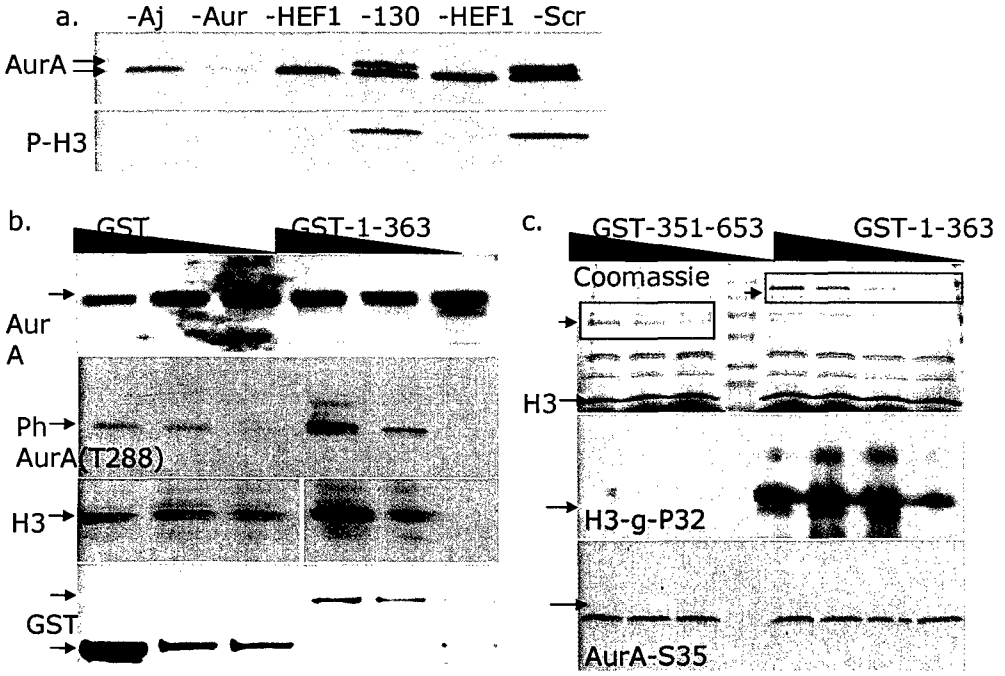

Figure 5. ***HEF1 is required for the activation of AuroraA kinase in vitro and in vivo.***
5a. MCF7 cells were treated with siRNA for 48 hours with siRNA to Ajuba (Aj), AurA (Aur), HEF1, p130Cas (130), or a scrambled control (Scr). Cells were lysed, then AurA was immunoprecipitated and used for Western (top) or in vitro kinase assay with γ-^{32}P-ATP, with a histone H3 substrate, to visualize level of histone phosphorylation (bottom).
5b. Increasing quantities (1, 2, or 4 μg) of GST-fused $HEF1_{1\text{-}363}$ or GST only were mixed with reticulocyte translated, recombinant AurA in an in vitro kinase reaction containing a histone H3 substrate. Reactions visualized with antibody to total AurA, to a phosphorylated form of AurA that reflects kinase activation (phospho-AurA, P-AurA), or GST, as indicated. Again, phosphorylated histone H3 is shown.
5c. Increasing quantities (1, 0.5, or 0.25 μg) of GST-fused $HEF1_{1\text{-}363}$ or GST-$HEF1_{351\text{-}653}$ were mixed with reticulocyte translated, ^{35}S-labelled AurA and H3 histone (AurA substrate) in the presence of γ-^{32}P-ATP, in an in vitro kinase reaction. Reactions were visualized via autoradiography, to indicate total ^{35}S AurA (2 days of exposure) and phosphorylated H3 (6h of exposure).

B-iii- **The codon 47 polymorphism of p53 is functionally significant**

The codon 47 polymorphism of p53 is functionally significant

Trainee: Xiaoxian Li, Ph.D.
Mentor: Maureen Murphy, Ph.D.
Period report: 1/1/2003-12/31/2004

Introduction:

More than one million people are diagnosed with breast cancer every year worldwide (1). It has been generally accepted that breast cancer is the most common malignancy in the female. The mechanism whereas breast cancer forms and develops remains unclear. Research results have clearly associated the initiation, development and prognosis of breast cancer with different types of genetic alterations of oncogenes and tumor suppressor genes. Among all the altered genes, the p53 gene has the most frequency of genetic mutations. The mutation of the p53 gene is found in about 20~40% of breast cancer and is often accompanied by loss the wild type allele. It has been known that germline mutation of the p53 gene is responsible for the Li-Fraumeni Syndrome (LFS). LFS patients, at early age, are much more prone to development of several types of cancers, among which, breast cancer is the most frequent one (2), indicating the importance of the p53 gene in the formation and development of breast cancer. Another example of the importance of p53 in initiation of breast cancer is that several studies have indicated that mutation of the p53 gene is found in ductal carcinoma in situ before the development of invasive breast cancer (3-5). Furthermore, the frequency of the p53 gene mutation has been found higher in large and invasive breast cancer (6). Accumulating evidence shows that mutations of the p53 gene is an independent risk factor conferring worse overall survival and some studies indicate the mutations of the p53 gene is the single most significant prognosis indicator (7).

Hormone therapy, chemo- and radio-therapy are the most used clinical regimes in treating breast cancers and have been proved successful. However some patients are more resistant to these clinical treatments and show worse prognosis and higher rate of relapse. Berns et al (8) show that patients with mutated p53 have the poorest response to chemotherapy, such as tamoxifen. Estrogen receptor (ER) is closely related to breast cancer. ER positive breast cancer cells grow more slowly, are better differentiated and tend to have better prognosis. The ER has been shown to interact with and protect the p53 protein from MDM2 mediated degradation (9). The finding the ER prolongs the half life of p53 at least partially explains why ER positive breast cancer is less malignant. Together, all the evidence shows the indispensable role of p53 in breast cancer.

P53 is a tumor suppressor protein. Mutation or deletion of p53 is found in about 50% of human cancers. P53 double knock out mice are prone to development of multi-types of cancers. Research shows that over-expression of p53 is sufficient to kill cancer cells. P53 induces apoptosis in tumor cells by its gene regulatory function or its direct effect on mitochondria to release cytochrome-c. The p53 protein transactives pro-apoptotic genes or suppresses anti-apoptotic genes when cells encounter DNA damages. Recently, the mitochondrial pathway through which p53 induces apoptosis has been reported (11).

The p53 tumor suppressor gene contains at least two coding region polymorphisms. A common polymorphism at codon 72 encodes either proline (P72) or arginine (R72). We recently reported that a common polymorphism in p53 at codon 72 is functionally significant. Codon 72 of p53 can encode either arginine (R72) or proline (P72). We found that the R72 form of p53 has up to

15-fold increased apoptotic ability compared to the P72 form, in both inducible cell lines and in cells with endogenous p53 homozygous for each variant (11). At least part of the increased apoptotic potential of R72 is due to enhanced mitochondrial localization of this protein, where we have found that p53 can interact directly with the pro-apoptotic protein BAK, displacing Mcl-1 and allowing BAK oligomerization (12). These functional studies on the codon 72 polymorphic variants of p53 have led to a number of studies testing the impact of this polymorphism on the risk and progression of human cancer. Several of these reports indicate that the lesser apoptotic P72 form is associated with increased risk of cancer (13-15). Another report indicated that individuals in families predisposed to colon cancer who are homozygous for the P72 allele have an earlier age of onset for cancer, and tend to have increased tumor number, compared to individuals homozygous for R72 (16). Recently a polymorphism in the gene encoding MDM2, which negatively regulates p53, leads to attenuated p53 function and increased cancer risk (17). The combined data support the hypothesis that identification of other functionally significant polymorphisms in the p53 tumor suppressor gene will have an impact on our understanding of genetic determinants of cancer risk and progression.

In the present report we provide data that another polymorphism in p53, at codon 47, is also functionally significant. Codon 47 encodes proline in wild type p53, but in a small subset of individuals it can encode serine (CCG -> TCG). A single study, performed over ten years ago, was done on the serine 47 (S47) polymorphic variant. In that study, the S47 polymorphism was found in less than 5% of African Americans, and not at all in Caucasians (18). A preliminary functional analysis failed to reveal differences between S47 and wild type p53; importantly however, the ability to induce apoptosis was not assessed (18). Additionally, it was not known at that time that phosphorylation of the adjacent residue, serine 46, was critical for p53's ability to induce apoptosis. One of the kinases that directly catalyzes serine 46 phosphorylation is the proline-directed kinase p38 MAPK. The importance of serine 46 phosphorylation by p38 MAPK to apoptosis induction by p53 is epitomized by the findings that mutation of serine 46 to alanine, incubation with specific chemical inhibitors of p38 MAPK, or overexpression of proteins that inhibit p38 MAPK, have all been shown to markedly inhibit p53-dependent apoptosis (19-22). Significantly, the serine 47 polymorphism in p53 replaces the proline residue necessary for phosphorylation of serine 46 by proline-directed kinases like p38 MAPK, raising the possibility that the S47 variant has decreased phosphorylation on serine 46, and impaired apoptotic ability.

In this report we present data indicating that the serine 47 polymorphic variant is a poorer substrate for phosphorylation by p38 MAPK. Consistent with this, we show that, in multiple clones of stably transfected cells containing equivalent levels of p53, the S47 variant has a 2 to 5-fold decreased ability to induce programmed cell death, compared to wild type p53. This decreased ability to induce programmed cell death is accompanied by a decreased ability to transactivate p53AIP1, as well as the pro-apoptotic p53 target gene PUMA. Down-regulation of PUMA using short interfering RNAs reduces the ability of wild type p53 to induce apoptosis, to levels roughly equivalent to the S47 variant. The combined data indicate that the codon 47 polymorphism in p53 is functionally significant, and suggest that studies on the influence of this polymorphism to the increased or altered cancer risk evident in African Americans should be assessed.

Body

Results

The serine 47 polymorphism may be linked to the proline 72 polymorphism in p53.

A previous study by Harris and colleagues first described the existence of a coding region polymorphism in the p53 gene at codon 47. This codon encodes proline in wt p53, but these researchers found it encodes serine in less than 5% of African Americans (18). Codon 47 occurs in exon 4 of p53, where we have shown another functionally significant polymorphism, at codon 72, also exists. Before testing the hypothesis that the S47 and wild type p53 proteins might have altered apoptotic function, it was necessary to determine the frequency with which this polymorphism was linked to either codon 72 variant (P72 or R72). Therefore, we analyzed both the codon 47 and the codon 72 polymorphisms in genomic DNA isolated from 200 African Americans from the Fox Chase Cancer Center Biosample Repository. We identified four DNA samples that were heterozygous for the S47 variant, for an allele frequency of 1% (4/400 alleles); this is somewhat less than the previous study, although that study had considerably smaller sample size. Sequence analysis revealed that in all four cases the S47 allele occurred in *cis* with the proline 72 polymorphism (P72), suggesting that the S47 and P72 polymorphisms may be linked. For the purposes of this study, which compares the function of S47 and wt p53, we focused on the S47-P72 allele (which we designate S47), and we compare it to the P47-P72 allele, which we designate as wild type (wt) p53.

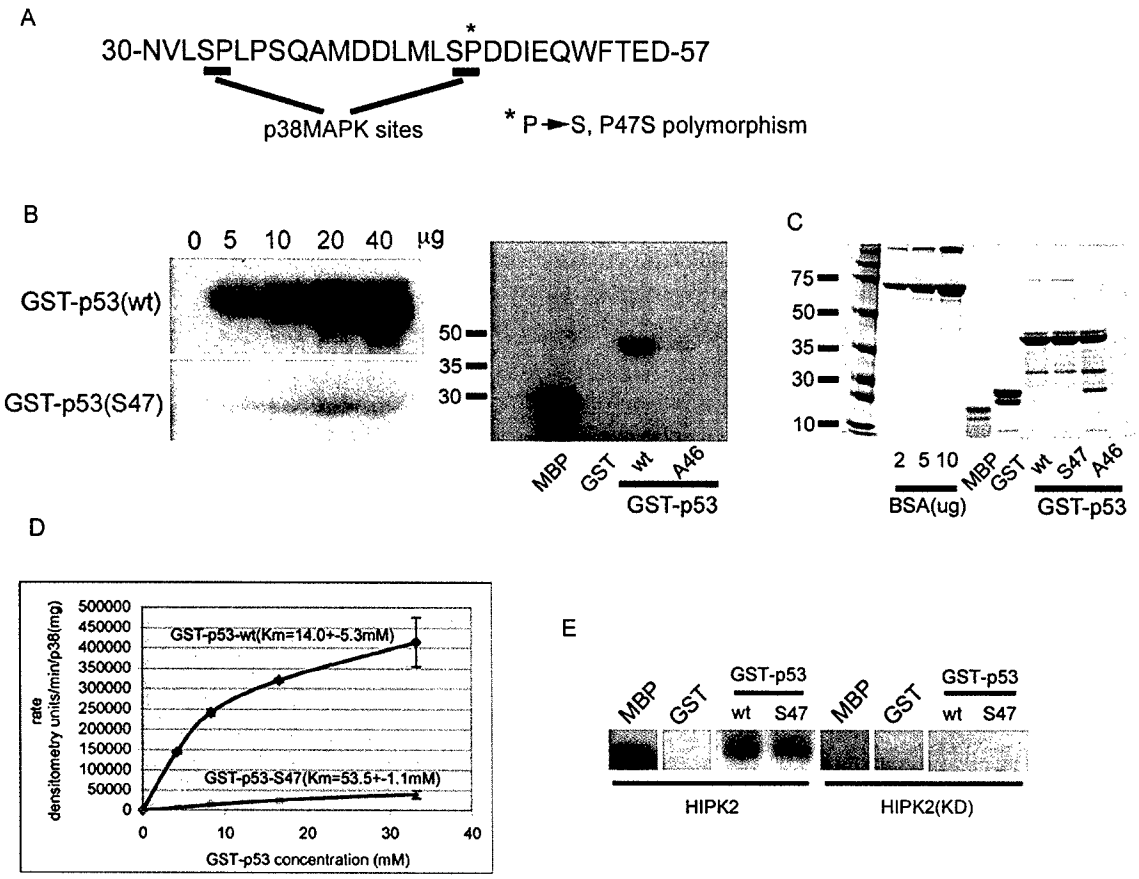

Figure 6. The S47 polymorphic variant of p53 is impaired for phosphorylation by p38 MAP kinase.
A. Amino acid sequence of residues 30-57 of human wt p53, with the p38 MAPK phosphorylation sites underlined, and the site of the serine 47 polymorphism marked with an asterisk.
B. (Left panel) Kinase assay using purified p38 MAPK (Upstate Biotechnology) and the indicated concentration of purified GST-p53 and GST-S47 (both containing amino acids 1-92, with serine 33 replaced by alanine). (Right panel) p38 MAPK assay using myelin basic protein (MBP) as a positive control, and as a negative control, GST alone and GST (1-92) with serines 33 and 46 replaced with alanine (A46), 10 ug of substrate per reaction.

C. Coomassie stained gel verifying the loading and purity of GST fusion proteins used in A; Bovine serum albumin (BSA) is included as a standard.

D. The Michaelis Menton model was fit to the averaged data from three independent experiments performed in A, using GraphPad Prism v. 3.0a (GraphPad Software, San Diego CA). The K_m for wt p53 and S47 are indicated; the V_{max} for p38 MAPK for wt p53 is estimated to be eight-fold greater than for S47. Rate is indicated on the y axis as the densitometry units of phosphorylation per minute per micro-gram of enzyme.

E. Flag-tagged HIPK2, or a kinase-dead version of this enzyme, were immunoprecipitated with anti-flag antibody following transient transfection of H1299 cells and incubated with myelin basic protein (MBP), GST alone, GST-p53 or GST-S47 (the latter two encode amino acids1-92 of human p53, with alanine at amino acid 33).

The S47 protein is a poorer substrate for phosphorylation by p38 MAPK

p38 MAPK is a proline-directed kinase, and requires a proline residue adjacent to the target phosphorylation site for efficient recognition of that site; notably, the S47 polymorphism replaces this proline with serine (Fig. 6A). In order to test the hypothesis that the S47 polymorphism alters serine 46 phosphorylation by p38 MAPK, we created GST fusion proteins representing amino acids 1-92 of wt p53 (wt) and the S47 variant (S47). As a control for these studies we generated a p53 construct in which serine 46 was mutated to alanine (A46). Because serine 33 is also phosphorylated by p38 MAPK (Fig. 6A), these constructs were generated with an alanine substitution at amino acid 33; this replacement has no effect on phosphorylation of serine 46 (23 and our unpublished results). Increasing amounts of GST-p53 and GST-S47 were incubated with a constant amount of purified active p38 MAPK (Upstate Biotechnology) and γ^{32}P-ATP, using kinase conditions previously described (11). Phosphorylated p53 was then resolved by SDS-PAGE and autoradiography. As depicted in Figure 6, wt p53 was efficiently phosphorylated by p38 MAPK (Fig. 6B). In contrast, the S47 variant protein was phosphorylated markedly less well. As expected, neither GST alone nor the A46 mutant was detectably phosphorylated under these conditions (Fig. 6B). Coomassie staining of the input proteins confirmed equal loading and purity of the wt, S47 and A46 substrates (Fig. 6C). Notably, decreased phosphorylation of the S47 variant by p38 MAPK was also evident using GST fusion proteins containing serine at amino acid 33, except that the background level of phosphorylation was higher (data not shown).

The Michaelis Menton model was fit to the averaged data from three independent p38 MAPK kinase experiments performed using S47 and wt p53 as substrates. This modeling revealed a three-fold decrease in the K_m, and an eight-fold decrease in the V_{max}, for S47 compared to wt p53 (Fig. 6D). These data suggest that the S47 protein can bind to p38 MAPK, but that the ability of this enzyme to phosphorylate serine 46 is markedly reduced. To control against the possibility that the S47 protein was denatured or misfolded, we tested the ability of another kinase, the homeo-domain interacting protein kinase-2 (HIPK2) to phosphorylate S47 and wt p53. Like p38 MAPK, HIPK2 also phosphorylates serine 46, but it is not reported to be a proline-directed kinase (23,24). As shown in Figure 6E, following transfection into p53 null cells, immunoprecipitated FLAG-tagged HIPK2 was able to phosphorylate S47 and wt p53 proteins identically. In contrast, a kinase dead version of HIPK2 (K221R; D'Orazi et al, 2002) did not detectably phosphorylate either protein (Fig. 6E). These data indicate that the S47 variant of p53 is impaired for phosphorylation on serine 46 by the proline-directed kinase p38 MAPK.

The S47 variant has decreased apoptotic ability *in vivo*

We next determined whether the S47 polymorphism alters p53 function *in vivo*. We generated stably-transfected cell lines containing inducible versions of wild type p53 (wt) and the S47 variant, as well as the A46 mutant. These p53 variants were generated using the temperature sensitive version of p53 encoding valine at amino acid 138. This temperature-sensitive form p53 is well characterized; the p53 protein is denatured and inactive when cells are cultured at 39 degrees.

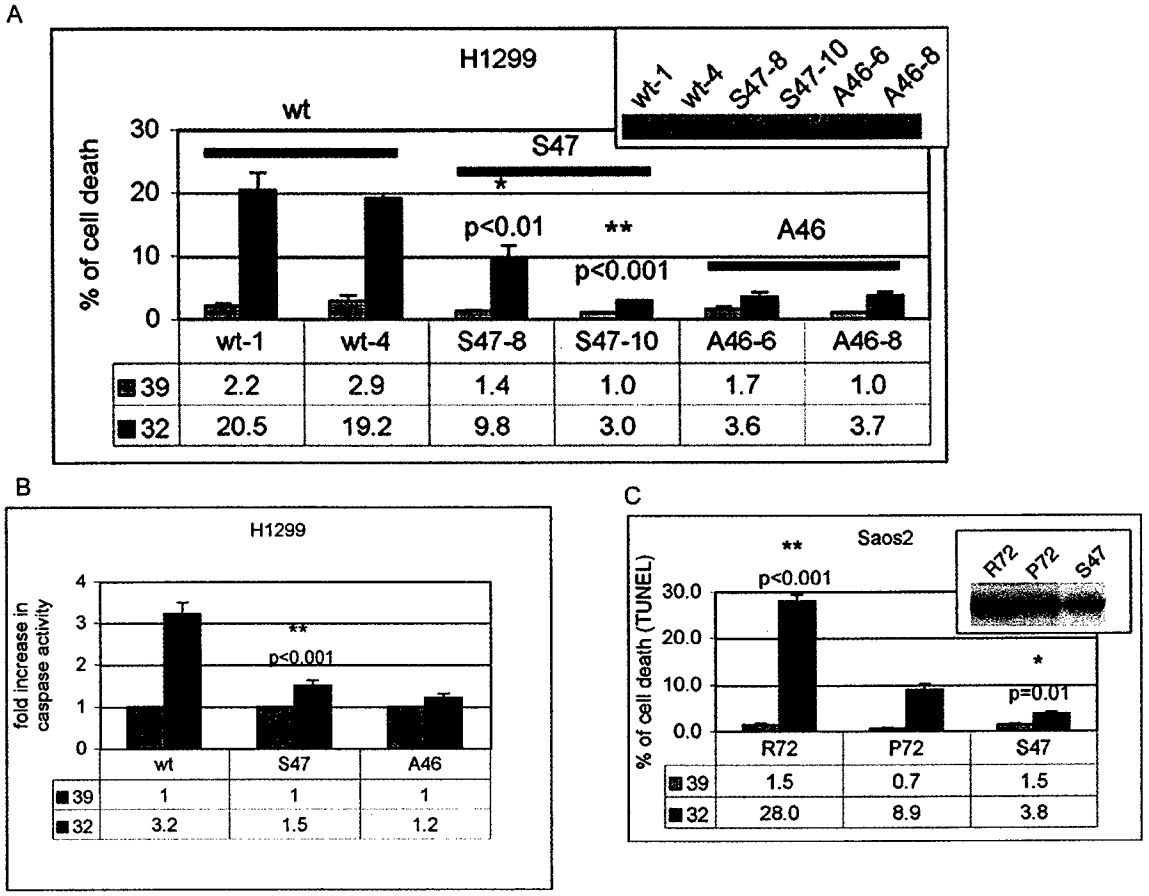

Figure 7. The S47 variant has impaired ability to induce apoptosis, relative to wt p53.

A. TUNEL assay results from individual clones of cells stably transfected with inducible versions of p53, as indicated. Western analysis for total p53 in each clone is indicated in the inset. Values of TUNEL positive cells are given at 39 degrees (mutant p53) and 32 degrees (wild type p53 conformation) following twenty-four hours of temperature shift. Values given are the mean +/- standard error of measurement from three independent experiments. p values reflect comparison of indicated clones to clone wt-4.

B. Multi-caspase activity assay in clones wt-4, S47-8 and AP-8 from A, following twenty-four hours of temperature shift. Levels of caspase activity in uninduced samples (39 degrees, mutant conformation p53) were set to 1, and the fold increase is depicted. The values shown are the averaged results from three independent experiments, with standard error of measurement. The p value indicated is relative to clone wt-4 at 32 degrees.

C. TUNEL analysis of clones of Saos2 cells stably transfected with each p53 polymorphic variant (R72, P72 and S47), analyzed by western analysis for p53 level (see inset) and for TUNEL positive cells after twenty-four hours of temperature shift. Values are expressed as the mean +/- standard error of measurement. p values are given for each cell line (R72 and S47) compared to wt p53 (P72) at 32 degrees.

Temperature shift of cells to 32 degrees results in wild type p53 conformation and apoptosis induction (23,26). Twenty independent clones for each variant (wt, S47 and A46) were generated in the human lung adenocarcinoma cell line H1299 (p53-/-); this line was chosen because it contains high levels of active p38 MAPK, as determined by western blotting using antisera specific for the active enzyme (data not shown). Two clones for each variant were selected for further analysis based upon western analysis indicating comparable levels of p53 protein (Fig. 7A, inset western). These six clones were analyzed for apoptosis induction following temperature shift using TUNEL assay (terminal dUTP nick end labeling); additionally, three of these clones (wt-clone 4, S47-clone 8 and A46-clone 8) were further analyzed using an assay that measures multi-caspase activation. As depicted in Figure 7, TUNEL analysis following temperature shift indicated that the S47 variant consistently had between 2 to 5-fold decreased ability to induce apoptosis, relative to wt p53, while the A46 variant was almost completely compromised for apoptosis induction (Fig. 7A). Consistent with this, analysis of multi-caspase activation indicated that the S47 variant had significantly decreased ability to activate caspases, relative to wt p53 ($p<0.001$).

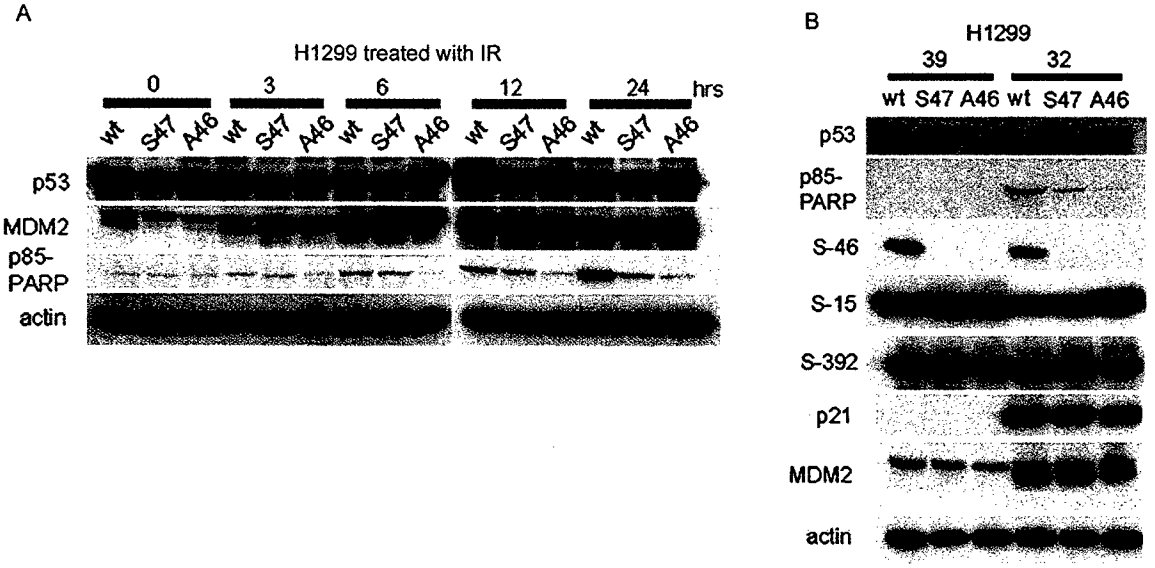

Figure 8. The S47 variant has reduced apoptotic ability, but apparently normal transactivation of MDM2 and p21/waf1.

A. Western analysis of apoptosis induction (appearance of the caspase-cleaved form of poly (ADP) ribose polymerase, p85-PARP) in cells harvested at the indicated timepoints after temperature shift. Just prior to temperature shift, cells were exposed to 6 Gy of radiation. The clones depicted are the same as those in Figure 7B. 39 degrees is mutant (inactive) p53, and 32 degrees is wild type conformation and activity. Levels of β-actin are included as a loading control.

B. Western analysis for p53 level, apoptosis (p85-PARP) and phosphorylated serines 46, 15 and 392, using phospho-specific antisera (Cell Signaling), as well as induction of the p53 target genes MDM2 and p21/waf1. Cells were temperature shifted for 24 hours. Levels of β-actin are included as a loading control.

The ability of A46 to induce apoptosis was more compromised than S47 (Fig. 7B), possibly due to residual phosphorylation of S47 by p38 MAPK or HIPK2. To confirm these findings in another cell background, we generated stably-transfected wt and S47 cell lines in the p53-null human osteosarcoma cell line Saos2. Again, clones were selected that contained equivalent levels of p53

(Fig. 7C, inset western). For this comparison we also included a Saos2 cell line containing an inducible version of the arginine 72 (R72) polymorphic variant; in this way, all three polymorphic variants of p53 could be compared for apoptosis induction (S47, P72 and R72). As shown in Figure 2C, TUNEL analysis following temperature shift in these cell lines indicated there was an over 2-fold decrease in apoptosis in the S47 cell line compared to wild type p53 (P72, $p = 0.01$), and a 7-fold decreased ability when compared to R72 ($p<0.001$).

We extended these analyses to include a time course of apoptosis in the inducible wt, S47 and A46 cell lines following exposure to gamma radiation (clones wt-4, S47-8 and A46-8 from Figure 7, which were analyzed for the remainder of this study). In this experiment, apoptosis was measured as the appearance of the 85 kDa caspase cleavage product of Poly (ADP) ribose polymerase (PARP), using an antibody specific for this caspase cleavage product (p85 PARP). Decreased abundance of p85 PARP following induction of S47 compared to wt p53 could be seen at all time points, although at later time points the difference was more marked (2-fold difference at 6 hours, and 10-fold difference at 24 hours, see Fig. 8A). Similar findings were seen following treatment with doxorubicin as the source of DNA damage (not shown). We next examined the phosphorylation pattern of p53 in these inducible cell lines following temperature shift, using antisera specific for p53 phosphorylated at serines 15, 46 or 392. These analyses revealed no difference in the phosphorylation pattern on serines 15 or 392 between the wt, S47 and A46 proteins (Fig. 8B). There was however a marked decrease in reactivity for the serine 46 phospho-specific antibody for the S47 variant, although we cannot rule out the possibility that the proline-to-serine change in the S47 variant interferes with recognition by this antibody. Interestingly, despite clear differences in apoptosis induction, we saw no evidence of a gross difference in the transactivation potential of these proteins. The ability of the S47 and A46 variants to transactivate the p53-response genes MDM2 and p21/waf1 was indistinguishable from wt p53 in a time course following radiation (MDM2, see Fig. 8A) or following temperature shift (p21 and MDM2, Fig. 8B).

The p38 MAPK inhibitor SB-203580 inhibits serine 46 phosphorylation and apoptosis

The combined data support the hypothesis that the S47 variant has decreased apoptotic ability relative to wt p53, due in part to decreased phosphorylation on serine 46 by p38 MAPK. To solidify these findings, we made use of a well-characterized inhibitor of p38 MAPK, SB-203580 (27). We temperature-shifted our inducible H1299 clones in the presence of SB-203580 or dilution vehicle, and apoptosis induction and the phosphorylation pattern of p53 were assessed. As depicted in Figure 9, western analysis using an antibody specific for phosphorylated serine 46 confirmed that the p38 MAPK inhibitor effectively inhibited phosphorylation on this residue. Specifically, prior to temperature shift wt p53 was already phosphorylated on serine 46 (Fig. 9A, lane 1, S-46). Following temperature shift and assumption of a wild type conformation, this phosphorylation of p53 increased approximately 2-fold (lane 4, S-46), while temperature shift in the presence of SB-203580 reduced serine 46 phosphorylation to starting levels (lane 7). This decrease in serine 46 phosphorylation was accompanied by a marked decrease in apoptosis. Specifically, incubation with SB-203580 brought the levels of the p85 PARP caspase cleavage product, and TUNEL positive cells, to levels comparable to the untreated S47 variant (Figs. 9A and 9B, respectively). SB-203580 also marginally

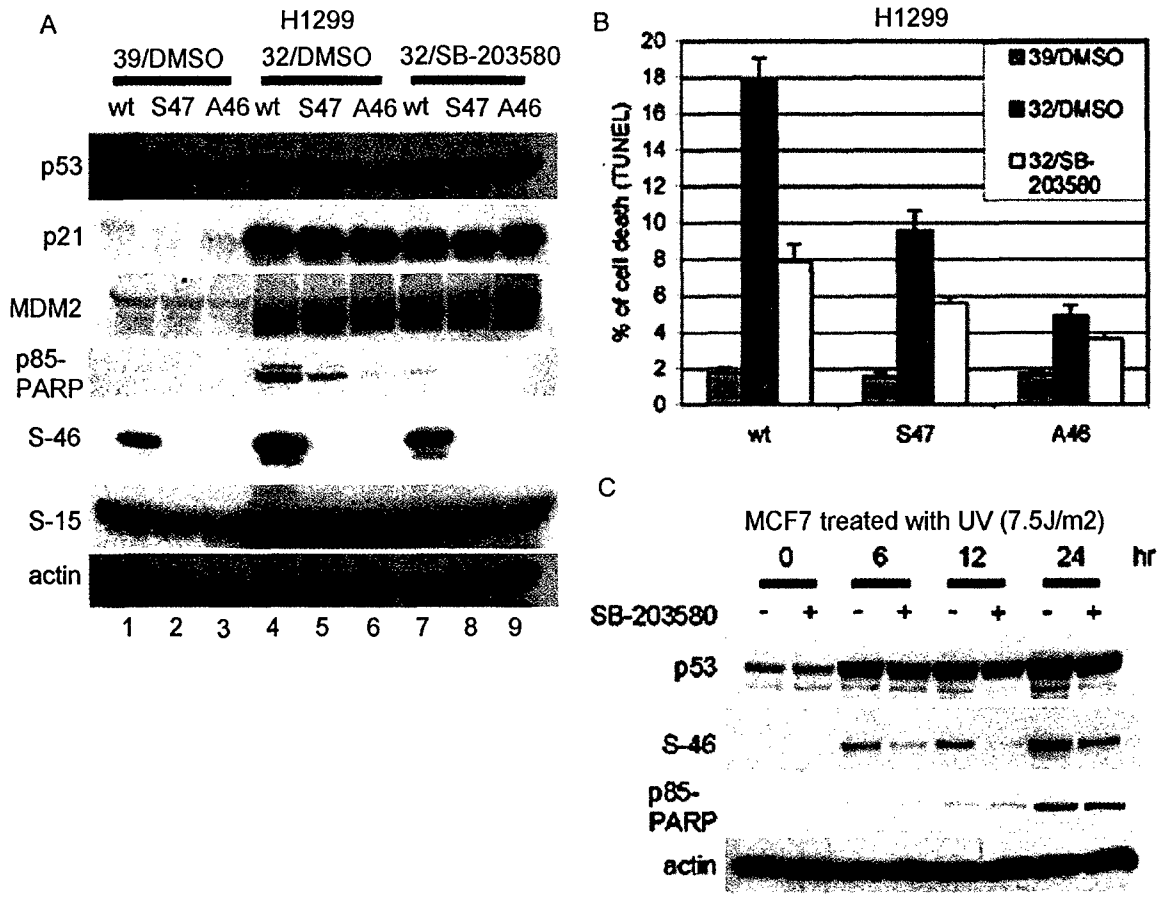

Figure 9. The p38 MAPK inhibitor SB-203580 inhibits phosphorylation of p53 serine 46 and abrogates p53-dependent apoptosis.

A. Western analysis for the proteins indicated of H1299 clones containing the indicated inducible proteins (wt, S47 and A46) treated with the p38 inhibitor SB-203580 or vehicle alone (dimethyl sulfoxide, DMSO) 30 minutes prior to temperature-shift to 32 degrees to induce wild type p53 conformation. The data depicted are representative of three independent experiments. Levels of β-actin are included as a loading control.

B. Quantitation of apoptosis using TUNEL assay on the inducible H1299 clones indicated, following 24 hours of temperature shift; cells were pre-treated for 30 minutes prior to temperature shift with p38 MAPK kinase inhibitor (SB-203580) or vehicle alone (DMSO). Apoptosis was quantitated on a Guava Personal Cell Analysis machine (Guava Technologies).

C. Western analysis of asynchronously growing MCF-7 breast carcinoma cells treated with ultra-violet light (7.5 J/m2) and harvested after the times indicated. Cells were pre-treated for 30 minutes with SB-203580 to a final concentration of 40 uM, or vehicle alone (DMSO), before harvesting and western analysis using antisera to the proteins indicated.

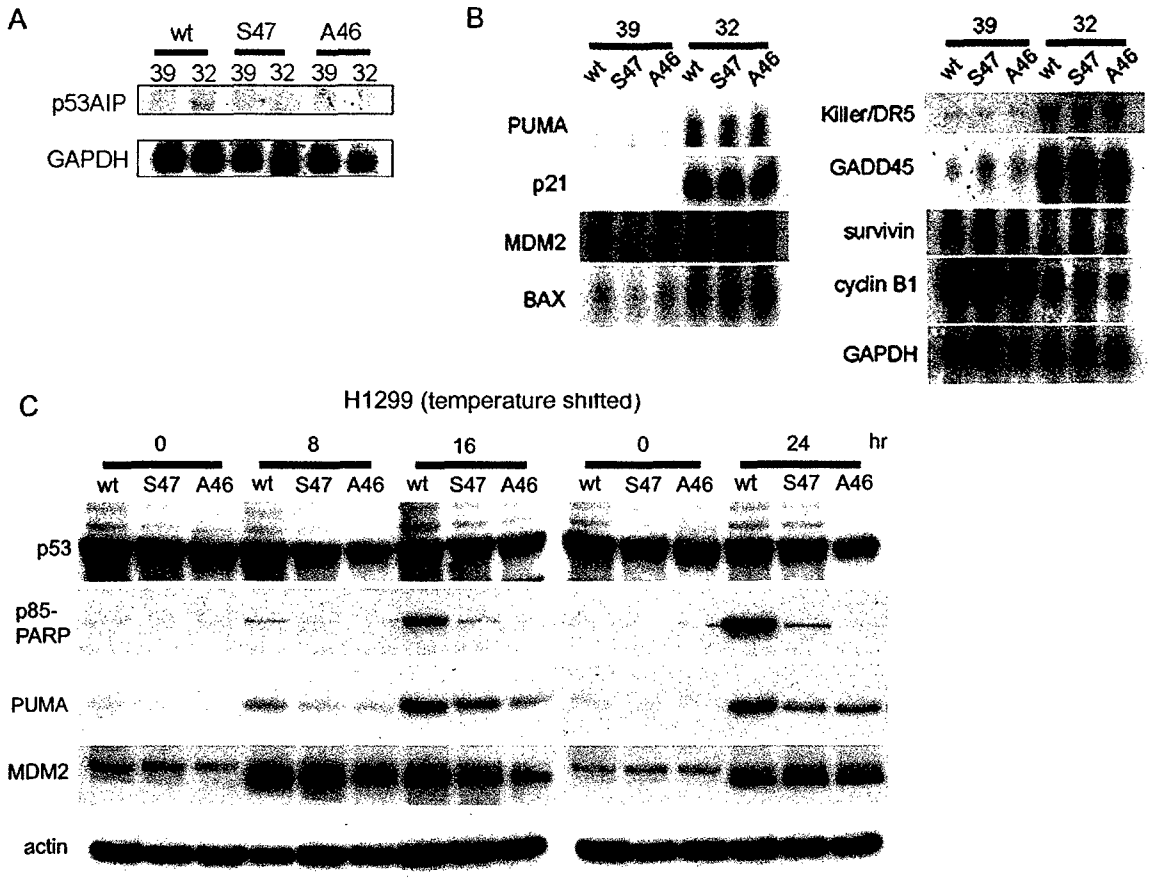

Figure 10. The S47 variant has impaired ability to transactivate the p53-response genes p53AIP1 and PUMA.

A. Northern analysis of 2 ug of polyadenylated RNA isolated from the inducible H1299 clones indicated probed with cDNA specific for p53AIP1 and gapdh (glyceraldehyde 3 phosphate dehydrogenase). Temperature shift is for 24 hours.

B. Northern analysis of total RNA isolated from the H1299 clones indicated, following 24 hours of temperature shift. Results are representative of 3 independent experiments. Densitometry indicates a consistent 3 to 4-fold decrease in PUMA level in S47 and A46, relative to wt p53. Gapdh is included as a control for loading and integrity.

C. Western analysis of a time course of p53 induction in the H1299 clones indicated for p53 level, apoptosis (p85-PARP) and PUMA level. Levels of β-actin are included as a loading control.

inhibited apoptosis induced by the S47 variant, possibly due to residual phosphorylation of serine 46, or to phosphorylation of serine 33 by p38 MAPK, which can also play a role in apoptosis induction (27). Consistent with these data, we found that the SB-203580 inhibitor also effectively inhibited phosphorylation of serine 46, and apoptosis (p85 PARP appearance), in MCF-7 cells (wt p53) treated with ultra-violet light, which activates p38 MAPK (Fig. 9C).

The S47 variant has impaired ability to transactivate p53AIP1 and PUMA

It has been reported previously that serine 46 phosphorylation is not required for the ability of p53 to transactivate the majority of target genes. However, at least one, the pro-apoptotic target gene p53AIP1, requires this phosphorylation event for efficient transactivation (20). In line with this, we analyzed poly-adenylated RNA isolated from our inducible H1299 cell lines, and found that while there was only a modest induction of p53AIP1 in cells containing wt p53, there was no evidence for

induction in lines containing the S47 or A46 variants (Fig. 10A). Unfortunately we have been unable to detect p53AIP1 protein using commercially available antibodies, possibly because the level of p53AIP1 in the cell types employed in this study (H1299, Saos2 and MCF-7) is extremely low following p53 induction. The low level of p53AIP1 in these cells prompted us to broaden this analysis to include other p53-target genes. Northern analysis of the level of other p53 response genes in total RNA revealed no difference in the ability of S47, A46 and wt p53 proteins to transactivate the p53-induced genes *Killer/DR5*, *Gadd45*, *p21/waf1*, *Mdm2* or *bax*, or to repress the genes encoding *survivin* or *cyclin B1*. Interestingly, however, there was a consistent decrease in the ability of the S47 and A46 variants to transactivate the p53 response gene PUMA (p53 up-regulated modulator of apoptosis, Fig. 10B). Western analysis confirmed that the S47 variant had a decreased level of

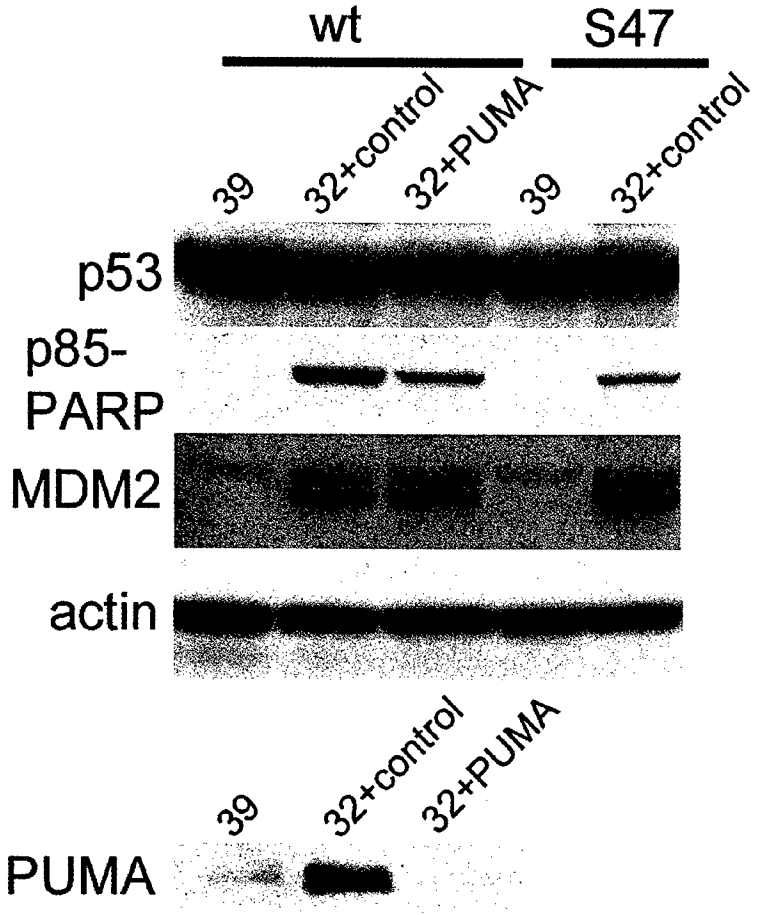

Figure 11. Decreased ability to induce PUMA underlies in part the decreased apoptotic potential of the S47 variant.
H1299 cells containing the inducible versions of p53 indicated were temperature shifted for 24 hours; 24 hours prior to temperature shift cells were transfected with siRNA specific for PUMA, or control scrambled oligonucleotide. Western analysis was performed using the antisera indicated, and levels of β-actin are included as a loading control.

PUMA induction (2-fold decrease compared to wt p53 at 8 hours, 7-fold decrease at 24 hours, see Fig. 10C). In contrast, transactivation of MDM2 was comparable in these experiments (Fig. 10C). Decreased PUMA levels correlated with decreased apoptosis, as measured by the appearance of p85 PARP (Fig. 10C). These data suggest that PUMA transactivation is sensitive to serine 46 phosphorylation. In support of this premise, we found that the p38 MAPK inhibitor SB-203580

efficiently inhibited PUMA transactivation in MCF-7 cells following treatment with ultra-violet light (data not shown).

Down regulation of PUMA using short interfering RNA decreases apoptosis in cells with wt p53 to levels equivalent to the S47 variant

In order to confirm the significance of decreased PUMA transactivation to the decreased apoptotic potential of the S47 polymorphic variant, we used transfection of short interfering RNA oligonucleotides specific for the PUMA transcript to reduce its level in cells with inducible wt p53. Apoptosis in these cells was measured as the appearance of the caspase cleavage product p85 PARP.

As depicted in Figure 11, western analysis of cells treated with siRNA specific for PUMA (SmartPool RNA, Dharmacon), or control scrambled RNA, indicated that the PUMA siRNA efficiently reduced the levels of this transcript, while the control siRNA had no effect. Additionally, exposure to siRNA for PUMA, or controls oligos, had no effect on the ability of p53 to transactivate MDM2 (Fig. 11). Significantly, reduction of PUMA in cells with wt p53 reduced the level of apoptosis in these cells, as measured by p85 PARP appearance, to a level equivalent to cells containing the inducible S47 variant (Fig. 11). These data support the premise that impaired transactivation of PUMA by the S47 variant underlies at least part of the apoptotic defect of this protein

***B-iv.*- Development of a Mouse Model for the Targeted Disruption of the *Appl* Gene in Mammary Gland**

Trainee: Huihong You, Ph.D
Mentor: Joseph Testa, Ph.D.
Period reported: August 1, 2003 – to December 31, 2004

Introduction

Like other AKT/protein kinase B (PKB) family members, AKT2 is activated by various growth factors through phosphatidylinositol 3-kinase (PI3K) and thereby mediates signals involved in diverse cellular processes, including apoptosis inhibition, cell proliferation, and insulin signaling. AKT is an integral player in a signal transduction pathway of which many components have been linked to oncogenesis. Activated forms of AKT and its upstream activator, PI3K, are responsible for the transforming activities of certain viruses, and a negative regulator of this pathway, PTEN, is a tumor suppressor.

To facilitate our understanding of the cellular function of AKT2, we had previously used the yeast two-hybrid system to identify two candidate AKT2 partners. Multiple independent isolates of two clones were obtained in a screen of a human fetal brain cDNA library. We have designated one of the putative AKT2 interactors APPL (28). Although a number of important substrates and regulators of AKT/PKB have been identified, our data indicate that APPL is not a substrate but, instead, is an adaptor. To date, APPL is the only adaptor reported to interact with AKT kinases. Moreover, under the conditions tested thus far, this interaction has been strongest with the AKT2 isoform. Since AKT2 appears to play a more prominent role in human neoplasia than other members of the AKT family, the characterization of APPL may provide important insights regarding oncogenic mechanisms involving AKT2.

Recently, APPL(or APPL1, also called DIP13-alpha) has been identified as a Rab5 effector, which resides on a subpopulation of endosomes. APPL1 translocates from the membranes to the nucleus where it interacts with the nucleosome remodeling and histone deacetylase multiprotein complex NuRD/MeCP1 in response to extracellular stimuli (29).

Another study showed that APPL interacts with a region on the cytoplasmic domain of DCC (deleted in colorectal cancer, which is a candidate tumor suppressor gene), which is required for the induction of apoptosis. Co-expression of DCC and DIP13-alpha results in an increase in apoptosis (304).

Apoptosis occurs during normal growth and development of the mammary gland. During involution and remodeling of the breast after lactation, apoptosis is a prominent feature. Most of the secretary epithelium in the lactating breast undergoes apoptosis as the mammary gland regresses and is reorganized for another cycle of lactation. The expression of activated Akt is regulated in this process, such that Akt1 activation peaks in pregnancy and lactation, and decreases during mammary involution (reviewed in reference 31). To provide insights regarding how the loss of *Appl* regulates Akt activation and the normal apoptotic process, and how loss of *Appl* affects mammary development during lactation and involution, we are generating an *Appl* conditional knock-out (KO) mouse model. Since Akt2 and Her2 overexpression or *Pten* deletion play important roles in mammary gland development and mammary tumorigenesis, we propose to elucidate the biochemical significance of Appl in these processes. To address these questions, we intend to cross *Appl* KO mice with MMTV-*Akt2* or MMTV-*Her2* transgenic mice, or with *Pten* KO mice.

Body

To date, we have finished Specific Aim 1 and 2. They include: aim1: screen phage libraries derived from 129Sv mouse genomic DNA to identify phage clones containing the *Appl* coding region; and construct a plasmid for gene-targeted disruption of APPL; aim 2: electroporate ES cells with the KO construct and screen the resultant transfected clones for homologous recombination of the gene-targeted construct using Southern blot analysis and PCR.

1) A phage 129Sv mouse genomic library (Stratagene) was screened and clones containing the *Appl* coding region were identified.

Based on the human *APPL* genomic sequence and restriction mapping, we decided to target Exon 5 of the mouse *Appl* gene. We generated a probe specific for Exon 5 of the mouse *Appl* gene, based on mouse EST sequences, and used this probe to screen the library. We identified 5 positive clones, which are about 15.5 kb in length and contain *Appl* genomic sequences that flank exon 2 to 7 or exon 5 to 11.

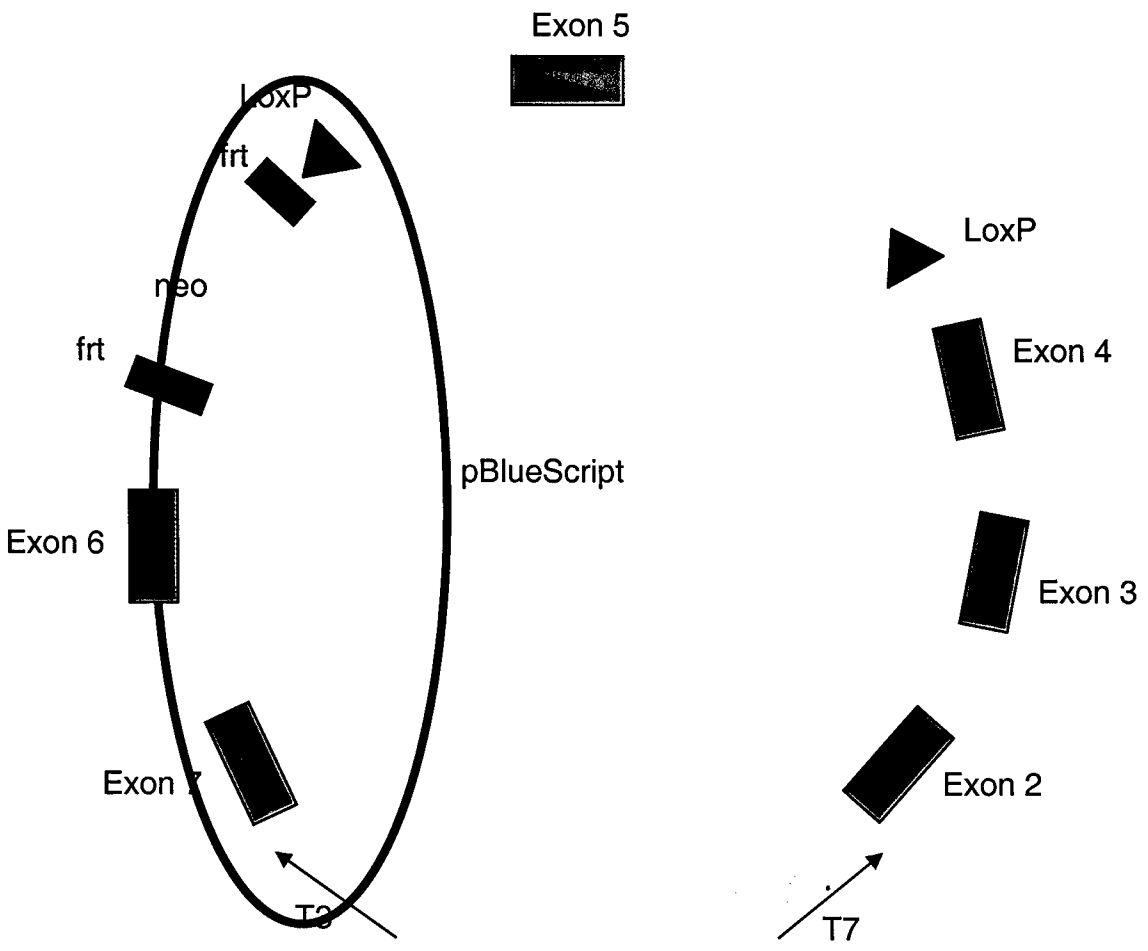

Figure12: KO targeting construct for disruption of Exon 5 of Appl. Processing of the Appl ORF will be disrupted after Exon 4.

2) A construct to conditionally disrupt *Appl* expression/function was synthesized.

The *Appl* gene has 22 exons distributed over ~60 kb. Exon 5 is 88 bp in length and is flanked by two very large introns, which maximize the chance that our engineered cassette will recombine specifically with the *Appl* locus. Disruption of Exon 5 will result in a frame shift in the *Appl* ORF, which is predicted to disrupt endogenous *Appl* gene transcription. We devised a detailed restriction map of the region of interest. With this information, a targeting vector was designed to add one LoxP site upstream of Exon 5 and another LoxP and a selectable neomycin-resistance gene (*neo*) cassette flanked by two FRT sites downstream of Exon 5. Unique restriction fragments have been identified that can distinguish between the wild-type and the LoxP/*neo-Appl* genes by Southern blot and PCR analyses.

Overlapping subclones obtained from the phage genomic library encompass approximately 15.5 kb of sequence. Figure 12 depicts the complete *Appl* KO construct that was constructed for the investigations described. In brief, the 9.3-kb genomic sequence flanking Exon 2 to Exon 7 of mouse *Appl* has been directly excised by restriction enzyme digestion from a subclone derived from a 129Sv mouse genomic library. This 9.3-kb insert was cloned into a pBluescript vector (with mutated KpnI site, XbaI site, SpeI site and BamHI site in its multiple cloning region). An oligo with a LoxP sequence and an EcoRI site has been cloned into the BamHI site of the vector upstream of Exon 5. Another LoxP site with FRT-flanked neo sequence derived from plasmid pK-11/pM-30 (32) has been cloned into the vector downstream of Exon 5, between EcoRV and KpnI sites.

3) Embryonic stem (ES) cell clones containing the conditional *Appl* KO sequence and *Neo* cassette were identified.

We electroporated mouse ES cells with the KO construct and screened the resultant transfected clones for homologous recombination of the gene-targeted construct using Southern blot analysis and PCR and electroporated positively identified gene-targeted ES cells with plasmids, which can express Flp site-specific recombinase to remove the neo selection cassette.

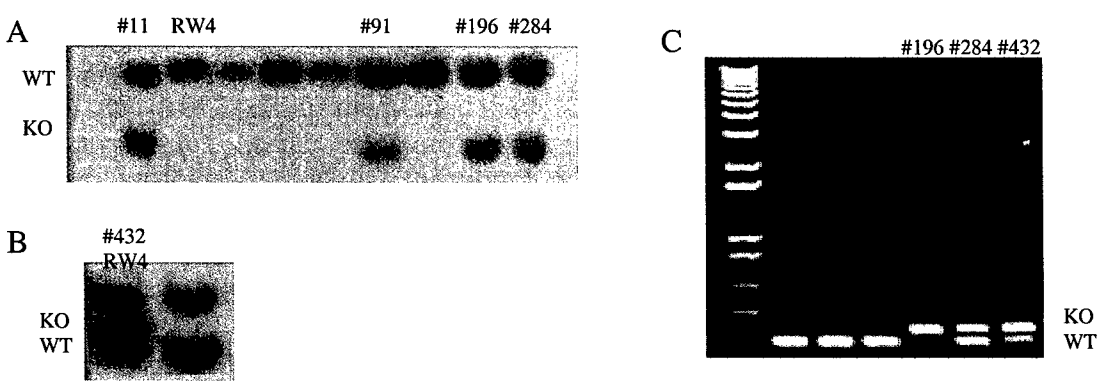

Figure 13. Southern-blot analysis of control and homologous recombined clones after digestion with XbaI (A) or AvaI (B) and hybridization with the 3' (A) or 5'(B) external probe. C: PCR using primers that detect wildtype and loxP containing knockout alleles. WT, wild-type band; KO, knock out band.

a) *ES cell culture and selection:*

A unique XhoI restriction site within the vector itself and near homologous *Appl* intron sequences has been used to linearize the construct prior to transfection of RW4 ES cells. Electroporation and drug selection of ES cells have been performed. Transfected cells were drug-selected (resistance to G418) for 10 days, and then individual stem cell clones were isolated in 24-well plates. Once sufficient cell numbers were obtained, clones were split into two sets of plates (one for freezing of viable cells, the other for generation of DNA). These ES cell clones have been screened for homologous recombination using PCR with specific primers and Southern blot analyses, using restriction enzymes (XbaI for 3' and AvaI for 5') that yield fragments of a predicted molecular weight and genomic probes flanking the targeting sequence. Both 5' and 3' probes and *Neo* probe have been used in order to confirm double homologous recombination and *Neo* insertion. 791 ES cell clones have been screened, and 9 of them were identified as positive homologous recombined clones in this targeting strategy (Figure 13).

b). Karyotyping positive ES clones

After identified the homologous recombined clones, we karyotyped 3 of them in the Cytogenetics Research Facility at Fox Chase Cancer Center (Table1).

Table 1. Karyotype of positive ES clones

Clone number	Normal diploid cells	Abnormal cells
196	18	2
284	19	1
432	19	1

c). Removal of Exon 5 with an adenoviral Cre expression vector:

To test for positive homologous recombination resulting in Exon 5 deletion of *Appl,* clone 284 was infected with an adenoviral Cre expression vector. After infection, 30 clones were picked and screened by PCR and sequencing. One clone was identified that had a deletion of Exon 5 (Figure 14).

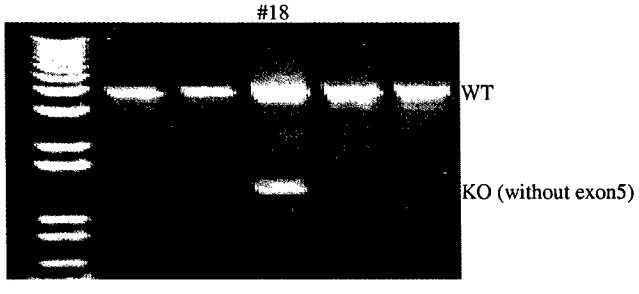

Figure 14. PCR screening Ad-Cre virus infected clones using primers that detect wildtype and knockout alleles. WT, wild-type band; KO, knock out band (without exon5).

d). Removal of the neo selection cassette:

We transiently transfected 2 clones (clone 284 and 432) by electroporating plasmids that express Flp site-specific recombinase in order to remove the Neo selection cassette. After transfection, we used one half of the cells for drug selection to identify clones lacking the Neo cassette. ES clones that are sensitive to G418 were identified and expanded for freezing and screening using Southern blot analysis and PCR. About 1300 clones were picked and drug (G418) selected in two rounds of electroporations, but none of the *Neo*-minus clones retained both loxP sites.

4) Derive mice for future KO studies and breed chimeric mice to obtain germline transmission and mice heterozygous or homozygous for LoxP incorporated *Appl* alleles.

To date, we have injected 3 positive ES clones into 129 mouse blastocysts. Chimeric mice have been obtained and are being mated with B6 female mice. PCR/southern blotting will be used for genotyping of agouti offspring, using mouse tail DNA to see if there is germline transmission of the conditional KO *Appl* sequence.

C- KEY RESEARCH ACCOMPLISHMENTS.

C-1. *Predisposition to genomic instability in breast cancer: analysis of molecular mechanisms*

a) Recent work has emphasized the dual activity of centrosomes in contributing to control of cell polarization in interphase and cell migration but also in coordinating polarity of the mitotic spindle in M-phase progression.

b) Our work on HEF1 is the first and only study that has clearly indicated an important function of the CAS family of focal adhesion signaling proteins in profound changes in the physical organization of cells during mitosis. We have shown HEF1 is localized to the centrosome throughout cell cycle, but increased significantly at G2/M boundary. HEF1 directly interacts with the AurA kinase. AurA kinase is over-expressed in more then 50% of breast cancers. The N-terminal domain of HEF1 is involved in this interaction. HEF1 is an AurA substrate. Phosphorylation of HEF1 by AurA is important for interaction between AurA and HEF1. HEF1 – AurA interaction causes the activation and might be involved in AurA activation during mitotic onset.

C-ii- The codon 47 polymorphism of p53 is functionally significant.

a) The S47 variant shows significantly decreased phosphorylation of serine 46.

c) The S47 variant shows compromised apoptotic ability.

d) The p38 kinase is a key player in the phosphorylation of serine 46 by interaction with proline 47. When p38 is inhibited, the phosphorylation of serine 46 is inhibited, as well as the apoptotic ability of p53.

e) The S47 variant has compromised apoptotic ability because it possesses decreased ability to transactivate p53AIP and PUMA.

C-iii- *Development of a Mouse Model for the Targeted Disruption of the Appl Gene in Mammary Gland.*

a) We have isolated and characterized genomic fragments of Appl from a phage 129Sv mouse genomic library. A 9.3-kb sequence, flanking exon 2 to exon 7 of Appl, was used to generate a targeting construct containing LoxP sites and neomycin resistance sequence.

b) We are using this homologous construct to electroporate embryonic stem cells that will be selected for resistance to G418 and homologous recombination of the targeting construct.

D- REPORTABLE OUTCOMES

Presentations:

1. Pugacheva, E.N American Society for Cell Biology, December 14-18th, San Francisco, CA, 2002(poster)

2. Pugacheva, E.N Fox Chase Cancer Center Postdoc Day, 6 June 2003, Philadelphia, PA (poster)

3. Pugacheva, E.N The Engelhardt Institute for Molecular Biology Biennial Meeting, June 29th – July 5th 2003, Moscow, Russia (talk)

4. Pugacheva, E.N American Society for Cell Biology, December 14-18th, San Francisco, CA,2003 (poster)

5. Pugacheva, E.N American Society for Cell Biology, December 4-8th, Washington, DC, 2004 (poster)

6.Li, X., Dumont P., Della Pietra A. Shetler C. and Murphy M. (2003). Proline 47 is important in mediating p53-dependent apoptosis. Fox Chase Cancer Center Pharmacology Department Meeting. Philadelphia, PA.

7.Li, X., Dumont P., Della Pietra A. Shetler C. and Murphy M. (2003). Graduate and Postdoc Day at the Fox Chase Cancer Center. Philadelphia, PA.

8.Li, X., Dumont P., Della Pietra A. Shetler C. and Murphy M. (2004). Graduate and Postdoc Day at the Fox Chase Cancer Center. Philadelphia, PA.

9. You, H. and Testa, J.R. Involvement of Akt in vitamin E succinate-induced apoptosis. Graduate and Postdoctoral Day at the Fox Chase Cancer Center. Philadelphia, PA.2004

Publications:

1. Serebriiskii, I.G., Mitina, O., Pugacheva, E., Benevolenskaya, E., Kotova, E., Toby, G.G., Khazak, V., Kaelin, W.G., Chernoff, J., and Golemis, E.A. Detection of peptides, proteins, and drugs that selectively interact with protein targets. Genome Res 12: 1785-1791, 2002.

2. Pugacheva, E.N.and Golemis, E.A Deregulation of HEF1 induces defects in centrosomal dynamics and formation of the mitotic spindle. Manuscript was submitted 2004 (Cell).

3.Li, X., Dumont P., Della Pietra A. Shetler C. and Murphy M. The codon 47 polymorphism of p53 is functionally significant. (Submitted)

E- CONCLUSIONS AND SIGNIFICANCE:

E-1- Predisposition to genomic instability in breast cancer: analysis of molecular mechanisms.

Defects in the integrity of cellular division at mitosis are important predisposing factors to breast cancer, as reflected by the defects in ploidy and over-duplication of centrosomes in many primary breast cancers. The phenotypes we have observed in cells overexpressing or depleted of HEF1 is exactly coincident with the cells similarly manipulated for AuroraA kinase. A detailed analysis of the consequences of positively or negatively deregulating the activity of HEF1 indicates that HEF1 function is essential for centrosomal maturation and mitotic spindle formation. HEF1 also interacts with and controls the activation of AurA, suggesting an important role for HEF1 in regulation of mitotic entry. Interestingly, the functions we have identified for HEF1 are not completely shared with its well-studied family member p130Cas, while both proteins have much more pronounced activity in epithelial cells versus fibroblasts. These results indicate that HEF1 provides a crucial bridge coordinating attachment and cell division processes at M-phase in human breast epithelial cells.

ii- **- The codon 47 polymorphism of p53 is functionally significant.**

Our data indicate that the S47 variant of p53 has decreased ability to serve as a substrate for phosphorylation by p38 MAPK, as well as decreased ability to induce apoptosis *in vivo*. Underlying this apoptotic defect we have found that the S47 variant exhibits decreased ability to transactivate the p53 response genes p53AIP1 and PUMA. In contrast, we have seen no differences in the ability of S47 to bind to DNA, induce G1 arrest, or to localize to mitochondria, compared to wt p53 (X. Li and M. Murphy, unpublished observations). These data are the first to suggest that the serine 47 polymorphism is functionally significant, and to implicate serine 46 phosphorylation in the transactivation of the p53 target gene PUMA. While the changes in PUMA transactivation by S47 appear to range only from 2- to 7-fold, transactivation of PUMA is known to be particularly critical for apoptosis induction by p53 (32-34). Additionally, even the heterozygous PUMA knock-out mouse (Puma +/-), with 2-3 fold reduction in PUMA levels, has a marked defect in apoptosis of irradiated thymocytes, compared to wild type mice (34).

Our data indicate that there are two polymorphisms in p53 that are functionally significant, at codons 47 and 72. It remains to be determined if the S47 polymorphism has an impact on cancer risk; however, in support of this possibility, missense mutations of amino acid 47 (proline to leucine) are reported in the p53 mutation data base (35). It remains to be determined why functionally significant polymorphic variants in a tumor suppressor gene that decrease its function would persist in the human population. It is of note that both of the polymorphic variants of p53 that are associated with decreased apoptotic potential (P72 and S47) are more prevalent in populations whose origin is near the equator (Africa). This suggests that the selection for these variants may have occurred as a response to exposure to high levels of ultraviolet light. We speculate that the decreased apoptotic potential of p53 may have been selected for in environments of high UV exposure in order to enable cells to more efficiently repair DNA, or to accumulate the pigmentation necessary to inhibit over-fixation of vitamin D, which can be toxic in such environments. In contrast, the higher apoptotic potential of the R72 variant, which is associated with skin of lighter pigmentation (36), would be selected for in environments where UV exposure was limited, and the increased absorption of UV rays afforded by lighter pigmentation would enhance vitamin D fixation. The combined data suggest that a careful epidemiological analysis of the impact of the S47 polymorphism on cancer risk, progression, and the efficacy of chemotherapy and radiation therapy is warranted. Additionally, it will be important to determine if the ethnic bias of this polymorphism explains some of the differences in cancer incidence between Caucasian and African American populations.

iii- ***Development of a Mouse Model for the Targeted Disruption of the Appl Gene in Mammary Gland.***

A 9.3-kb DNA genomic sequence, flanking exon 2 to exon 7 of Appl, was isolated and characterized, and was used to generate a targeting construct containing LoxP sites and neomycin resistance sequence. In order to understand the significance of the Appl during cellular processes and the potential interaction with other signaling molecules such as AKT2, it is important to analyze this gene in the context of a living animal. In particular, the generation of Appl mice with targeted disruption of Appl in the mammary gland will elucidate the role of Appl in mammary development. Mating Appl mice with other mouse models of breast cancer will reveal the potential of Appl in contributing to breast tumorigenesis. We will breed chimeric mice to obtain mice heterozygous and homozygous for LoxP incorporated *Appl* alleles. We will breed these mice with MMTV-Cre or WAP-Cre transgenic mice to disrupt the *Appl* gene in mammary gland, delineate the phenotype of *Appl*-targeted disruption in the mammary gland, and elucidate the function of Appl in breast development and during mammary involution. These studies may provide insights regarding *in vivo* mammary-specific apoptotic signaling and potential targets for therapeutic intervention. We also intend to breed floxed *Appl* mice to EIIa-Cre transgenic mice to generate mice with *Appl* deleted during embryogenesis. If disrupting the *Appl* gene during embryogenesis is not lethal, we will breed these mice with *Akt2* KO mice to further delineate the role of Appl in mammary gland development, or with *Pten* KO mice, MMTV-Akt2, or MMTV-Her2 transgenic mice to study the function of Appl in mammary tumorigenesis. Previous data from our laboratory showed that Akt plays a critical role in mammary gland involution. By breeding *Appl* KO mice with MMTV-*Akt2* transgenic mice or with *Akt2* KO mice, we will determine if Appl can regulate Akt2 function in normal mammary gland development, especially during lactation and involution. About 60% of *Pten*-deficient mice develop breast cancer by 10 months. By breeding *Pten* KO mice or MMTV-*Her2* transgenic mice with *Appl* KO mice, we will be able to investigate whether Appl deficiency can alter the incidence, size, or aggressiveness of mammary tumors. In order to unravel the full spectrum of *Appl* function, it is important to analyze this gene in the context of a living animal. The use of *Appl* conditional KO mice will complement our laboratory's ongoing *in vitro* studies. Gene inactivation through homologous recombination is an unambiguous means to target *Appl,* thereby eliminating its function and establishing a phenotype for Appl loss-of-function. The resulting *Appl* KO mice will be interbred with WAP-Cre or MMTV-Cre transgenic mice, EIIa-Cre transgenic mice, and other transgenic or knockout mice with genetic defects in the Akt signaling pathway to determine if Appl has an important physiological function in mammary gland development and mammary tumorigenesis.

F- REFERENCES

1. Parkin DM, Bray F, Ferlay J, Pisani P. (2000) *Int J Cancer* 94:153-6.
2. Malkin D, Li FP, Strong LC, et al. (1990) *Science* 250:1233-8.
3. Ho GH, Calvano JE, Bisogna M, et al. (2000) *Cancer* 89:2153-60.
4. Done SJ, Arneson CR, Ozcelik H, Redston M, Andrulis IL (2001) *Breast Cancer Res Treat.* 65:111-8.
5. Done SJ, Eskandarian S, Bull S, Redston M, Andrulis IL (2001) *J Natl Cancer Inst.* 93:700-4
6. Norberg T, Klaar S, Karf G, et al. (2001) *Cancer Res.* 61:8317-21
7. Borresen-Dale AL. (2003) *Int J Biol Markers.* 18:54-6.
8. Berns EM, Foekens JA, Vossen R, et al. (2000) *Cancer Res.* 60:2155-62.
9. Liu G, Schwartz JA, Brooks SC. (2000) *Cancer Res.* 60:1810-4.
10. Murphy M, Ahn J, Walker KK, Hoffman WH, Evans RE, Levine AJ and George DL. (1999) *Genes & Dev* 13:2490-2501.
11. Dumont P, Leu JI, Della Pietra AC, George DL, Murphy M. (2003) *Nat Genet.* 33:357-65.
12. Leu JI, Dumont P, Hafey M, Murphy ME, George DL. (2004) *Nature Cell Biology*, 6:443-50.

13. Hishida A, Matsuo K, Tajima K, Ogura M et al. (2004) *Leuk Lymphoma* 45:957-64.
14. Xi YG, Ding KY, Su XL, Chen DF, You WC, Shen Y, Ke Y (2004) *Carcinogenesis* 25:2201-6.
15. Granja F, Morari J, Morari EC, Correa LA, Assumpcao LV, Ward LS. (2004) *Cancer Lett* 210:151-7.
16. Jones JS, Chi X, Gu X, Lynch PM, Amos CI, Frazier ML. (2004) *Clin Cancer Res* 10:5845-
17. Bond GL, Hu W, Bond EE, Robins H et al. (2004) *Cell* 119:591-602.
18. Felley-Bosco E, Weston A, Cawley HM, Bennett WP, Harris CC (1993) *Am J Hum Genet.* 53:752-9.
19. Bulavin DV, Demidov ON, Saito S, Kauraniemi P et al. (2002) *Nat Genet* 31:210-215
20. Oda K, Arakawa H, Tanaka T, Matsuda K et al. (2000) *Cell* 102:849-62 .
21. Sanchez-Prieto R, Rojas JM, Taya Y, and Gutkind JS. (2000) *Cancer Res* 60:2462-72.
22. Takekawa M, Adachi M, Nakahata A, Nakayama I, Itoh F, Tsukuda H, Taya Y, Imai K. (2000) *EMBO J.* 19:6517-26.
23. D'Orazi G, Cecchinelli B, Bruno T, Manni I, et al. (2002) *Nat Cell Biol.* 4:11-19.
24. Hofmann TG, Moller A, Sirma H, Zentgraf H, Taya Y, Droge W, Will H, and Schmitz ML. (2002) *Nat Cell Biol* 4:1-10.
25. Pochampally R, Li C, Lu W, Chen L, Luftig R, Lin J and Chen J. (2000) *Biochem Biophys Res Commun* 279:1001-1010.
26. Martinez J, Georgoff I, Martinez J, Levine AJ. (1991) *Genes Dev.* 5:151-9.
27. Bulavin DV, Saito S, Hollander MC, Sakaguchi K, Anderson CW, Appella E, Fornace AJ Jr. (1999) *EMBO J.*18:6845-54 .
28. Mitsuuchi, Y., Johnson, S. W., Sonoda, G., Tanno, S., Golemis, E. A., and Testa, J. R. Identification of a chromosome 3p14.3-21.1 gene, APPL, encoding an adaptor molecule that interacts with the oncoprotein-serine/threonine kinase AKT2. Oncogene *18:* 4891-4898, 1999
29. Miaczynska, M., Christoforidis, S., Giner, A., Shevchenko, A., Uttenweiler-Joseph, S., Habermann, B., Wilm, M., Parton, R.G., and Zerial, M. APPL proteins link Rab5 to nuclear signal transduction via an endosomal compartment. Cell. 116(3):445-56, 2004.
30. Liu, J., Yao, F., Wu, R., Morgan, M., Thorburn, A., Finley, R.L. Jr, and Chen, Y.Q., Mediation of the DCC apoptotic signal by DIP13 alpha. J Biol Chem. 277(29):26281-5, 2002.
31. Strange, R., Metcalfe, T., Thackray, L., and Dang, M. Apoptosis in normal and neoplastic mammary gland development. Microsc. Res. Tech. *52*: 171-181, 2001.
32. Yu J, Zhang L, Hwang PM, Kinzler KW, Vogelstein B. (2001) *Mol Cell* 7:673-82.
33. Villunger A, Michalak EM, Coultas L, Mullauer F, Bock G, Ausserlechner MJ, Adams JM, Strasser A. (2003) *Science* 302:1036-8.
34. Jeffers JR, Parganas E, Lee Y, Yang C, et al. (2003) *Cancer Cell* 4:321-8
35. Olivier M, Eeles R, Hollstein M, Khan MA, Harris CC, Hainaut P. (2002) *Hum Mutat.* 19:607-14. (Database version R9, July 2004).
36. McGregor JM, Harwood CA, Brooks L, Fisher SA et al. (2002) *J Invest Dermatol.* 119:84-90.

Appendices

JOSE RUSSO, M.D., F.C.A.P., FASCP

A- Publications:

1. Serebriiskii, I.G., Mitina, O., Pugacheva, E., Benevolenskaya, E., Kotova, E., Toby, G.G., Khazak, V., Kaelin, W.G., Chernoff, J., and Golemis, E.A. Detection of peptides, proteins, and drugs that selectively interact with protein targets. Genome Res 12: 1785-1791, 2002.

2. Pugacheva, E.N., Yungfeng Feng; Gregory D. Longmore and Erica A Golemis,. HEF1 regulates centrosomal maturation and spindle formation through control of the Aurora A Kinase. Manuscript was submitted 2004 (Cell).

3.Li, X., Dumont P., Della Pietra A. Shetler C. and Murphy M. The codon 47 polymorphism of p53 is functionally significant. (Submitted)

Methods

Detection of Peptides, Proteins, and Drugs That Selectively Interact With Protein Targets

Ilya G. Serebriiskii,[1] Olga Mitina,[1,2] Elena N. Pugacheva,[1] Elizaveta Benevolenskaya,[3] Elena Kotova,[1] Garabet G. Toby,[1,4] Vladimir Khazak,[5] William G. Kaelin,[3] Jonathan Chernoff,[1] and Erica A. Golemis[1,6]

[1]Division of Basic Science, Fox Chase Cancer Center, Philadelphia, Pennsylvania 19111, USA; [2]Department of Molecular Biology and Medical Biotechnology, Russian State Medical University, Moscow, Russia; [3]Dana-Farber Cancer Institute, Boston, Massachusetts 02115, USA; [4]Cell and Molecular Biology Group, University of Pennsylvania School of Medicine, Philadelphia, Pennsylvania 19104, USA; [5]Morphochem, Inc., Monmouth Junction, New Jersey 08852, USA

Genome sequencing has been completed for multiple organisms, and pilot proteomic analyses reported for yeast and higher eukaryotes. This work has emphasized the facts that proteins are frequently engaged in multiple interactions, and that governance of protein interaction specificity is a primary means of regulating biological systems. In particular, the ability to deconvolute complex protein interaction networks to identify which interactions govern specific signaling pathways requires the generation of biological tools that allow the distinction of critical from noncritical interactions. We report the application of an enhanced Dual Bait two-hybrid system to allow detection and manipulation of highly specific protein–protein interactions. We summarize the use of this system to detect proteins and peptides that target well-defined specific motifs in larger protein structures, to facilitate rapid identification of specific interactors from a pool of putative interacting proteins obtained in a library screen, and to score specific drug-mediated disruption of protein–protein interaction.

[Supplemental material is available online at http://www.genome.org. The following individuals kindly provided reagents, samples, or unpublished information as indicated in the paper: A. Taliana, M. Russell, M. Berman, and R. Finley.]

Since its inception (Fields and Song 1989), the two-hybrid system has been utilized in increasingly complex strategies to analyze interactions between proteins of biological interest and known or novel cognate partners including other proteins, RNA sequences, pharmacological agents, and peptides (for review, see Serebriiskii et al. 2001). More recently, a number of groups have exploited the potential of two-hybrid systems as a tool for understanding protein interactions on a genome-level scale, with pilot studies involving elucidation of large sets of protein interactions developed in *Saccharomyces cerevisiae* (Schwikowski et al. 2000; Ito et al. 2001) providing a model for ongoing work in higher eukaryotes. Given the increasing realization that protein interaction networks involve the interaction of discrete signaling molecules with multiple partner proteins in different biological circumstances, accurate description of the function of a given protein now implicitly involves dissection of its interaction domains, ranking of its interaction affinity with each of its partners, and determination of physiological conditions under which each pair of proteins preferentially interacts. These determinations pose significant technological hurdles in high-throughput efforts.

We have described previously a proof-of-concept experiment for a two-hybrid Dual Bait system that provides internal controls for interaction specificity, and could theoretically be used to selectively compare the interaction of a protein with more than one partner molecule (Serebriiskii et al. 1999). Building from this preliminary study, we have now developed a complete system of reagents that can be used to score interaction of one transcriptional activation domain (AD)-fused prey protein with either of two DNA-binding domain (DBD)-fused bait proteins over a range of different interaction affinities. In three different library screening applications, we demonstrate that these reagents can be used to identify proteins or peptides that target short sequence elements of biological importance within a larger protein structure. We further demonstrate that the system can be used in a bait swap application for rapid secondary screening to sort multiple library hits into subgroups most likely to be reproducible and physiologically relevant. Finally, we describe the use of the reagents in a subtractive two-color visualization procedure that can discriminate specific from nonspecific drug-induced inhibition of protein interactions. These studies, together with our other work involving use of the system to build enhanced specificity derivatives of signaling proteins engaged in complex interactions, indicate the Dual Bait is a useful tool in dissection of complex cellular regulatory machinery.

[6]Corresponding author.
E-MAIL EA_Golemis@fccc.edu; FAX (215) 728-3616.
Article and publication are at http://www.genome.org/cgi/doi/10.1101/gr.450702.

RESULTS AND DISCUSSION

In the Dual Bait two-hybrid system (Fig. 1), the use of two parallel bait-reporter systems allows simultaneous and com-

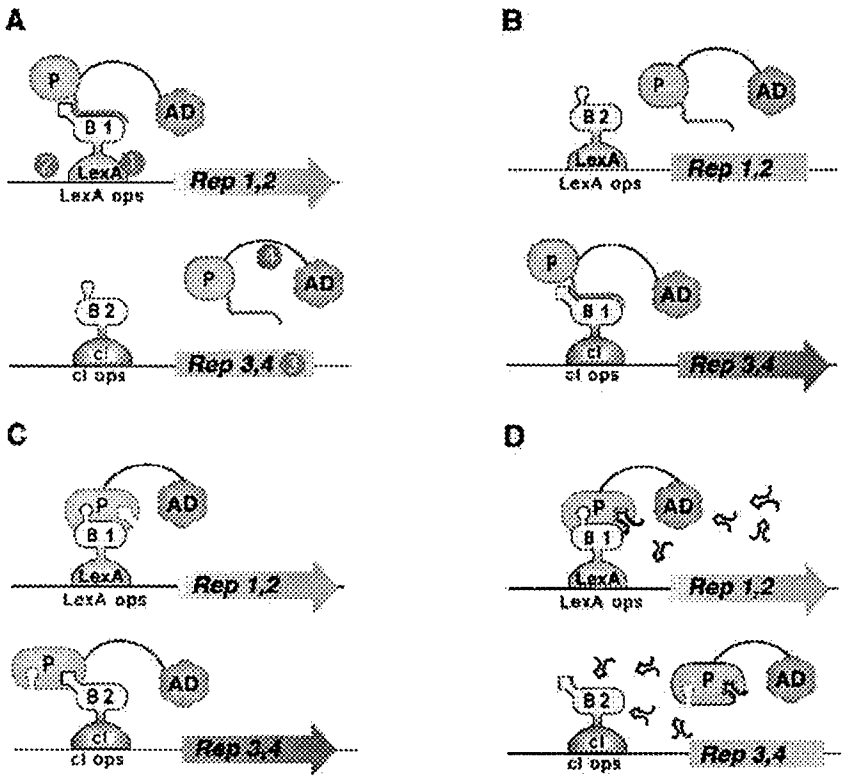

Figure 1 Outline of Dual Bait System. (*A*) An activation domain-fused prey (P) interacts with a LexA-fused bait (B1) to drive transcription of *lexAop*-responsive *LEU2* and *lacZ* reporters, but does not interact with a cI-fused bait (B2) and, thus, does not turn on transcription of *clop*-responsive *LYS2* and *gusA* reporters. The prey may represent a protein, as in Applications 1 and 3, or a peptide aptamer, as in Application 2. Note, in this example, the cI-Bait is drawn as representing a negative control for prey binding; the system can also be configured so that prey interacts with either or both baits, as in Serebriiskii et al. (1999). Points addressed in optimization of the Dual Bait two-hybrid system in this study (Table 1) are as follows: (1), varying expression level of baits; (2), enriching polylinkers to facilitate cloning of baits; (3), varying sensitivity of reporters; (4), diversifying plasmid antibiotic markers to facilitate isolation of library plasmid in *E. coli*. In addition, we have developed a robust yeast strain, SKY473, which is suitable both for bait testing and interaction mating in this system. (*B*) As described in Application 3, preys isolated against LexA-B1 and counterselected against cI-B2 are subsequently challenged with cI-B1 and LexA-B2, in a bait swap experiment. Those preys binding specifically to the B1 domain (as opposed to B1 specifically in the context of a LexA-B1 fusion protein) are retained preferentially. (*C*) One protein (P) may use different surface motifs to bind two different partners (B1, B2). (*D*) Application of a small molecule (drug or peptide) that obstructs one of the interactions shown in *C* will selectively turn off two of the four reporter genes, allowing subtractive scoring.

parative assessment of the interaction of a protein with two discrete partners. The bacterial LexA protein and the bacteriophage λ cI protein provide DBDs for the two baits. Each bait directs the transcription of two matched reporter genes, one colorimetric and one auxotrophic, such that *lacZ* and LEU2 are transcriptionally responsive to LexA fusions, and *GusA* and LYS2 are transcriptionally responsive to cI fusions.

On the basis of prior experience optimizing and characterizing functionality of the Interaction Trap (Gyuris et al. 1993; Estojak et al. 1995), a simple two-hybrid precursor of the Dual Bait system, we have noted several points at which it is desirable to have reagent flexibility, to maximize the range of proteins that can be productively studied. These include control of bait expression level, inducible expression of baits, and range of reporter sensitivity. In addition, convenience of use is improved by the availability of bait expression plasmid variants with diverse polylinkers, plasmids with alternative *Escherichia coli* selectable markers to aid plasmid recovery from yeast, robust strains useful for interaction mating approaches (Finley and Brent 1994), and antibodies allowing bait detection. We have developed an array of reagents that address these points for the Dual Bait. New reagents are described in Table 1, whereas a complete set of available Dual Bait and compatible Interaction Trap reagents are summarized in Supplemental Table 1. Control data demonstrating the efficacy of the new reagents at achieving graduated bait expression and reporter induction are provided in Supplemental Figure 1. This information and detailed protocols for system use are also presented at our Web site (http://www.fccc.edu/research/labs/golemis/InteractionTrapInWork.html).

We have now applied the enhanced Dual Bait reagents to a diverse group of biological problems involving determination of protein–protein interaction specificity. The results of four different categories of application are summarized below, with representative data.

Application 1

Identification of Proteins that Target a Specific Sequence Motif in a Larger Protein

In the first example, the Dual Bait system was used to identify and analyze effector proteins for members of the Rho subfamily of the Ras superfamily, namely Cdc42 and Rac. Activated Rac and Cdc42 induce actin reorganization and can themselves induce DNA synthesis and cell-cycle progression, and are required for transformation by Ras. The insert region found in Rho GTPases is a short (13 amino acid) sequence motif that is present in all Rho-family GTPases but absent from Ras and other small GTPases (Thapar et al. 2002). Deletion of the insert region from Rac1 or Cdc42 leads to their inability to transform cells, but not to the loss of other functions. These results imply that the insert region is required for the binding of one or more effectors that mediate the effects of Rac1 and Cdc42 on cell transformation.

We adapted the Dual-Bait interaction trap system to find effectors specific for interaction with the insert region. LexA–Cdc42 L28 (encoding an activated, transforming allele of Cdc42) and cI-Cdc42 L28-Δ8 [activated Cdc42, insert region replaced with a sequence from Ras (Wu et al. 1998)] were used as selective baits to screen an AD-fused HeLa library. Among the isolated clones, two of note include SPEC1 (small protein effector of Cdc42; Pirone et al. 2000), which bound equivalently to Cdc42 with or without the insert region, and FBP17

Table 1. Summary of New Dual Bait-Compatible Reagents

cI Fusion plasmids

Plasmid name (frames)	Selection in yeast/in *E. coli*		Comment/Description
pGKS3# AB pGKS4* AB	*HIS3*	Ap^R Km^R	ADH1 promoter expresses cI followed by polylinker
pGKS6# ABC pGKS7* AB			ADH1 promoter expresses cI followed by polylinker Modified ADH1 promoter expresses ~5× higher level of expression of cI bait
pGKS8# AB	Zeo^R		Dual purpose vector. ADH1 promoter expresses cI followed by polylinker, whereas cI-responsive *gusA* reporter cassette (with 3 *cI ops*) is integrated into the same plasmid backbone
pGBS9* AB pGBS10* AB	$G418^R$	Km^R	ADH1 promoter expresses cI followed by polylinker Modified ADH1 promoter ensures higher level of expression of cI
pGMS11* A	Zeo^R		GAL1 promoter expresses cI followed by polylinker; for
pGMS12* B	$G418^R$	Km^R	use with baits whose continuous presence is toxic to yeast

Reporter Plasmids

Plasmid name	Selection in yeast/in *E. coli*		No. of operators	
pRG64* pRG62*			4 cI 2 cI	cI operators direct transcription of the *gusA* gene: sensitivity to transcriptional activation is a function of operator number
pRG61*	*URA3*	Km^R	1 cI	
pDR8*			8 lexA 3 cI	LexA-responsive *lacZ* reporter is comparable with pMW112, whereas cI-responsive *gusA* reporter has sensitivity comparable to pRG62

***LEU2/LYS2* Selection Strains**

Strain name	Genotype	No. of operators	
SKY48	MATα *trp1, his3, ura3, lexAop-LEU2, clop-LYS2*	6 lexA 3 cI	Stringent selection for interaction partners of cI-fused baits; most sensitive LexA-responsive *LEU2* reporter
SKY191		2 lexA 3 cI	Most stringent LexA-responsive *LEU2* reporter; and more sensitive cI-responsive *LYS2* reporter versus SKY48
SKY473*	MATa *his3, leu2, trp1, ura3, lexAop-LEU2 clop-LYS2*	4 lexA 3 cI	Sensitivity of *LEU2* reporter is intermediate between sensitivity of *LEU2* in SKY48 and SKY191. Sensitivity of *LYS2* reporter is the same as sensitivity of *LYS2* in SKY191. Can be used as mating partner for SKY48 and SKY19 strains.

Reagents newly constructed (*) or modified (#) (change of reading frame and/or sequence of polylinker) in this work are indicated. SKY48 and SKY191 have been described previously (Serebriiskii et al. 1999), but are noted here to provide context for SKY473. A complete listing of dual bait-compatible reagents is provided at http://www.fccc.edu/researchy/labs/golemis/InteractionTrapInWork.html, as are links to detailed protocols for system use. The newly described cI plasmids provide options to regulate expression levels of baits using either constitutive or galactose inducible promoters (useful for toxic baits), and to use *HIS3*, Zeo^R or $G418^R$ as selectable markers in yeast, and either Ap^R or Km^R as selectable markers in *E. coli*, to maximize compatibility with other yeast two-hybrid systems. A newly developed DR8 dual reporter contains both *lacZ* and *gusA* genes, simplifying transformations, whereas the pRG reporter series allows variation of sensitivity levels for gauging cI-responsive transcription. Finally, the SKY473 reporter strain is an extremely robust MATa reporter strain that is optimal as an interaction mating partner with pre-existing Dual Bait or other two hybrid strains.

(formin binding protein 17; Fuchs et al. 2001), which bound preferentially to Cdc42 containing the insert region (Fig. 2A). SPEC1 has been described previously as a Cdc42 interactor (Pirone et al. 2000), whereas FBP17 has been noted as having putative Rho-family interaction motifs (Fuchs et al. 2001), although no interaction has been demonstrated previously. Both proteins may serve as small GTPase effectors in control of the actin cytoskeleton, with further characterization of FBP17 in this context of particular interest, due to its interaction requirement for the insert region, and its recently determined role as a component of a translocation breakpoint in acute myelogenous leukemia (Fuchs et al. 2001).

Application 2

Identification of Peptides that Target a Specific Motif in a Larger Protein

HEF1 belongs to a family of focal adhesion-localized docking proteins that assemble protein complexes regulating cellular attachment, motility, apoptosis, and oncogenic transformation (O'Neill et al. 2000). As cells enter mitosis, the full-length HEF1 protein is cleaved at a DLVD consensus site for caspases 3 and 7, and the carboxy-terminal processed species is proteasomally degraded, leading to replacement of full-length HEF1 with an amino-terminal p55 species that localizes to the mitotic spindle (Law et al. 1998). Production of p55 is completely eliminated by the mutation of DLVD site to DLVA (Law et al. 1998). As a first step to studying potential mitosis-specific functions of HEF1, we wished to identify peptide aptamers (Colas et al. 1996) targeted to the DLVD motif that might regulate HEF1 cleavage.

A LexA-HEF1(DLVD) bait was used for interaction mating with a peptide aptamer library (in collaboration with R. Finley), and positive interactors rescreened against LexA-HEF1(DLVD) and cI-HEF1(DLVA). Of a series of peptides thus identified, some interacted with both DLVD and DLVA HEF1 variants (DLVD = DLVA), whereas some were specific to the DLVD WT form (DLVD>>DLVA), and hence, predicted to bind near the caspase consensus site (Fig. 2B). Binding of all peptides to endogenous HEF1 in cells was confirmed by pull-down with GST-fused peptides (DLVD = DLVA, DLVD > DLVA, or nonspecific) or GST only (Fig. 2C). However, only peptides that bound DLVD, but not DLVA variants were able to selectively bind a DLVD, but not a DLVA mutant of full-length HEF1 in mammalian cells (E. Pugacheva, I. Serebriiskii, R. Finley and E. Golemis, unpubl.).

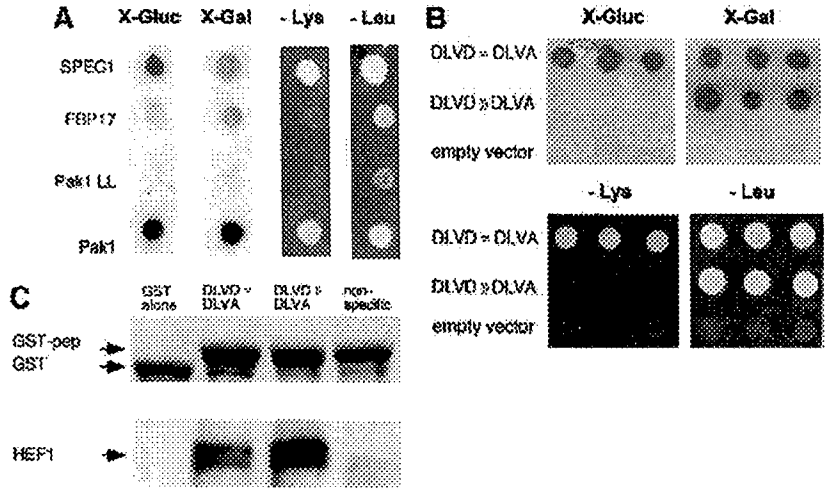

Figure 2 Targeting of interacting proteins or peptides to small sequence motifs. (*A*) Differential interaction of Cdc42 effectors as detected by the Dual Bait procedure. Two Cdc42-interacting proteins, FBP17 (Fuchs et al. 2001) and SPEC1 (Pirone et al. 2000) were isolated by a yeast two-hybrid screen with LexA-Cdc42-L28. In this screen, 10^7 diploids arising from an interaction mating (Finley and Brent 1994)-based screen yielded 25 positive colonies showing interactions with LexA-Cdc42 L28. Counterscreening against cI fused to activated Cdc42 lacking the insert region (Cdc42 L28-Δ8) revealed two clones, both containing the same cDNA, showing differential binding. All yeast shown contain both baits, and AD-fusions as indicated at *left*. Beside AD-fused FBP17 (specific for Cdc42-L28) and SPEC1 (bound both forms equivalently), AD-Pak1, which binds both forms of Cdc42, and AD-Pak1 LL, which cannot bind either form of Cdc42 (Sells et al. 1997), are included as controls. Results with growth and colorimetric reporters for Cdc42-L28-Δ8 [gusA (X-Gluc) and *LYS2*, first and third lines] and LexA-Cdc42-L28 [*lacZ* (X-Gal) and *LEU2*, second and fourth lines], are shown. (*B*) Selection of peptides specifically targeting HEF1-DLVD. A LexA-HEF1(DLVD) bait was used to identify interacting peptide aptamers, in collaboration with R. Finley. Selected peptides were rescreened in parallel against LexA-HEF1(DVLD) or cI-HEF1(DLVA), differing from the original bait by only a D363A substitution. Shown are peptides that interact with both DLVD and DLVA variants (DLVD = DLVA; activates all four reporters; representative sequence HHASTPRRESPGIMSPL); or with DLVD but not DLVA (DLVD>>DLVA; activates *lacZ* and *LEU2* only; representative sequence, SGKFGEALPGWLSSACWCFG), and a nonspecific control peptide (negative; activates no reporters; representative sequence, EQLKYNRFWPWQWWGGRRLR). (*C*) Confirmation that peptides interact with HEF1 in an *in vitro* system, using pulldowns of endogenous HEF1 from cell lysates with the three GST-fused peptides from *B*, or with GST only. (*Top*) Levels of GST peptide or GST only in reaction; (*bottom*) associated HEF1.

Application 3

Rapid Confirmation of Specific Interactions from a Library Screen

Some proteins of considerable biological interest, such as retinoblastoma (Rb), have a tendency to sometimes identify many nonspecifically interacting proteins from two-hybrid library screens, making it experimentally desirable to improve means to rapidly sort through sometimes large numbers of putative positives. In introducing this application, we note that alterations in the DNA sequence of retinoblastoma (*Rb*) gene contribute to the development of retinoblastoma with different penetrance. Low penetrant mutants give rise to retinoblastoma at a much lower frequency than expected for a null allele. Such mutants are expected to retain some protein-binding activities of wild-type pRB, which are of considerable interest for cancer biology, whereas high penetrant mutants are thought to have lost many of these interactions. RBΔ663 is a synthetic mutant that behaves similarly to the low-penetrant pRB mutants (see discussion in Sellers et al. 1998). The Dual Bait system was used to screen for proteins that interact with LexA-RBΔ663 but not with a high-penetrant (cI-RB Δex22, lacking exon 22) mutant of pRB (Fig. 3, top). In screening of three cDNA libraries, we identified several proteins that showed such binding specificity. Of interest, the E7 oncoprotein of human

Screen Step	Description	Fetal Liver	Fetal Brain/ B42	Fetal Brain/ GAL4
1	LEU+LacZ+	49	84	20
2	LEU+LacZ+GusA+	47	67	20
3	# genes	7	6	20
4	post-swap LEU+LacZ+GusA+	20	56	1
5	# genes	5	2	1
6	# final validated genes	4	2*	1*

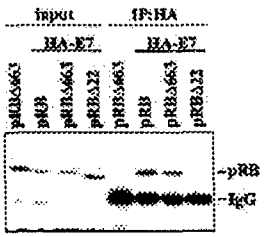

Figure 3 Use of Dual Bait reagents to reduce false positive background. (*Top*) The RBΔ663 and RBΔex22 mutants of pRB are described in Sellers et al. (1998), and were expressed in the context of a large pocket domain of pRB containing amino acids from 379 to 928. SKY48 yeast expressing LexA-RBΔ663 and cI-RBΔex22 baits were used to screen three different libraries. (Lines *1,2*) Numbers of clones positive for LexA-RBΔ663-responsive (*LEU2*, *lacZ*) but negative for cI-RBΔex22-responsive (*gusA*) reporters. (Line *3*) Number of discrete genes represented among the clones. (Line *4*) Number of clones positive for cI-RBΔ663-responsive (*GusA*), but not LexA-RBΔex22-responsive (LEU, *lacZ*) reporters; note, this reduction from line *2* values was not observed with retransformation testing with the original LexA-RBΔ663 and cI-RBΔex22 baits. (Line *5*) Number of genes represented in line *4* set of clones. (Line *6*) Number of surviving genes that were validated by coimmunoprecipiation and other techniques. (*) Note, papillomavirus E7 was identified from two different fetal brain libraries with B42 or GAL4 as activation domains. Although a legitimate pRB interactor, as E7 is not normally expressed in brain, it may represent an artifact of the libraries' construction. (*Bottom*) HA-tagged E7 and pRB derivatives were overexpressed in Saos-2 (*Rb−/−*) osteosarcoma cells and their interaction was determined by immunoprecipitation with anti-HA antibody (HA 11, BAbCO). The precipitated proteins pRB, pRBΔ663, and RBΔex22 (RBΔ22 in figure) were detected by immunoblotting with anti-RB antibody (XZ56). Input proteins are 10% of that used in immunoprecipitation.

papilloma virus HPV-18 was isolated from two different libraries by this approach. E7, a known wild-type pRB interactor (Munger et al. 1989), was, for the first time, shown to interact with the low pentetrant RBΔ663 but not the high-penetrant Δex22 mutant.

As in Application 1, this is a demonstration of the capacity of the system to identify interactors with specific requirement for a binding motif in a larger protein. However, whereas in some libraries, positives represented multiple hits on a small number of genes, in others (fetal brain, GAL4), unique isolates of a large number of genes were obtained, suggesting specific interactions (Serebriiskii and Golemis 2001). To further improve specificity of the screen, we performed a bait swap, now expressing LexA-RBΔex22 and cI-RBΔ663 rather than LexA-RBΔ663 and cI-RBΔex22. Simultaneous retransformation of initially isolated preys with yeast containing swapped DBD fusions in parallel with the original baits eliminated a substantial number of the originally isolated clones, which were presumptively binding to a unique but artifactual configuration of the original baits (Fig. 3, top).

For the fetal brain/GAL4 library, this single step reduced the number of possible specific interacting clones from 20 to 1. With a single exception, all of the clones that interacted selectively with both LexA- and cI-RBΔ663 were confirmed by additional assays including coimmunoprecipitation (Fig. 3, bottom). The ease of swapping the two baits while remaining in the same reporter strain background, and using the same precalibrated reporter genes, is not matched by any other two hybrid-based system.

Application 4

Scoring Specific Disruption of Protein Interactions by Small Molecule Inhibitors

It has been of interest to try to develop small molecule inhibitors of specific protein–protein interactions as an intelligent

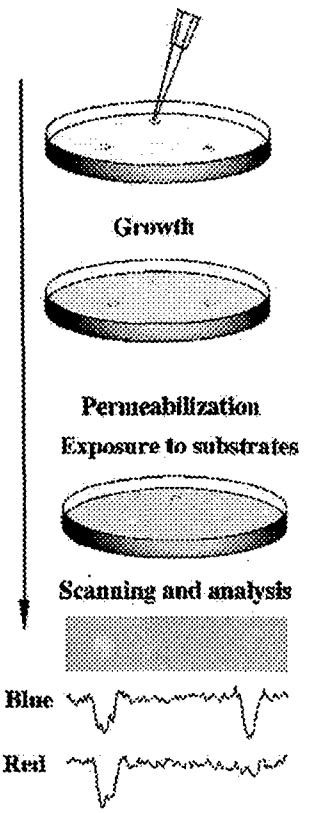

Figure 4 Drug disruption of protein–protein interactions. (*Top*) Yeast containing baits and preys are mixed with low-melt agarose and poured over appropriate dropout growth medium. After agarose is set, 1 μL of each compound to be tested or solvent negative control is dropped on the plate. Yeast are incubated for 1–2 d, then permeabilized and overlaid with Z-buffer, Magenta-Gal (a red colorimetric substrate for LacZ) and X-Gluc (a blue colorimetric substrate for GusA). (*Bottom*) The result shown derives from a mixed population of yeast strains containing LexA-Ras and AD-Raf or cI-Ras and AD-RalGDS. In this example, only the colorimetric (*lacZ* and *gusA*) reporters are being assessed. Fungicide (*left*) inhibits both *lacZ* and *gusA* signal, whereas a specific Ras–Raf interaction inhibitor reduces only *gusA* (blue) output, leaving a red spot; solvent control produced no spots (data not shown). Shown below the spots are results obtained following a scan of plate, import of image into NIH Image, and performance of densitometry for signal intensity in blue versus red across the spot midline.

way to manipulate signal transduction networks (discussed in Golemis et al. 2002). By use of a two-hybrid approach, small molecule inhibitors of the interaction between the oncoproteins Ras and Raf have been obtained (J. Kato-Stankiewicz, V. Khazak, I. Serebriiskii, E. Golemis, , in prep.). Using this compound as a tool in comparison with a general fungicide, we demonstrate that the Dual Bait reagents can be used in a single-step, plate-based colorimetric counterscreen that has the potential to facilitate future yeast-based screening for drugs that inhibit specific protein–protein interactions. As shown in Figure 4, yeast containing cI- and LexA- baits, and interacting preys, can be embedded as a lawn in soft agar medium, and subsequently overlaid with Magenta-Gal and X-Gluc. Interaction of Ras with its effectors Raf and RalGDS induces both *lacZ* and *gusA* reporters, turning medium a uniform purple-blue, and thus providing a subtractive background to judge specific versus nonspecific reporter inhibition. Hence, whereas spotting a fungicide results in loss of both blue and red coloration, resulting in a white patch, and spotting of solvent has no effect, specific inhibition of the Ras–Raf interaction results in selective inhibition of *GusA* activation, resulting in a red patch. Prior discussions of drug screening applications of two hybrid have emphasized the use of counterselectable reporters such as *URA3* (with 5-FOA) to score inhibition of interaction (Vidal and Endoh 1999); however, a difficulty with the use of counterselections in yeast is the frequency at which drug-insensitive mutants are likely to be selected. In this case, no growth pressure is applied, but selective differences in activity of a specific versus nonspecific reporter can be seen on the basis of color difference. Further, scanning of plates, and image analysis for red-blue ratio can provide quantitation of data; and given that pharmaceutical screens are standardly done using compounds arrayed in microtiter plates, automation of such an approach, potentially through adaptation of imaging technologies currently used for, for instance, microarrays, would be highly feasible.

Summary

The development of a selective two-hybrid screening system has been of considerable general interest, and a number of groups have proposed strategies and reagent sets toward this end (discussed in Serebriiskii et al. 2001). For all new technologies, a key question is whether novel reagents demonstrated in proof-of-concept will prove broadly applicable, or problematic. We demonstrate that the enhanced Dual Bait reagents described here can be used in diverse applications involving proteins, peptides, and drugs, and in so doing, describe novel approaches that offer many advantages in probing and manipulating protein interaction specificity. We hope they will find productive use in the scientific community.

METHODS

Molecular and Microbiological Manipulation

Cloning of novel constructs was performed using conventional protocols. Yeast were cultured and manipulated by use of standard techniques. Details of the sequences and cloning sites encompassed in the panel of bait expression plasmids and reporter plasmids described in the Results section are available at (http://www.fccc.edu/research/labs/golemis/InteractionTrapInWork.html) and in Supplemental Figures 2–6. Further information concerning cloning strategies used for plasmid construction, or details of yeast strain construction, are available upon request, as are the plasmids and strains described herein. Expression of bait and prey proteins was confimed by Western analysis, with primary antibody to LexA, cI, or hemagglutinin (for preys).

For data presented in this work, two-hybrid experiments were performed as described (Estojak et al. 1995). For plate-based X-Gal and X-Gluc assays, chloroform/agarose overlay was used. For liquid β-glucuronidase or β-galactosidase assays, the procedure described in Serebriiskii et al. (1999) was used. Analysis of activation of *LYS2* or *LEU2* reporters was accomplished by replica plating yeast to plates lacking leucine or lysine, and monitoring growth over 4 d.

ACKNOWLEDGMENTS

These studies were supported by NIH grants GM54168 (to J.C.), CA63366 (to E.G.), and core grant CA06927 (to Fox Chase Cancer Center); and awards (to E.G.) from Ovarian SPORE and NCI Translational Pilot Projects, and the Pennsylvania Tobacco Health Research Formula Fund. E.N.P. is supported by DAMD 17-00-1-0429, from the Department of Defense Breast Cancer Research Program, managed by the U.S. Army Medical Research and Materiel Command. E.G. is a consultant to Morphochem. We thank Antje Taliana, Marijane Russell, and Michelle Berman for contributing work in the area of Dual Bait reagent construction. We gratefully acknowledge Russ Finley (Wayne State University) as a collaborator on dual bait peptide screening.

The publication costs of this article were defrayed in part by payment of page charges. This article must therefore be hereby marked "advertisement" in accordance with 18 USC section 1734 solely to indicate this fact.

REFERENCES

Colas, P., Cohen, B., Jessen, T., Grishina, I., McCoy, J., and Brent, R. 1996. Genetic selection of peptide aptamers that recognize and inhibit cyclin-dependent kinase 2. *Nature* **380:** 548–550.

Estojak, J., Brent, R., and Golemis, E.A. 1995. Correlation of two-hybrid affinity data with *in vitro* measurements. *Mol. Cell. Biol.* **15:** 5820–5829.

Fields, S. and Song, O. 1989. A novel genetic system to detect protein–protein interaction. *Nature* **340:** 245–246.

Finley, R. and Brent, R. 1994. Interaction mating reveals binary and ternary connections between *Drosophila* cell cycle regulators. *Proc. Nat. Acad. Sci.* **91:** 12980–12984.

Fuchs, U., Rehkamp, G., Haas, O.A., Slany, R., Konig, M., Bojesen, S., Bohle, R.M., Damm-Welk, C., Ludwig, J., Harbott, W.D., et al. 2001. The human formin-binding protein 17 (FBP17) interacts with sorting nexin, SNX2, and is an MLL-fusion partner in acute myelogeneous leukemia. *Proc. Natl. Acad. Sci.* **98:** 8756–8761.

Golemis, E.A., Tew, K.D., and Dadke, D. 2002. Protein interaction-targeted drug discovery: Evaluating critical issues. *Biotechniques* **32:** 636–638, 640, 642 passim.

Gyuris, J., Golemis, E.A., Chertkov, H., and Brent, R. 1993. Cdi1, a human G1 and S phase protein phosphatase that associates with Cdk2. *Cell* **75:** 791–803.

Ito, T., Chiba, T., Ozawa, R., Yoshida, M., Hattori, M., and Sakaki, Y. 2001. A comprehensive two-hybrid analysis to explore the yeast protein interactome. *Proc. Natl. Acad. Sci.* **98:** 4569–4574.

Kato-Stankiewicz, J., Hakim, I., Zhi, C., Zhang, J., Serebriiskii, I., Guo, L., Edamatsu, H., Koide, H., Agarwal, S., Hess, S. et al. 2002. Novel inhibitors of Ras/Raf1 interactions identified by two-hybrid screening revert Ras-dependent transformation phenotypes in human cancer cells. *Proc. Natl. Acad. Sci.* (in press).

Law, S.F., Zhang, Y.-Z., Klein-Szanto, A., and Golemis, E.A. 1998. Cell-cycle regulated processing of HEF1 to multiple protein forms differentially targeted to multiple compartments. *Mol. Cell. Biol.* **18:** 3540–3551.

Munger, K., Werness, B.A., Dyson, N., Phelps, W.C., Harlow, E., and Howley, P.M. 1989. Complex formation of human papillomavirus E7 proteins with the retinoblastoma tumor suppressor gene product. *EMBO J.* **8:** 4099–4105.

O'Neill, G.M., Fashena, S.J., and Golemis, E.A. 2000. Integrin signaling: A new Cas(t) of characters enters the stage. *Trends Cell*

Biol. **10:** 111–119.
Pirone, D.M., Fukuhara, S., Gutkind, J.S., and Burbelo, P.D. 2000. SPECs, small binding proteins for Cdc42. *J. Biol. Chem.* **275:** 22650–22656.
Schwikowski, B., Uetz, P., and Fields, S. 2000. A network of protein–protein interactions in yeast. *Nat. Biotechnol.* **18:** 1257–1261.
Sellers, W.R., Novitch, B.G., Miyake, S., Heith, A., Otterson, G.A., Kaye, F.J., Lassar, A.B., and Kaelin, Jr., W.G. 1998. Stable binding to E2F is not required for the retinoblastoma protein to activate transcription, promote differentiation, and suppress tumor cell growth. *Genes & Dev.* **12:** 95–106.
Sells, M.A., Knaus, U.G., Bagrodia, S., Ambrose, D.M., Bokoch, G.M., and Chernoff, J. 1997. Human p21-activated kinase (Pak1) regulates actin organization in mammalian cells. *Curr. Biol.* **7:** 202–210.
Serebriiskii, I.G. and Golemis, E.A. 2001. Two hybrid system false positives, and approaches to their detection and elimination. In *Two-hybrid systems, methods and protocols.* (ed. P.N. MacDonald), pp. 123–134. Humana Press, Totowa, NJ.
Serebriiskii, I., Khazak, V., and Golemis, E.A. 1999. A two-hybrid dual bait system to discriminate specificity of protein interactions. *J. Biol. Chem.* **274:** 17080–17087.
Serebriiskii, I.G., Khazak, V., and Golemis, E.A. 2001. Redefinition of the yeast two-hybrid system in dialogue with changing priorities in biological research. *BioTechniques* **30:** 634–655.
Thapar, R., Karnoub, A.E., and Campbell, S.L. 2002. Structural and biophysical insights into the role of the insert region in rac1 function. *Biochemistry* **41:** 3875–3883.
Vidal, M. and Endoh, H. 1999. Prospects for drug screening using the reverse two-hybrid system. *Trends Biotechnol.* **17:** 374–381.
Wu, W.J., Lin, R., Cerione, R.A., and Manor, D. 1998. Transformation activity of Cdc42 requires a region unique to Rho-related proteins. *J. Biol. Chem.* **273:** 16655–16658.

WEB SITE REFERENCE

http://www.fccc.edu/research/labs/golemis/InteractionTrapInWork.html; Web site for this project.

Received May 22, 2002; accepted in revised form August 30, 2002.

APPENDIX 2

HEF1 regulates centrosomal maturation and spindle formation through control of the Aurora-A kinase.

Elena N. Pugacheva[1], Yungfeng Feng[2], Gregory D. Longmore[2], and Erica A. Golemis[1,*]

[1]Division of Basic Science, Fox Chase Cancer Center, 333 Cottman Ave., Philadelphia, PA 19111, [2]Departments of Medicine and Cell Biology, Washington University, St. Louis 63110

Running Title: HEF1 regulates centrosomes through Aurora-A

Key words: HEF1, centrosome, attachment, spindle, mitosis, Aurora-A, Ajuba

Number of Characters: 62,242

* corresponding author:
Erica Golemis, W406
Fox Chase Cancer Center
333 Cottman Ave.
Philadelphia, PA 19111
Phone: 215-728-2860
Fax: 215-728-3616
Email: EA_Golemis@fccc.edu

Abstract.

The HEF1 scaffolding protein has a well-defined role in mediating integrin-dependent attachment signaling at focal adhesions. We have previously shown that HEF1 relocalizes to the spindle asters at mitosis, but the significance of this migration was unclear. We report here that HEF1 controls mitotic spindle formation through action at centrosomes in the G2 phase of cell cycle. Increased levels of HEF1 induce supernumerary centrosomes, and multipolar spindles. Conversely, depletion of HEF1 results in premature centrosomal splitting, monoastral or asymmetric spindles, and transient appearance of >4N populations. The G2/M localization profile and overexpression phenotypes of HEF1 resemble those of the mitotic regulator Aurora A (AurA) kinase. We show that HEF1 associates with and controls activation of AurA at the centrosome, with these interactions mediated in part through HEF1 interactions with the AurA-associated protein Ajuba. These results suggest a novel mechanism for the coordination of cell attachment status with cell division in mitosis, and may provide insight into the induction of genomic instability in cancer.

Introduction.

Organismal development requires the synchronized interaction of cell differentiation, polarization, and division controls to enable the creation of highly organized structures from an isolated oocyte. At present, although the mechanisms by which these different processes are coordinated are not well understood, studies predominantly in *C. elegans* and *D. melanogaster* have led to the identification of a number of proteins that act at cell-cell or cell-substrate interfaces in interphase, and at the mitotic machinery in M-phase. The complex functions of these proteins allow the direct specification of cleavage plane to be coordinated with the establishment or maintenance of a polarized cellular identity (Knust and Bossinger, 2002; Nance et al., 2003; Severson and Bowerman, 2003). Some, including the PAR family of proteins in *C. elegans*, play critical roles in early embryogenesis. In one elegant recent example, the fly Adenomatous Polyposis Coli (APC) ortholog was shown to organize a bridge between cell cortex and the centrosome in male germline cells that oriented the mitotic spindle and subsequent division plane, thus specifying the differentiation status of daughter cells based on their post-cleavage proximity to a divisional "hub" (Yamashita et al., 2003). A number of the proteins identified in these studies have homologs with presumably orthologous functions in higher eukaryotes. However, studies of mammalian signaling proteins typically have not focused on very early development, but rather emphasize the study of cell processes and protein function in 2-dimensional cell culture models. Because the coordination of cell division polarity with cellular attachment status is less readily perceived and analyzed in such models, this topic is only recently beginning to be addressed.

It has long been known that loss of basal cell adhesion can cause mitotic defects in mammalian cells, most notably by causing failure of cytokinesis (Ben-Ze'ev and Raz, 1981; Orly and Sato, 1979). This failure is not simply due to the loss of traction forces that cells use to physically separate, as it has been documented that the presence of too high a level of cell attachment can similarly reduce cytokinetic efficiency (Piel et al., 2001). These results imply communication between the cell division machinery and the focal adhesions that provide basal cell attachment. However, because cell adhesion is most readily observable in interphase cells, and focal adhesions tend to minimize or disappear in mitotic cells, accompanied by the

downregulation of some key focal adhesion-associated signaling proteins (Law et al., 1998; Yamaguchi et al., 1997; Yamakita et al., 1999), little work has investigated a possible requirement or alternative role for focal adhesion-associated proteins in M-phase. Notably, in the past several years, investigations of the nuclear cell cycle have also documented the coordination of nuclear signaling events in time and space during M-phase progression in higher eukaryotes, emphasizing the roles of proteins associated with structures such as the centrosome, the contractile ring, the central spindle, and the midbody in controlling the timing of progression through different cell cycle stages (e.g. (Raff et al., 2002); reviewed in (Glotzer, 2001)). These structures exist in close contact with or are derived from the actin and tubulin cytoskeletons. An economical view of cellular function would suggest that the re-use of proteins which govern cytoskeletal dynamics in interphase cells might not only be efficient, but might also provide a means to synchronize changes in cell contacts during the mitotic process.

Of all the mitotic structures, a number of recent studies suggest that the centrosome might be a primary signal integration point. Recent work has emphasized the dual activity of centrosomes in contributing to control of cell polarization in interphase cell migration (Etienne-Manneville and Hall, 2003; Yvon et al., 2002), but also in coordinating polarity of the mitotic spindle in M-phase (Segal and Bloom, 2001). Centrosomally-associated signaling activities also govern the timing of mitotic entry (Jackman et al., 2003). Mechanistically, the activation of cyclin B1 at mitosis has been proposed to depend on an initial recruitment of activated AurA kinase to the centrosome in late G2, following AurA interaction with the LIM domain protein Ajuba (Hirota et al., 2003). The subsequent destruction of cyclin B later in M-phase, required for the metaphase-anaphase transition, is also regulated from the centrosome, based on the initial assembly and activation of the anaphase promoting complex/cyclosome at this structure (Raff et al., 2002). Finally, some studies have also indicated that the centrosome performs a key licensing function at the point of cytokinesis (Piel et al., 2001).

HEF1 is a member of a group of scaffolding proteins that includes p130Cas and Efs/Sin (Bouton et al., 2001; O'Neill et al., 2000). This group of Cas proteins localizes to focal adhesions in interphase cells, and acts as intermediates in a variety of integrin-dependent signaling processes, including establishment of cell attachments, migration, and cell survival

signaling. In 1998, our group first raised the possibility that HEF1 might have a previously unsuspected function in mitosis (Law et al., 1998), based in large part on the observation that the HEF1 protein relocalized from focal adhesions to the mitotic spindle asters in M-phase. Since that time, reports have appeared suggesting of the association of other focal adhesion-associated proteins, such as zyxin (Hirota et al., 2000), paxillin (Herreros et al., 2000), FAK, and Pyk2 (Rodriguez-Fernandez et al., 1999) with the mitotic spindle or other relevant structures such as the microtubule organizing center (MTOC) or centrosome. One question that has not been well addressed is whether these changes have any functional significance for spindle function, or are simply reflections of the considerably changed signaling landscape that accompanies focal adhesion disassembly in mitotic versus interphase cells.

In this study, we have tested the hypothesis that HEF1 localization to the mitotic spindle reflects an active role for this protein in M-phase. We have found that HEF1 association with the spindle follows an initial HEF1 localization to the centrosome that peaks in late G2 phase. A detailed analysis of the consequences of positively or negatively deregulating the activity of HEF1 indicates that HEF1 function is essential for centrosomal maturation and mitotic spindle formation. HEF1 also interacts with and controls the activation of AurA, suggesting an important role for HEF1 in regulation of mitotic entry. Interestingly, the functions we have identified for HEF1 are not completely shared with its well-studied family member p130Cas, while both proteins have much more pronounced activity in epithelial cells versus fibroblasts. These results indicate that HEF1 provides a crucial bridge coordinating attachment and cell division processes at M-phase in mammalian cells.

Results.

Cell cycle-regulated progression of HEF1 localization from the centrosome in G2 to the spindle in M-phase. The initial goal of this study was to analyze potential consequences of deregulated HEF1 signaling for formation and function of the mitotic spindle. Mitotic spindles generally are nucleated from centrosomes, and defective signaling by centrosomally associated proteins is frequently associated with aberrant spindle formation and/or progression through mitosis (e.g. (Mailand et al., 2002; Marumoto et al., 2003)). Moreover, in many cases, spindle-associated signaling proteins first associate with and become activated at the centrosome, prior to propagation of signals to the spindle (e.g.(Raff et al., 2002)). Therefore, as a prelude to this work, we first examined whether HEF1 localizes only to the spindle, or also to the centrosome.

Immunofluorescence analysis of cell cycle-synchronized MCF-7 cells with antibodies to HEF1 and to the centrosomal protein gamma-tubulin indicated that HEF1 localizes to the centrosome in a cell cycle regulated manner (Figure 1A). HEF1 was essentially undetectable at centrosomes in G1 cells, and only weakly visible as a centrosome associated mass in S phase. This corresponds to relatively low levels of HEF1 detectable in cells at these stages (Figures 1B, 1C). HEF1 levels markedly increase during G2, and HEF1 is strongly detected at the centrosome in mid- and particularly late G2, prior to the movement of a significant fraction of HEF1 to the spindle in mitosis. As mitosis progresses to later stages, HEF1 remains associated with the spindle and moves to the midzone. However, HEF1 is no longer detectable at the centrosome at cytokinesis. The endogenous HEF1 localization pattern described here was blocked by the peptide against which the HEF1 antibody was raised, supporting signal specificity (not shown). Further, transient over-expression of GFP-fused HEF1 revealed similar centrosomal (Figure 1D) and spindle (not shown) localizations. Using GFP- and FLAG epitope-fused HEF1 derivatives (Figure 1E, F), we have performed preliminary mapping of sequence determinants necessary for localization of HEF1 to the mitotic spindle. Based on this analysis, we have identified a minimal sequence of amino acids 1-405 required for strong association with the centrosome, with sequences between 363-405 an essential localization determinant. In addition to this fragment, carboxy-terminal derivatives of HEF1 (aa 351-653, and 654-834) also showed some association with the centrosome, although this was not as pronounced as the 1-405 fragment.

Up- or down-regulation of HEF1 expression causes centrosomal and spindle abnormalities. To determine the functional significance of HEF1 association with the centrosome and the mitotic spindle, we established three independent systems for manipulation of HEF1 in MCF-7 cells. First, we overexpressed the full length HEF1 protein under control of a tetracycline-repressible promoter (Figure 2A). Second, based on prior data indicating HEF1 cleavage and proteolysis at mitosis and apoptosis (discussed further below), we stabilized full length endogenous HEF1 using peptide aptamers targeted to a previously mapped primary cleavage site (Law et al., 2000; Law et al., 1998; Serebriiskii et al., 2002) (Figure 2B). Third, we used an siRNA approach to deplete endogenous HEF1 (Figure 2C). For each manipulation, a matching negative control set was used, corresponding to tetracycline-regulated GFP (for overexpression), use of non-specific peptides, and use of a scrambled siRNA (for depletion).

Both overexpression of exogenous HEF1 and peptide stabilization of endogenous HEF1 induced a high frequency of cells with spindle defects by 48 hours following cell treatment (Figure 3A, B). Most notable was the increase in the number of cells with multipolar spindles, which represent 12% of the population with overexpression, and >16% with specific HEF1-targeted peptides, as compared to 2-3% for all negative controls. These defects are likely to arise from a primary defect at the centrosome, as for every cell with multipolar spindles, each spindle originated from a supernumerary centrosome (Figure 3A). In other cells, while no multipolar spindles were observed, nevertheless the spindle was defective. A common phenotype was the presence of "bent" spindles, which would arise if the spindle poles had not fully moved to opposite sides of the nucleus. Overexpression of full length HEF1, or introduction of HEF1-stabilizing peptides, was also found to consistently induce centrosomal amplification, with >10% of cells containing in excess of 4 centrosomes within 48 hours following treatment (Figures 3B).

Depletion of HEF1 using siRNA also induced a distinct mitotic phenotype. In contrast to the results with overexpressed HEF1, this was marked by high percentages of cells with monoastral spindles (Figure 3C, center panels), or with poorly formed or asymmetric spindles (Figure 3C, right panels). SiRNA depletion is not completely homogenous among cells in a population; using antibodies to HEF1, we determined that cells with monoastral or deformed spindles consistently represented cells with the most complete HEF1 depletion, whereas those

cells with apparently normal bipolar spindles had detectable HEF1 signal (data not shown). In examining the centrosomes of mitotic HEF1-depleted cells, two consistent abnormalities were observed (Figure 3C). First, the centrosomes of cells with defective spindles showed weaker reactivity with antibody to gamma-tubulin than did cells with higher HEF1 levels, and apparently normal spindles. Second, although two distinct gamma-tubulin or GFP-centrin centrosomal structures were observed in all mitotic cells with depleted HEF1, there was invariably asymmetry in the ability of the two centrosomal structures to nucleate spindle formation. Gamma-tubulin is known to accumulate during centrosomal maturation in the G2 phase of cell cycle (Bornens, 2002; Meraldi and Nigg, 2002; Rieder et al., 2001). Therefore, these observations suggested that HEF1 depletion might be interfering with this maturation process, rendering one centrosomal daughter incompetent to act as a microtubule-organizing center.

We also inspected the status of centrosomes in non-mitotic HEF1-depleted cells. Notably, two distinct, widely separated, GFP-centrin-positive structures (Figure 3D) were observed in >80% of HEF1-depleted cells (>500 cells counted in 5 separate experiments), but in less than 10% of cells treated with a scrambled siRNA. In the normal centrosomal duplication cycle, the single "mother" centrosome remaining in a cell after cytokinesis undergoes duplication in S-phase, with the two centrosomes remaining linked while the "daughter" matures through G2. Normally, two widely separated centrosomes are not observed until the G2/M transition (Bornens, 2002; Meraldi and Nigg, 2002). FACS analysis of HEF1-depleted cells versus scrambled siRNA-treated controls confirmed that their cell cycle profile does not show significant G2 enrichment (Figure 3E). Hence, the primary defect is likely one of centrosome cohesion, resulting in premature splitting, rather than a secondary consequence of altered cell cycle compartmentalization.

HEF1 interacts with AurA and Ajuba and is required for the activation of AurA kinase at the centrosome. The centrosomal maturation phenotypes observed with HEF1 depletion, and the centrosomal amplification/multipolar spindle phenotype observed with HEF1 overexpression, are similar to those reported for inhibition or overexpression of other proteins known to exert a key role in centrosomal maturation, including notably the AurA kinase (Hannak et al., 2001; Marumoto et al., 2003). AurA activation at the centrosome has recently been reported to require

interaction with the LIM domain/scaffolding protein Ajuba (Hirota et al., 2003), which had previously been thought to function primarily at cell junctions and in the nucleus. Suggestively, an Ajuba bait used in a two-hybrid screen in yeast directly isolated the carboxy terminal two-thirds (amino acids 365-834) of HEF1 (results not shown). Therefore, we asked whether HEF1 might directly regulate AurA signaling through interactions with Ajuba and/or AurA at the centrosome.

In HEF1-depleted MCF-7 cells in the G2 phase of cell cycle, total levels of AurA at the centrosome were similar to those found in MCF-7 cells treated with a matched scrambled siRNA (Figure 4A, B). In contrast, levels of phospho-AurA, indicative of kinase activation (Hirota et al., 2003), were greatly reduced or absent under conditions of HEF1 depletion (Figure 4A, B), implying that HEF1 plays an important role in the activation of AurA. This role could be direct, with HEF1 physically a component of an Ajuba-AurA activation complex, or it might be indirect, with HEF1 causing defects at an early stage of the centrosomal cycle so that AurA is subsequently unable to be activated in association with an immature centrosomal structure. Antibody directed at HEF1 co-immunoprecipitated endogenous AurA, while antibody to AurA precipitated HEF1 (Figure 4C). This suggested HEF1 control of AurA activation was direct, through interaction with an AurA-containing complex.

Based on the two-hybrid prediction of HEF1-Ajuba association, we then analyzed the HEF1 interaction with Ajuba. As no highly specific antibodies to Ajuba were available, we first transfected cells with FLAG-tagged HEF1, and N- and C-terminal derivatives; and Myc-tagged full length Ajuba, Ajuba preLIM region, or a negative control (GFP) (Figure 5A). Immunoprecipation with FLAG demonstrated strong association of full length HEF1 with full length Ajuba, weak association of the N-terminal domain of HEF1 with full length Ajuba, and strong association between the aa 351-653 fragment of HEF1 and both the full length Ajuba, and the preLIM region of Ajuba (Figure 5A). In a reciprocal experiment, full length Ajuba, and to a lesser degree the isolated Ajuba LIM region, co-immunoprecipitated HEF1 (Figure 5B): full length Ajuba also weakly co-immunoprecipitated the HEF1 N-terminus (Figure 5C). Combining these results with the earlier observation that the carboxy-terminal domain of HEF1 was sufficient to interact with Ajuba in a two-hybrid screen, we propose that the Ajuba LIM region

interacts with the HEF1 N-terminus, whereas the Ajuba preLIM region has the potential to interact with the HEF1 C-terminus, but this is masked in the context of full length HEF1 sequences. These data indicated that HEF1, AurA, and Ajuba might exist in a complex.

We further tested the functional interaction between HEF1 and AurA. We demonstrated above that amino acids 1-405 are a minimum determinant of strong HEF1 association with the centrosome, with a critical localization determinant located in the serine-rich amino acids from 363-405 (Figure 1). Using antibody to GFP for co-immunoprecipitation, we find that GFP-HEF1$_{1\text{-}405}$ is also sufficient to interact with AurA *in vivo*, while GFP-HEF1$_{1\text{-}363}$ is not (Figure 6A). We have also determined that HEF1 can function as an AurA substrate. Purified activated AurA was incubated with equal quantities (Figure 6B, top) of GST-fused domains of HEF1, with the AurA substrate histone H3 as a positive control, and GST and histone H1 as negative controls. AurA efficiently phosphorylated both the HEF1$_{1\text{-}363}$ and HEF1$_{1\text{-}405}$ proteins to a degree comparable to or exceeding the histone H3 positive control, while not phosphorylating either of the negative controls (Figure 6B). In further test, we have used GST-HEF1 derivative proteins in *in vitro* pulldowns to gauge association with AurA (Figure 6C). This experiment confirms the primary site of HEF1 interaction with AurA is contained within HEF1$_{1\text{-}363}$. These results indicate that under *in vitro* conditions, HEF1 can associate with AurA in the absence of other proteins, and that the HEF1 sequences from 363-405 are not required for HEF1 association with or phosphorylation by AurA, suggesting the primary role of these sequences in promoting the interaction *in vivo* is through allowing HEF1 to associate with the centrosome, where endogenous AurA concentrates. Together, these results indicate that phosphorylation by AurA is not required for HEF1 recruitment to the centrosome, compatible with the observed accumulation of HEF1 at the centrosome prior to AurA activation at G2/M transition (Figure 1). We sought to test this idea by depleting AurA, and examining HEF1 centrosomal localization. We were unable to do so, because interestingly, siRNA depletion of AurA markedly depressed the steady state levels of HEF1 (Figure 6D). This stabilization was seen both in nocodazole- and thymidine-arrested cells, so was not cell cycle-stage specific. Both AurA (Kiat et al., 2002) and HEF1 (Liu et al., 2000; Nourry et al., 2004) have been shown to bind proteins that promote their degradation by the proteasome. Our data suggest loss of association between AurA and HEF1 may render HEF1 more susceptible to proteolysis, as treatment of AurA- or scrambled-siRNA

depleted cells with the proteasome inhibitor ALLN significantly stabilized the levels not only of AurA, but also of HEF1 (Figure 6D).

Finally, our earlier results (Figure 3) predicted that HEF1 interaction with AurA might serve to activate the kinase. To directly test this idea, we titrated the GST-HEF11-363 AurA-interacting domain versus GST into an in vitro kinase reaction containing reticulocyte lysate-translated 35-S-labeled AurA (Figure 6E). Increasing levels of GST-HEF1, but not of GST, clearly induced the auto-phosphorylation of AurA, indicating that the association with HEF1, as with the previously reported association with Ajuba, is sufficient to promote AurA catalytic activity (Hirota et al., 2003).

Separation of HEF1 effects at the centrosome, and in attachment. The main functions previously ascribed to HEF1 and the Cas family of proteins have been in regulation of cell attachment and motility (Bouton et al., 2001; O'Neill et al., 2000). We had previously shown that over-expression of HEF1 induced cell spreading (Fashena et al., 2002; O'Neill and Golemis, 2001), whereas overexpression of the HEF1 carboxy-terminus had a dominant negative function on cell attachment, causing cell rounding (O'Neill and Golemis, 2001). To evaluate whether HEF1 control of cell attachment, and regulation of centrosome-associated functions, were linked or separable, GFP-fused HEF1 and HEF1 truncations were transfected into MCF7 and HeLa cells, and the ability of different HEF1 domains to act as dominant negatives by inducing centrosomal splitting versus inhibiting cell attachment was scored (Figures 6ABC). Based on this analysis, the $HEF1_{1\text{-}405}$ domain proved to have a potent phenotype, and the $HEF1_{351\text{-}653}$ fragment a weaker phenotype, in inducing centrosomal splitting (Fig 6A), while neither affected the degree of cell spreading (Fig 6B). Conversely, $HEF1_{654\text{-}834}$ induced significant cell rounding (Fig 6B), as reported before, but did not affect centrosomal splitting (Fig 6A). These results indicated that separable HEF1 domains were required for centrosomal and attachment activities.

In further test, we determined the consequences of varying the degree of cellular attachment induced by extrinsic stimuli on HEF1-associated centrosomal phenotypes. Cells with induced overexpressed HEF1 (Figure 6D), depleted HEF1 (Figure 6E), or overexpressed dominant negative $HEF1_{1\text{-}405}$ (Figure 6F) were plated on either normal tissue substrates, or on

poly-L-lysine, fibronectin, or laminin to increase spreading. Cells plated on the latter 3 substrates were significantly more spread, and were marked by more pronounced paxillin staining at focal adhesion structures (results not shown). However, in scoring the number of supernumerary centrosomes induced by overexpressed HEF1 (Figure 6D), or the number of split centrosomes induced by removal or dominant negative blockade of HEF1 function (Figures 6E,F), the greater attachment status did not strikingly affect the observed phenotypes. Together with the earlier results, these findings suggested the HEF1 functions in attachment and centrosomal dynamics were distinct.

Comparison of HEF1 and p130Cas regulation of centrosome status and AurA activation. The HEF1 protein has been documented as being particularly abundant in epithelial and lymphoid lineages, and less abundant in fibroblasts (Law et al., 1998; Minegishi et al., 1996), while a second Cas family member, p130Cas, is more ubiquitously expressed. We investigated whether the HEF1 role in centrosome maturation was specific to cells of epithelial lineages, and whether p130Cas had similar activities. FF2425 fibroblasts (Figure 8A, 8B) and other human fibroblast lines (MCR5-hTERT, results not shown) express minimal levels of HEF1. Treatment of FF2425 or MCR5-TERT fibroblasts with siRNA to HEF1 produced no phenotype under conditions where centrosomal splitting was observed in 41% of centrosomes in HeLa and 78% in MCF-7 cells (Figure 8A). This result confirmed the specificity of the HEF1-directed siRNA in the experiments described above – i.e., in a cell type in which no HEF1 is detected by Western blot or immunoflurescence, the HEF1-directed siRNAs have no effect. In MCF-7 cells, and HeLa cells, depletion of p130Cas produced 45% and 12% percent splitting, respectively (Figure 7A), in contrast to the much greater effect seen with HEF1 depletion. Based on Western analysis (Figure 8B, and results not shown), p130Cas was effectively depleted, excluding limited depletion of p130Cas as an explanation for the more limited phenotype.

Interestingly, p130Cas depletion did not cause centrosomal splitting in FF2425 cells or MCR5-hTERT cells (Figure 8A, 8B and results not shown). Antibodies to p130Cas do not reveal localization of this protein to centrosomes. However, comparison of cells transfected with plasmids overexpressing p130Cas and HEF1 suggest that the two proteins can localize to centrosomes with comparable efficiency under conditions of overexpression,whether in either

fibroblasts or epithelial cells (Figure 8C). One speculative explanation for these differing results is that p130Cas is known to exist as numerous differentially phosphorylated isoforms within different cellular compartments (Polte and Hanks, 1997): it may be that endogenous p130Cas localized to the centrosome is not well recognized by antibodies to the protein. Finally, we compared levels of AurA and phospho-AurA at the centrosome in p130Cas- versus HEF1-depleted cells. Phospho-AurA activation was not notably diminished following p130Cas depletion, (Figures 8D, E), in contrast to the results seen with HEF1 (Figure 4, 8E), again suggesting a less important function for centrosome maturation.

Based on the phenotypes described above, a long-term consequence of HEF1-dependent defects in centrosomal and spindle dynamics might be predicted to be the development of aneuploid population of cells. FACS analysis of a total population of MCF-7 or MCF12F epithelial cells depleted for HEF1 for 48 hours did not reveal a large number of such aneuploid cells (results not shown; also see Figure 3E). However, elutriation of a population of cells treated with HEF1-directed or control siRNAs, followed by FACS analysis, clearly indicated the presence of distinct 6N and 8N populations in some fractions (Figure 8E, top two panels). The elutriated fractions containing significant levels of 6N and 8N cells were returned to culture, propagated for an additional 24 hours, then re-assayed by FACS. Over 24 hours, these >4N cell populations were lost (Figure 8E, bottom two panels), and cells adapted a more normal cell cycle distribution. These observations could be most readily explained as clearance of the hyperploid cells by the spindle checkpoint surveillance machinery, suggesting loss of HEF1 from epithelial cells predisposes to, but is insufficient for, genomic instability.

Discussion.

The data in this study indicate that the HEF1 protein is a novel and important regulator of centrosomal function. In particular, depletion studies reveal a requirement for HEF1 in centriolar cohesion in interphase cells; centrosomal maturation, as marked by the recruitment of gamma-tubulin and ability to act as a microtubule-organizing center in mitosis; and centrosomal signaling, reflected by loss of ability to activate AurA at mitotic entry. HEF1, AurA, and Ajuba physically interact, and HEF1 is itself phosphorylated by AurA kinase, and present at reduced levels in the absence of AurA. The general similarity between HEF1 and AurA overexpression phenotypes (Dutertre et al., 2002; Goepfert et al., 2002; Zhou et al., 1998) is striking, and in the context of our other data implies that HEF1 and AurA functions are closely linked. As discussed below, the consequence of HEF1 depletion is similar to, but more profound than, AurA depletion, implying a more general HEF1 requirement at the centrosome. Although HEF1 has additional well-defined activities as a regulator of cell attachment, the functions reported here for centrosomal dynamics are clearly separable, involving different HEF1 domains and partners. Finally, although the HEF1-related p130Cas protein seems less important than HEF1 at the centrosome, depletion of p130Cas nevertheless induced some centrosomal defects. Together, these results support the idea that the focal-adhesion associated Cas proteins function in a distinct sphere to control mitotic entry.

In this study, we found that overexpression of HEF1 induced supernumerary centrosomes and multipolar spindles. An ongoing debate in the centrosome field is whether centrosomal amplification in tumors is a primary event regulated at the level of the centrosomal duplication cycle, or whether it results from failed cytokinesis (Dutertre et al., 2002; Kramer et al., 2002; Meraldi and Nigg, 2002). In previous studies of AurA overexpression, failed cytokinesis has been suggested as a contributing factor to the centrosomal amplification observed (Marumoto et al., 2003; Meraldi et al., 2002; Meraldi and Nigg, 2002). In further work, we have determined that HEF1 overexpression does not induce centrosomal amplification in cells arrested by thymidine in G1/S for 16 hours, but such amplification becomes apparent at 48 hours after HEF1 induction (results not shown). Hence, this mechanism may apply in the present study.

Regulation of the activation of AurA is a novel and important activity of HEF1. Our data indicate that the HEF1 interaction with AurA requires at minimum the amino terminal 363 amino acids of HEF1 (Figure 6B, C), and can occur in the absence of any additional proteins in an environment in which the proteins are freely diffusible (i.e. in vitro), although in cells HEF1 requires additional sequences allowing association with the centrosome to efficiently interact with AurA (Figures 1E, 1F). HEF1 can associate with unphosphorylated AurA (Figure 8E; also, work in process suggests HEF1 has higher affinity for unphosphorylated than phosphorylated AurA), and both HEF1 and inactive AurA co-accumulate at the centrosome through the S and G2 phases of cell cycle. HEF1 also interacts extensively with Ajuba (Figure 5). Ajuba has previously been shown to be required and sufficient for activation of the AurA kinase in vitro (Hirota et al., 2003); however, our results with HEF1 depletion clearly indicate that in the absence of HEF1, AurA cannot be activated in vivo (Figures 4AB; 8E), while co-incubation of the $HEF1_{1\text{-}363}$ fragment and AurA in vitro results in activation of the AurA in vitro kinase activity against a histone H3 substrate (Figure 6E). Based on these summed results, we propose that HEF1 is part of a ternary complex that assembles at the centrosome, and triggers activation of AurA at mitotic entry through the joint action of Ajuba and HEF1.

HEF1 activity at the centrosome is likely to be more extensive than regulation of AurA. Depletion of AurA has been variously described as inhibiting gamma-tubulin accumulation at the centrosome, and causing the two centrosomes to collapse to one centrosome, causing monoastral spindles, in early M phase. Likewise, depletion of HEF1 inhibits gamma-tubulin accumulation, and induces a monoastral spindle. However, the premature splitting phenotype we describe here occurs prior to activation of AurA, and has not been reported for AurA depletion. One possibility is that HEF1 also controls the activity of the centrosomally localized Nek2 kinase, a NimA family kinase that controls centrosomal cohesion through phosphorylation of the coiled-coil protein Nap1 (Fry, 2002). It is becoming well established that Nim, Aurora, and Polo-like kinases function coordinately at the centrosome in progression to and through mitosis (O'Connell et al., 2003). Given the capacity of HEF1 to act as a scaffolding protein (O'Neill et al., 2000), it is a reasonable candidate to play a role in this coordination.

Our data suggest a more important role for HEF1 than Cas in promoting AurA activation and centrosomal maturation, and imply that epithelial cells are more prone to centrosomal dysfunction than fibroblasts following Cas protein depletion. Indeed, an essential function for p130Cas at the centrosome is incompatible with the observation that p130Cas knockout mice die only at embryonal day 11.5 (Honda et al., 1998), and that harvested cells from these mice are viable (Honda et al., 1999). Our data are congruent with an increasing number of studies that note a cell-type specific component to centrosomal regulation (Yvon et al., 2002) and AurA function. AurA is most commonly upregulated in epithelial cancers (Anand et al., 2003). APC and its partner beta-catenin, proteins that are predominantly expressed in epithelial cells and associate with epithelial-specific structures, have been shown to also interact directly or indirectly with the centrosome, controlling its organization and function (Etienne-Manneville and Hall, 2003; Ligon et al., 2001; Yamashita et al., 2003). Elegant genetic studies in lower eukaryotic models for development such as *C. elegans* (reviewed in (Salisbury, 2003; Schneider and Bowerman, 2003)) have begun to elucidate a model in which dynamic interconnections between the centrosome and structures at the cell cortex controls the plane of mitotic spindle orientation, and cleavage furrow formation. Control of cleavage plane direction is of critical importance in developing organisms, because of the necessity to program growth in specific directions. Speculatively, it is reasonable to propose that control of cleavage plane is more importance in epithelial cells than in fibroblasts in higher eukaryotes, because the intrinsic function of epithelial cells in vivo is to maintain polarized structures that serve barrier functions. In this context, the association of an epithelially-enriched protein such as HEF1 with mitotic structures may contribute to coordination of centrosomal orientiation with the focal structures at the basolateral surface of epithelial cells.

Finally, the results presented here have interesting implications for the process of cancer development. A first study by Lingle et al. in 1998 demonstrated that the centrosomes of breast adenocarcinoma cells generally were characterized by abnormal structure, and increased microtubule nucleating capacity in comparison to centrosomes of normal breast epithelial and stromal tissues (Lingle et al., 1998). A number of subsequent studies have firmly documented the association between over-amplification of centrosomes, multipolar mitoses, genomic instability characterized by frequent aneuploidy, and development of aggressive breast cancer

(e.g. (Brinkley, 2001; D'Assoro et al., 2002; Deng, 2002; Duesberg et al., 2000; Hollander and Fornace, 2002; Kramer et al., 2002; Lingle et al., 2002; Weaver et al., 2002)). Some proteins that have well-established signaling roles in breast cancer have been found to take part in the normal centrosomal duplication cycle. For example, the tumor suppressor BRCA1 normally associates with the centrosome, and interacts with the central centrosomal protein gamma-tubulin. Through interactions at the centrosome with gamma-tubulin and other proteins, BRCA1 restricts centrosomal replication to once per cell cycle; in BRCA1-deficient cells, centrosome amplification is common (Deng, 2002; Weaver et al., 2002); BRCA1 has recently been shown to be an AurA substrate (Ouchi et al., 2004). Overexpression of AurA (also known as BTAK, for breast tumor amplified kinase) has been shown to occur early in breast cancer development, and induce centrosome amplification and aneuploidy (Goepfert et al., 2002; Zhou et al., 1998). However, in many tumors, the provenance of centrosomal defects is not known. Intriguingly, a previous study has associated upregulated expression of a Cas family member in breast cancers as associated with increased malignancy and poor prognosis (van der Flier et al., 2000). Our data raise the possibility that deregulated Cas proteins may not only impact cancer development based on their functions in cell migration (metastasis) and resistance to apoptosis, but also in the acquisition of genome instability.

Methods.

Plasmids and constructs. The generation of full length, GFP-tagged HEF1 (O'Neill and Golemis, 2001), GST-HEF1 (Law et al., 1996). FLAG-tagged HEF1 and deletion mutants were subcloned into the pCatch–FLAG vector (a gift of Dr. Jonathan Chernoff) to produce FLAG fusion proteins in eukaryotic cells. GFP- and GST-fused HEF1 derivatives were made by subcloning HEF1 fragments into the pEGFP-C4 (Clontech) and pGST (57) plasmids, respectively. *In vitro* translation was done from Aurora expressed from pCMV-SPORT6-C6 (OpenBiosystems). The human p130Cas cDNA was produced by RT-PCR from MCF-7 cells and was cloned into the pEGFP-C4 vector and pCatch-FLAG to produce GFP and FLAG–tagged proteins, respectively. HEF1-specific and non-specific peptides (Serebriiskii et al., 2002) were cloned in the retroviral vector pUP (a gift of Dr.Alexey Ivanov) and introduced into MCF-7 cells by infection. To create tet-repressible expression of HEF1 in MCF-7, the HEF1 cDNA was cloned into retroviral vector pUST-4 (A.Ivanov unpublished data). GP-293 cells were used as a packaging cell line to produce retrovirus for infection of the MCF-7-tTa cells (Clontech). To achieve uniform transient expression of HEF1 derivatives in MCF-7 cells, $HEF1_{1-363}$ and $HEF1_{1-405}$ were cloned in the lentiviral vector pLV-GFP (a gift of Dr. I. Verma). pCMV-6-myc-Ajuba, pCMV-6-myc-PreLim-Ajuba, and pCMV-6-myc-Lim-Ajuba have been described (Kanungo et al., 2000).

Cell culture. The human MCF-7 (breast adenocarcinoma), HeLa (cervical carcinoma), FF2425 (normal fibroblast), and MCR5-hTERT (immortalized fibroblast) cell lines were grown in DMEM supplemented with 10% fetal calf serum. The human MCF-12F (normal breast epithelial) cell line was grown in F12/DMEM media supplemented with 5% horse serum, EGFR, insulin, cholera toxin and hydrocortisone. The MCF-7-GFP-centrin2 and HeLa-GFP-centrin2 stable cell lines were obtained by transfection of the pEGFP-centrin2 plasmid ((D'Assoro et al., 2001), a gift of Dr. Jeffrey Salisbury) into MCF-7 and HeLa cells, and subsequent G418 selection. Tetracycline-regulated MCF-tTa-HEF1 stable cell lines were obtained by first infecting the parental MCF-7-tTa cell line (Clontech) with the pUST-4-HEF1 retroviral vector, then selecting with G418 and puromycin to produce a mass culture of MCF-7-tTa-HEF1 cells. For selection, G418 was used at 500 μg/ml, and puromycin at 1 μg/ml. For lentivirus, 293T cells

were used as a packaging cell line, and and recipient cells MCF-7 treated with the supernatant of 293T transfected cells within 24-48 hours post-transfection of HEF1 constructs. For growth of cells on poly-L-lysine, laminin, or fibronectin, a procedure comparable to that described in (O'Neill and Golemis, 2001) was used to prepare coverslips. Cells transfected with HEF1 GFP-fragments or siRNA, or stable cell lines induced to express HEF1, were plated on these versus uncoated (normal) coverslips, grown for 48 hours, then centrosomal composition and spreading scored. We note, we also attempted to examine the consequences of loss of adhesion for centrosomal phenotypes by plating cells on poly-HEMA, as previously described (O'Neill and Golemis, 2001): however, the onset of apoptosis within 24 hours induced by this treatment precluded reliable analysis (results not shown).

Protein expression, Western blotting, and immunoprecipitation . Recombinant proteins used for pulldown and IP were expressed in BL21 (DE3) bacteria, induced with 300 μM IPTG, and purified using the MicroSpin GST Purification module (Amersham Biotech.). Alternatively, pCMV-SPORT6-C6 AuroraA was in vitro translated in the presence of ^{35}S-Methionine using an SP6 transcription/translation reticulocyte kit (Promega) to produce labeled protein. For Western blotting and immunoprecipitation (IP), mammalian cells were disrupted by M-PER lysis buffer (PIERCE) or NET2 buffer (50mM Tris-HCl pH7.5, 150mM NaCl, 0.05% Triton-X100) in the presence of complete protease inhibitors cocktail, and equivalent protein loads of whole cell lysates used either directly for SDS-polyacrylamide gel electophoresis (SDS-PAGE), or for IP. IP samples were incubated overnight with antibody at 4°C, subsequently incubated for 2 hours with protein A/G-sepharose (Sigma), washed 3 times in lysis buffer supplemented with protease inhibitors, and resolved by SDS-PAGE. Western blotting was done using standard procedures and developed by chemoluminescence using the West-Pico system (Pierce Co.), following the manufacturer's recommendations.

Transiently transfected or infected cells were analyzed for protein expression at 24 - 96 hours hours post-transfection. Transfection procedures were carried out by 5 hour incubation in Lipofectamine 2000 reagent (Invitrogen) for plasmid transfection, or Oligofectamine (Invitrogen) for siRNA oligonucleotide transfection. Antibodies used for Western assay were the following: rabbit polyclonal antibody to HEF1 (Law et al., 1998), at a 1:100 dilution, anti-α-

tubulin-mouse monoclonal (Sigma; 1:10,000), mouse monoclonal anti-γ-tubulin (GTU-88, Sigma; 1:5,000), anti-p130Cas (Transduction Labs, 1:2000), anti-AuroraA (Pharmingen, 1:1,000), anti-Phospho-AuroraA (Cell Signaling, 1:1000), mouse monoclonal anti-Myc tag E910 (Santa Cruz: for IP), rabbit polyclonal anti-Myc (A14, Santa Cruz: for Western), and mouse monoclonal anti-FLAG (Sigma). Secondary anti-mouse or anti-rabbit HPR conjugated antibody (Amersham Biotech) were used at a dilution of 1:10000 or 1:20000.

siRNA experiments RNA oligonucleotides duplexes were synthesized targeted to HEF1, to p130Cas, to Aurora A, and to Ajuba. These and a negative control scrambled siRNA were obtained from (Dharmacon). After transfection of siRNAs, degree of depletion of target proteins was determined by Western blot.

Preparation of cells and synchronization procedures. For observation of cells initially synchronized at the G1/S boundary, cells were initially incubated for 16-18 hours in the presence of 2mM thymidine (Sigma). Some cells were then washed 2 times in PBS, then returned to fresh medium and allowed to grow for 9-12 hours to observe synchronized progression to mitosis. For synchronization at G2/M boundary, cells were incubated in 1μM nocodazole for 14 hours, and collected by shake-off. Collected cells were washed 3 times in PBS, then either replated in fresh medium on the glass cover slips and cultured at 37°C for up to 90 minutes, then fixed for immunofluorescence analysis; or lysed for Western and IP analysis. As an alternative drug-free synchronization approach, an elutriating centrifuge (Beckman J) was used to enrich for G1 or mitotic populations. For elutriation of MCF-7 cells the following conditions were used: speed 1800 rpm, 4°C, and a starting flow rate of 5.5 ml/min. Flow rate was stepped up by increments of 0.5 ml/min, with fractions collected at each step. In a typical experiment, G1 cells were found in fractions 1 and 2, while fractions 5 and 6 were enriched for cells in G2/M. For all the synchronization procedures, the predicted cell cycle compartmentalization was confirmed by use of fluorescence-activated cell sorter (FACS) analysis.

Immunofluorescence (IF). For IF, cells growing on cover slips were fixed with 4% paraformaldehyde for 10 minutes, washed with 1xPBS, then incubated with cold (-20°C) methanol for 2-3 minutes. They were permeabilized with 1% Triton X-100 in 1xPBS for 10

minutes, then blocked in 3% BSA, 0.1% Triton X-100 in 1xPBS for 1 hour. Cover slips were incubated with a primary antibody for 1 hour, washed 3 times with PBS, 0.1% Triton X-100, then incubated with secondary, fluorochrome-conjugated, antibody for 1 hour, and mounted in Vector shield mounting media (Vector). Primary antibodies included mouse monoclonal anti-AuroraA (Pharmingen, dilution 1:300), rabbit polyclonal anti-phospho-AuroraA Cell Signaling, 1:200), rabbit polyclonal anti-HEF1 1:100, rat monoclonal anti-α-tubulin (Abcam, 1:200), rabbit polyclonal anti-γ-tubulin (Abcam, 1:200), mouse monoclonal anti-pericentrin (Transduction Labs, 1:250), mouse monoclonal anti-phosphohistone 3 (Upstate). Secondary antibodies were anti-mouse-Alexa-488, anti-rabbit-Alexa488, anti- mouse-Alexa-568, anti-mouse-Alexa-633, anti-rabbit-Alexa 633 (Molecular Probes, Inc.). DNA was stained by TOTO-3 dye (Molecular Probes). Confocal microscopy was performed using a Radiance 2000 laser scanning confocal microscope (Bio-Rad laboratories, Hercules, CA) coupled to a Nikon Eclipse E800 upright microscope (Carl Zeiss, Thornwood, NY). Images were obtained separately by independent excitation at 488/568/633 nm to minimize overlapping signals. All optical sectioning was carried out in 0.5 μm increments. For composite panels, all individual components were recorded under identical conditions.

Cell spreading analysis was performed as described in (O'Neill and Golemis, 2001), with calculation of area based on scored pixels within a traced cell perimeter. In addition, immunofluorescence with primary antibody to paxillin was used to confirm increased size and formation of focal adhesions in cells plated on laminin and fibronectin (data not shown).

Kinase assay. For phosphorylation of HEF1, an in vitro kinase assay was performed using the GST-fused HEF1 deletion mutants prepared as described above for pulldowns. Histone H3 and H1 were used as positive and negative controls for Aurora A phosphorylation. 0.5 μg of recombinant proteins were treated at 30°C for 20 minutes in a 20 μl reaction with 5 ng catalytically active Aurora A kinase (Upstate) in supplied buffer plus 250 μM ATP and 10 μCi of γ-(^{32}P)ATP. An aliquot without γ-^{32}P(ATP) was processed for Coomassie staining in SDS-PAGE. For phosphorylation of AurA, a wild type AurA cDNA was translated in reticulocyte lysate, mixed with titrated quantities of GST-HEF11-363 or GST, immunoprecipitated with anti-AurA, and used for kinase reaction with γ-^{32}P(ATP) and 2 μg of histone H3. Aliquots of the reaction

mix (before immunoprecipitation) were used for SDS-PAGE and Western analysis to confirm levels of AurA, and GST proteins; phospho-histone H3 was visualized by autoradiography.

Acknowledgments. We are grateful to Tyson Moyer for assistance with some experiments. This work was supported by research grant NIH CA63366, the Susan Komen Breast Cancer Foundation, and Tobacco Settlement funding from the State of Pennsylvania (to EAG); by NIH core grant CA-06927 to Fox Chase Cancer Center; by research grant NIH CA75315 and the Washington University/Pfizer Biomedical Research Program (to GDL). ENP was supported by the Department of Defense Breast Cancer Training grant DAMD17-00-1-0249. We thank Drs. Peter Chumakov and Alexey Ivanov for the pUST and pUP vectors, and Dr. Jeffrey Salisbury for the GFP-centrin construct. We are grateful to Drs. Jonathan Chernoff, Elizabeth Henske, and Maureen Murphy for critical review of the manuscript.

References.

Anand, S., Penrhyn-Lowe, S., and Venkitaraman, A. R. (2003). AURORA-A amplification overrides the mitotic spindle assembly checkpoint, inducing resistance to Taxol. Cancer Cell *3*, 51-62.

Ben-Ze'ev, A., and Raz, A. (1981). Multinucleation and inhibition of cytokinesis in suspended cells: reversal upon reattachment to a substrate. Cell *26*, 107-115.

Bornens, M. (2002). Centrosome composition and microtubule anchoring mechanisms. Curr Opin Cell Biol *14*, 25-34.

Bouton, A. H., Riggins, R. B., and Bruce-Staskal, P. J. (2001). Functions of the adapter protein Cas: signal convergence and the determination of cellular responses. Oncogene *20*, 6448-6458.

Brinkley, B. R. (2001). Managing the centrosome numbers game: from chaos to stability in cancer cell division. Trends Cell Biol *11*, 18-21.

D'Assoro, A. B., Barrett, S. L., Folk, C., Negron, V. C., Boeneman, K., Busby, R., Whitehead, C., Stivala, F., Lingle, W. L., and Salisbury, J. L. (2002). Amplified centrosomes in breast cancer: a potential indicator of tumor aggressiveness. Breast Cancer Res Treat *75*, 25-34.

D'Assoro, A. B., Stivala, F., Barrett, S., Ferrigno, G., and Salisbury, J. L. (2001). GFP-centrin as a marker for centriole dynamics in the human breast cancer cell line MCF-7. Ital J Anat Embryol *106*, 103-110.

Deng, C. X. (2002). Roles of BRCA1 in centrosome duplication. Oncogene *21*, 6222-6227.

Duesberg, P., Stindl, R., and Hehlmann, R. (2000). Explaining the high mutation rates of cancer cells to drug and multidrug resistance by chromosome reassortments that are catalyzed by aneuploidy. Proc Natl Acad Sci U S A *97*, 14295-14300.

Dutertre, S., Descamps, S., and Prigent, C. (2002). On the role of aurora-A in centrosome function. Oncogene *21*, 6175-6183.

Etienne-Manneville, S., and Hall, A. (2003). Cdc42 regulates GSK-3beta and adenomatous polyposis coli to control cell polarity. Nature *421*, 753-756.

Fashena, S. J., Einarson, M. B., O'Neill, G. M., Patriotis, C. P., and Golemis, E. A. (2002). Dissection of HEF1-dependent functions in motility and transcriptional regulation. J Cell Sci *115*, 99-111.

Fry, A. M. (2002). The Nek2 protein kinase: a novel regulator of centrosome structure. Oncogene *21*, 6184-6194.

Glotzer, M. (2001). Animal cell cytokinesis. Annu Rev Cell Dev Biol *17*, 351-386.

Goepfert, T. M., Adigun, Y. E., Zhong, L., Gay, J., Medina, D., and Brinkley, W. R. (2002). Centrosome amplification and overexpression of aurora A are early events in rat mammary carcinogenesis. Cancer Res *62*, 4115-4122.

Hannak, E., Kirkham, M., Hyman, A. A., and Oegema, K. (2001). Aurora-A kinase is required for centrosome maturation in Caenorhabditis elegans. J Cell Biol *155*, 1109-1116.

Herreros, L., Rodriguez-Fernandez, J. L., Brown, M. C., Alonso-Lebrero, J. L., Cabanas, C., Sanchez-Madrid, F., Longo, N., Turner, C. E., and Sanchez-Mateos, P. (2000). Paxillin localizes to the lymphocyte microtubule organizing center and associates with the microtubule cytoskeleton. J Biol Chem *275*, 26436-26440.

Hirota, T., Kunitoku, N., Sasayama, T., Marumoto, T., Zhang, D., Nitta, M., Hatakeyama, K., and Saya, H. (2003). Aurora-A and an interacting activator, the LIM protein Ajuba, are required for mitotic commitment in human cells. Cell *114*, 585-598.

Hirota, T., Morisaki, T., Nishiyama, Y., Marumoto, T., Tada, K., Hara, T., Masuko, N., Inagaki, M., Hatakeyama, K., and Saya, H. (2000). Zyxin, a regulator of actin filament assembly, targets the mitotic apparatus by interacting with h-warts/LATS1 tumor suppressor. J Cell Biol *149*, 1073-1086.
Hollander, M. C., and Fornace, A. J., Jr. (2002). Genomic instability, centrosome amplification, cell cycle checkpoints and Gadd45a. Oncogene *21*, 6228-6233.
Honda, H., Nakamoto, T., Sakai, R., and Hirai, H. (1999). p130(Cas), an assembling molecule of actin filaments, promotes cell movement, cell migration, and cell spreading in fibroblasts. Biochem Biophys Res Commun *262*, 25-30.
Honda, H., Oda, H., Nakamoto, T., Honda, Z., Sakai, R., Suzuki, T., Saito, T., Nakamura, K., Nakao, K., Ishikawa, T., *et al.* (1998). Cardiovascular anomaly, impaired actin bundling and resistance to Src-induced transformation in mice lacking p130Cas. Nat Genet *19*, 361-365.
Jackman, M., Lindon, C., Nigg, E. A., and Pines, J. (2003). Active cyclin B1-Cdk1 first appears on centrosomes in prophase. Nat Cell Biol *5*, 143-148.
Kanungo, J., Pratt, S. J., Marie, H., and Longmore, G. D. (2000). Ajuba, a cytosolic LIM protein, shuttles into the nucleus and affects embryonal cell proliferation and fate decisions. Mol Biol Cell *11*, 3299-3313.
Kiat, L. S., Hui, K. M., and Gopalan, G. (2002). Aurora-A kinase interacting protein (AIP), a novel negative regulator of human Aurora-A kinase. J Biol Chem *277*, 45558-45565.
Knust, E., and Bossinger, O. (2002). Composition and formation of intercellular junctions in epithelial cells. Science *298*, 1955-1959.
Kramer, A., Neben, K., and Ho, A. D. (2002). Centrosome replication, genomic instability and cancer. Leukemia *16*, 767-775.
Law, S. F., Estojak, J., Wang, B., Mysliwiec, T., Kruh, G. D., and Golemis, E. A. (1996). Human Enhancer of Filamentation 1 (HEF1), a novel p130Cas-like docking protein, associates with FAK, and induces pseudohyphal growth in yeast. Mol Cell Biol *16*, 3327-3337.
Law, S. F., O'Neill, G. M., Fashena, S. J., Einarson, M. B., and Golemis, E. A. (2000). The docking protein HEF1 is an apoptotic mediator at focal adhesion sites. Mol Cell Biol *20*, 5184-5195.
Law, S. F., Zhang, Y.-Z., Klein-Szanto, A., and Golemis, E. A. (1998). Cell-cycle regulated processing of HEF1 to multiple protein forms differentially targeted to multiple compartments. Mol Cell Biol *18*, 3540-3551.
Ligon, L. A., Karki, S., Tokito, M., and Holzbaur, E. L. (2001). Dynein binds to beta-catenin and may tether microtubules at adherens junctions. Nat Cell Biol *3*, 913-917.
Lingle, W. L., Barrett, S. L., Negron, V. C., D'Assoro, A. B., Boeneman, K., Liu, W., Whitehead, C. M., Reynolds, C., and Salisbury, J. L. (2002). Centrosome amplification drives chromosomal instability in breast tumor development. Proc Natl Acad Sci U S A *99*, 1978-1983.
Lingle, W. L., Lutz, W. H., Ingle, J. N., Maihle, N. J., and Salisbury, J. L. (1998). Centrosome hypertrophy in human breast tumors: implications for genomic stability and cell polarity. Proc Natl Acad Sci U S A *95*, 2950-2955.
Liu, X., Elia, A. E. H., Law, S. F., Golemis, E. A., Farley, J., and Wang, T. (2000). A novel ability of Smad3 to regulate proteasomal degradation of a Cas family member, HEF1. EMBO J *19*, 6759-6769.
Mailand, N., Lukas, C., Kaiser, B. K., Jackson, P. K., Bartek, J., and Lukas, J. (2002). Deregulated human Cdc14A phosphatase disrupts centrosome separation and chromosome segregation. Nat Cell Biol *4*, 317-322.

Marumoto, T., Honda, S., Hara, T., Nitta, M., Hirota, T., Kohmura, E., and Saya, H. (2003). Aurora-a kinase maintains the fidelity of early and late mitotic events in HeLa cells. J Biol Chem.
Meraldi, P., Honda, R., and Nigg, E. A. (2002). Aurora-A overexpression reveals tetraploidization as a major route to centrosome amplification in p53-/- cells. Embo J *21*, 483-492.
Meraldi, P., and Nigg, E. A. (2002). The centrosome cycle. FEBS Lett *521*, 9-13.
Minegishi, M., Tachibana, K., Sato, T., Iwata, S., Nojima, Y., and Morimoto, C. (1996). Structure and function of Cas-L, a 105-kD Crk-associated substrate-related protein that is involved in beta-1 integrin-mediated signaling in lymphocytes. J Exp Med *184*, 1365-1375.
Nance, J., Munro, E. M., and Priess, J. R. (2003). C. elegans PAR-3 and PAR-6 are required for apicobasal asymmetries associated with cell adhesion and gastrulation. Development *130*, 5339-5350.
Nourry, C., Maksumova, L., Pang, M., Liu, X., and Wang, T. (2004). Direct Interaction Between Smad3, APC10, CDH1 and HEF1 in Proteasomal Degradation of HEF1. BMC Cell Biol *5*, 20.
O'Connell, M. J., Krien, M. J., and Hunter, T. (2003). Never say never. The NIMA-related protein kinases in mitotic control. Trends Cell Biol *13*, 221-228.
O'Neill, G. M., Fashena, S. J., and Golemis, E. A. (2000). Integrin signaling: a new Cas(t) of characters enters the stage. Trends Cell Biol *10*, 111-119.
O'Neill, G. M., and Golemis, E. A. (2001). Proteolysis of the docking protein HEF1 and implications for focal adhesion dynamics. Mol Cell Biol *21*, 5094-5108.
Orly, J., and Sato, G. (1979). Fibronectin mediates cytokinesis and growth of rat follicular cells in serum-free medium. Cell *17*, 295-305.
Ouchi, M., Fujiuchi, N., Sasai, K., Katayama, H., Minamishima, Y. A., Ongusaha, P. P., Deng, C., Sen, S., Lee, S. W., and Ouchi, T. (2004). BRCA1 phosphorylation by Aurora-A in the regulation of G2 to M transition. J Biol Chem *279*, 19643-19648.
Piel, M., Nordberg, J., Euteneuer, U., and Bornens, M. (2001). Centrosome-dependent exit of cytokinesis in animal cells. Science *291*, 1550-1553.
Polte, T. R., and Hanks, S. K. (1997). Complexes of focal adhesion kinase (FAK) and Crk-associated substrate (p130Cas) are elevated in cytoskeleton-associated fractions following adhesion and Src transformation. J Biol Chem *272*, 5501-5509.
Raff, J. W., Jeffers, K., and Huang, J. Y. (2002). The roles of Fzy/Cdc20 and Fzr/Cdh1 in regulating the destruction of cyclin B in space and time. J Cell Biol *157*, 1139-1149.
Rieder, C. L., Faruki, S., and Khodjakov, A. (2001). The centrosome in vertebrates: more than a microtubule-organizing center. Trends Cell Biol *11*, 413-419.
Rodriguez-Fernandez, J. L., Gomez, M., Luque, A., Hogg, N., Sanchez-Madrid, F., and Cabanas, C. (1999). The interaction of activated integrin lymphocyte function-associated antigen 1 with ligand intercellular adhesion molecule 1 induces activation and redistribution of focal adhesion kinase and proline-rich tyrosine kinase 2 in T lymphocytes. Mol Biol Cell *10*, 1891-1907.
Salisbury, J. L. (2003). Centrosomes: coiled-coils organize the cell center. Curr Biol *13*, R88-90.
Schneider, S. Q., and Bowerman, B. (2003). Cell polarity and the cytoskeleton in the Caenorhabditis elegans zygote. Annu Rev Genet *37*, 221-249.
Segal, M., and Bloom, K. (2001). Control of spindle polarity and orientation in Saccharomyces cerevisiae. Trends Cell Biol *11*, 160-166.

Serebriiskii, I. G., Mitina, O., Pugacheva, E., Benevolenskaya, E., Kotova, E., Toby, G. G., Khazak, V., Kaelin, W. G., Chernoff, J., and Golemis, E. A. (2002). Detection of peptides, proteins, and drugs that selectively interact with protein targets. Genome Res *12*, 1785-1791.
Severson, A. F., and Bowerman, B. (2003). Myosin and the PAR proteins polarize microfilament-dependent forces that shape and position mitotic spindles in Caenorhabditis elegans. J Cell Biol *161*, 21-26.
van der Flier, S., Brinkman, A., Look, M. P., Kok, E. M., Meijer-Van Gelder, M. E., Klijn, J. G., Dorssers, L. C., and Foekens, J. A. (2000). Bcar1/p130Cas protein and primary breast cancer: prognosis and response to tamoxifen treatment. J Natl Cancer Inst *92*, 120-127.
Weaver, Z., Montagna, C., Xu, X., Howard, T., Gadina, M., Brodie, S. G., Deng, C. X., and Ried, T. (2002). Mammary tumors in mice conditionally mutant for Brca1 exhibit gross genomic instability and centrosome amplification yet display a recurring distribution of genomic imbalances that is similar to human breast cancer. Oncogene *21*, 5097-5107.
Yamaguchi, R., Mazaki, Y., Hirota, K., Hashimoto, S., and Sabe, H. (1997). Mitosis specific serine phosphorylation and downregulation of one of the focal adhesion protein, paxillin. Oncogene *15*, 1753-1761.
Yamakita, Y., Totsukawa, G., Yamashiro, S., Fry, D., Zhang, X., Hanks, S. K., and Matsumura, F. (1999). Dissociation of FAK/p130(CAS)/c-Src complex during mitosis: role of mitosis-specific serine phosphorylation of FAK. J Cell Biol *144*, 315-324.
Yamashita, Y. M., Jones, D. L., and Fuller, M. T. (2003). Orientation of asymmetric stem cell division by the APC tumor suppressor and centrosome. Science *301*, 1547-1550.
Yvon, A. M., Walker, J. W., Danowski, B., Fagerstrom, C., Khodjakov, A., and Wadsworth, P. (2002). Centrosome reorientation in wound-edge cells is cell type specific. Mol Biol Cell *13*, 1871-1880.
Zhou, H., Kuang, J., Zhong, L., Kuo, W. L., Gray, J. W., Sahin, A., Brinkley, B. R., and Sen, S. (1998). Tumour amplified kinase STK15/BTAK induces centrosome amplification, aneuploidy and transformation. Nat Genet *20*, 189-193.

Figure Legends.

Figure 1. HEF1 localization to the centrosome: cell cycle and sequence dependence. A. Cell cycle synchronized populations are analyzed for HEF1 localization to the centrosome and mitotic apparatus. HEF1 is indicated in green. γ-tubulin (red) is used to indicate centrosomes (see arrows). DNA (blue) becomes condensed at mitotic entry. Enlarged views of indicated centrosomes are shown in the upper right. Images are merged confocal sections. 6 μm scale bar applies to top row, 8 μm scale bar applies to all other images. **B.** FACS analysis demonstrating synchronization of cells in G1, S, and G2/M phases, as used for immunofluorescence analysis. **C.** Western analysis of HEF1 levels in the indicated phases of cell cycle, with beta-actin as loading control. **D.** GFP-HEF1 fusion protein confirms GFP-HEF1 localization at the centrosome in late G2 (arrows), and at the spindle in mitosis. **E.** Cells transfected with plasmids expressing GFP-HEF1$_{1\text{-}363}$ or GFP-HEF1$_{1\text{-}405}$, and gamma-tubulin. **F.** Fragments of HEF1 analyzed as GFP- or FLAG epitope-tagged fusion proteins, amino acids (a.a.) and degree of localization to the centrosome indicated. HEF1$_{1\text{-}834}$ is full length HEF1. *, protein poorly expressed.

Figure 2. Overexpression, stabilization, and depletion of HEF1. A. MCF-7 cells with tetracycline-repressed expression of stably integrated HEF1 or GFP in the presence (+) or absence (-) of tetracycline, measured at 24 or 48 hours after medium change. Western analysis with antibody to HEF1 demonstrates induction following tetracycline removal: the beta-actin protein was used as a loading control. **B.** Western blot analysis of MCF-7 cells infected retroviruses expressing HA-tagged thioredoxin (TRX)-peptide fusion proteins. Levels of HEF1 are stabilized by specific HA-TRX peptides (P1-HEF1, P2-HEF1), but not by non-specific HA-TRX peptides (P1-NS), or by HA-TRX with no peptide inserted (NP). HA shows comparable expression of HA-TRX fusions in all lanes. **C.** Western blot analysis of MCF-7 cells treated with siRNAs to HEF1 (siHEF1) or a scrambled control (Scr) shows efficient and specific HEF1 depletion. β-actin is used as a loading control.

Figure 3. Overexpression, stabilization, and depletion of HEF1 induce defects in the centrosomes and the mitotic spindle. A. MCF-7 cells with tet-repressed HEF1 were uninduced

(left panel) or induced by tetracycline removal (+HEF1, right 4 panels). Cells were treated to visualize DNA (blue) alpha-tubulin (green) and gamma-tubulin (red) for immunofluorescence; 4 representative mitoses are shown. Scale bar for images in this panel is 4 μM. **B.** Quantitation of multipolar spindles scored in cells with induced indicates the percentage of cells with multipolar spindles in the presence (+) or absence (-) of overexpressed HEF1, an overexpressed GFP control, or following treatment with HEF1-specific (H) or non-specific (NS) peptide, or negative control (NP) HA-TRX fusions. 3 independent experiments were performed, resulting in the assessment of 150 mitoses in total for each condition. **C.** MCF-7 cells were transfected with either a control scrambled (left panels), or an siRNA specific for HEF1(-HEF1; center and right panels) for 48 hours, then processed for immunofluorescence using markers to gamma-tubulin (red), alpha-tubulin (green), and DNA (blue). Shown, representative mitoses: top panels are a merged image. Scale bar for images in this panel is 5 μM. **D.** Immunofluorescence analysis of MCF-7 cells with stably expressed GFP-centrin2 (green) 48 hours post-transfection of scrambled (Scr) or HEF1-directed (-HEF1) siRNAs was used to calculate the frequency of split (top panel, -HEF1) versus closely paired (bottom panel, Scr) centrioles (indicated by arrows, and shown in insets). For quantification (discussed in Results), data were collected from at least three independent experiments, and 150 cells were counted for HEF1-depleted or control cells. DNA is shown in blue: note uncondensed DNA in HEF1-depleted cells with splitting. Scale bar for images in this panel is 5 μM. **E.** FACS analysis of cells depleted with indicated siRNAs at 48 hours post-transfection.

Figure 4. HEF1 associates with AurA and control AurA activation. **A.** MCF-7 cells were depleted with HEF1-directed siRNA (-HEF1) or a scrambled control (Scr). Mitotic cells stained with antibodies directed at AurA (green), phospho-AurA (P-AurA, red), and DNA (blue) are shown. Scale bar applies to all panels. **B.** MCF-7 cells were transfected with scrambled control (Scr) or HEF1-directed (-HEF1) siRNA for 48 hours, then collected and part of the sample elutriated. Non-elutriated (Asyn.), G1/S, or G2-M enriched populations were used for Western blot analysis using the antibodies indicated (left). **C.** MCF-7 cells prepared as in **B** were used for co-immunoprecipitation. Top, immunoprecipitation with control IgG or Cas antibody (cross-reactive with p130Cas and HEF1; efficient direct precipitation of both proteins), and Western blot using antibodies as indicated to left. Bottom, immunoprecipitation with control IgG or

AurA antibody, and Western blot as indicated. For each experiment, co-immunoprecipitation is compared in cells depleted for HEF1, or treated with scrambled siRNA, to confirm specific requirement of HEF1 in co-immunoprecipitation.

Figure 5. Mapping the HEF1-Ajuba interaction. **A.** Cells were transfected with FLAG-tagged full length HEF1 (Flag-FL), N-terminus (Flag-N), or C-terminus (Flag-C), in combinations with GFP or Myc-tagged full length Ajuba (Aj) or the Ajuba preLIM region (PL). Top three panels, left: input Ajuba derivatives, visualized with Myc antibody. Right panel: input HEF1 derivatives, visualized with FLAG antibody. Bottom three panels, left: Ajuba co-immunoprecipitated by FLAG antibody, visualized with Myc antibody. **B.** Cells transfected with HA-tagged full length HEF1, and either Myc vector or Myc tagged full length Ajuba (Aj), Ajuba preLIM region (PL), or LIM region (L). Right panels, input. Left panels, top, coimmunoprecipitated HEF1, visualized with antibody to HA; bottom, immunoprecipitated Ajuba. **C.** Experimental setup as in B, except cells contain full length HEF1 (left) or N-terminal HEF1 (right).

Figure 6. Delineation of the HEF1-AurA interaction. **A.** MCF-7 cells were mock-infected or infected with a pLV- plasmid encoding GFP-HEF1$_{1-363}$ or GFP- HEF1$_{1-405}$, immunoprecipitated with either control IgG (left lane) or antibody to GFP (right two lanes), and Western blot visualization with antibodies to GFP or AurA, as indicated. Note, both GFP-HEF1 fusion proteins display similar mobility here because high percent acrylamide gel was run to also visualize GFP (not included in image). **B.** In vitro kinase assay. Comparable levels of GST, GST-fusion proteins, or histone H1 or H3 (Coomassie stain, left panel) were incubated with AurA and gamma-32-P in vitro. Right panel, autoradiograph of in vitro phosphorylated AurA substrates. M, molecular weight marker. **C.** In vitro translated 35S-labelled AurA was mixed with 3 different GST-fused fragments of HEF1 or GST, and pulled down with glutathione beads, resolved by SDS-PAGE, and visualized by autoradiography (top panel) and Coomassie blue (CB) staining to show GST-fusions (bottom panel). In the lane "R", 20% of a total AurA 35S-labelled reaction mixture is shown: for each pulldown, a complete reaction mixture is used. **D.** MCF-7 cells were treated with either scrambled siRNA (Scr), or AurA-targeting siRNA (-AurA). Nocodazole arrested or thymidine arrested cells, either treated or untreated with ALLN, were

lysed, and blotted with antibodies as indicated at left. **E.** Increasing quantities (1, 2, or 4 μg) of GST-fused $HEF1_{1-363}$ or GST only were mixed with reticulocyte translated, ^{35}-S-labelled AurA in an in vitro kinase reaction. Reactions visualized with antibody to phospho-AurA, or GST, as indicated; or via autoradiography, to indicate total 35-S AurA.

Figure 7. Separation of HEF1 activities at the centrosome, and in cell attachment. A. Degree of centrosomal splitting in GFP-positive cells transfected with HEF1 truncations. Top, MCF7 cells; bottom, HeLa cells. Red, split centrosomes; blue, unsplit. Three (MCF7) and two (Hela) independent experiments were performed, with 100 cells counted in each experiment. **B.** Degree of cell spreading in GFP-positive cells transfected with HEF1 truncations. Top, MCF7 cells; bottom, HeLa cells. Scale reflects total pixels contained within trace of imaged cells. 2 experiments were performed, with 100 cells counted in each experiment. **C.** Western analysis of expression of different HEF1 truncations expressed as GFP-fused proteins in MCF7 (lanes 1-5) or HeLa (lanes 6-10) cells. Blot probed with antibody to GFP. Lanes are GFP-fusions to 1, 654-834; 2, 351-363; 3, 1-363; 4, FL; 5, 1-405; 6, 1-363; 7, 351-653; 8. 654-834; 9, FL; 10, 1-405. **D.** Mitotic spindle defects induced by HEF1 overexpression in cells plated on different matrices. A tetracycline-repressible MCF-7 derived cell lines was grown in the presence (-) or absence (+HEF1) of tetracycline after plating on glass coverslips (-), or coverslips coated with poly-L-lysine (PLL), fibronectin (FN), or laminin (LAM). Blue, normal bipolar spindles; red, multipolar spindles, or spindles with obvious malformations. Three independent experiments were performed, with 100 cells counted in each experiment. **E,F.** Centrosomal splitting induced by depletion of HEF1, or overexpression of dominant negative HEF1, in cells plated on different matrices. **E**, MCF7 cells with integrated GFP-centrin were transfected with siRNA containing scrambled sequence (Scr) or targeted to HEF1 (-HEF1). **F**, MCF7 cells were transfected with GFP-fused $HEF1_{1-363}$ or $HEF1_{1-405}$, and centrosomes visualized by antibody to gamma-tubulin. Following treatment, cells were plated on glass coverslips (-), or coverslips coated with poly-L-lysine (PLL), fibronectin (FN), or laminin (LAM). Red, split centrosomes; blue, unsplit. Three independent experiments were performed, with 100 cells counted in each experiment.

Figure 8. Comparison of HEF1 and p130Cas action at the centrosome. A. FF2425, MCF-7, or HeLa cells were depleted with siRNA targeting HEF1 (-HEF1), p130Cas (-130) or a

scrambled control (Scr). The percent of split centrosomes was scored; blue, un-split; red, split centrosomes. For each data point, 50 cells were counted in each of 3 separate experiments (150 cells total). **B.** Western blot, analyzing levels of HEF1 and p130Cas in MCF-7 cells treated with siRNA as for A. beta-actin represents a loading control. **C.** GFP-fused p130Cas (GFP-Cas) or GFP-fused HEF1 (GFP-HEF1) were expressed in either FF2425 or MCF-7 cells. Inset top right of each panel, enlarged view of centrosomes (indicated with arrows in main figure). Scale bar applies to all panels. **D.** MCF-7 cells with siRNA-depleted p130Cas, visualizing AurA, phospho-AurA (P-AurA), and phospho-histone H3 (P-H3). **E.** MCF7 cells were treated with siRNA for 48 hours, lysed, AurA immunoprecipitated, and used for Western or in vitro kinase assay with P-32-γ-ATP with a histone H3 substrate. Top, Immunoblot of immunoprecipitated AurA; bottom, autoradiography of phospho-histone H3. *, phosphorylated AurA. **F.** Transient appearance of >4N populations in HEF1-depleted cells. FACS analysis of fraction 5 of elutriated MCF-7 cells 48 hours after treatment with HEF1-directed (-HEF1) or scrambled control (Scr) siRNAs (Top); or after 24 additional hours of growth following elutriation prior to FACS analysis. See results for details. Comparable results were obtained in MCF12F cells (data not shown).

Figure 1

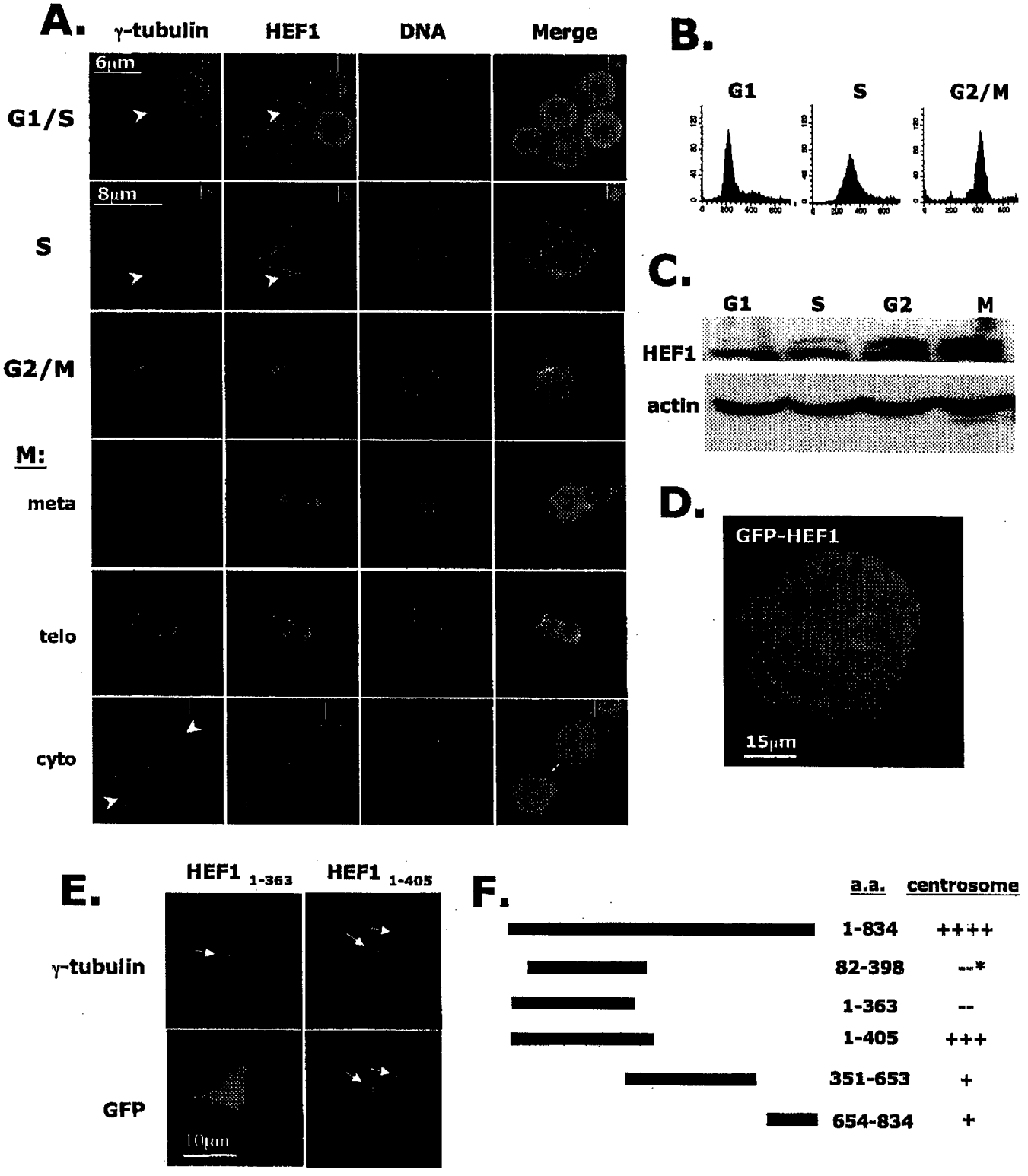
A.
γ-tubulin
HEF1
DNA
Merge
6μm
8μm
G1/S
S
G2/M
M:
meta
telo
cyto
B.
G1
S
G2/M
C.
G1
S
G2
M
HEF1
actin
D.
GFP-HEF1
15μm
E.
HEF1 1-363
HEF1 1-405
γ-tubulin
GFP
10μm
F.
a.a.
centrosome
1-834
++++
82-398
--*
1-363
--
1-405
+++
351-653
+
654-834
+

Figure 2

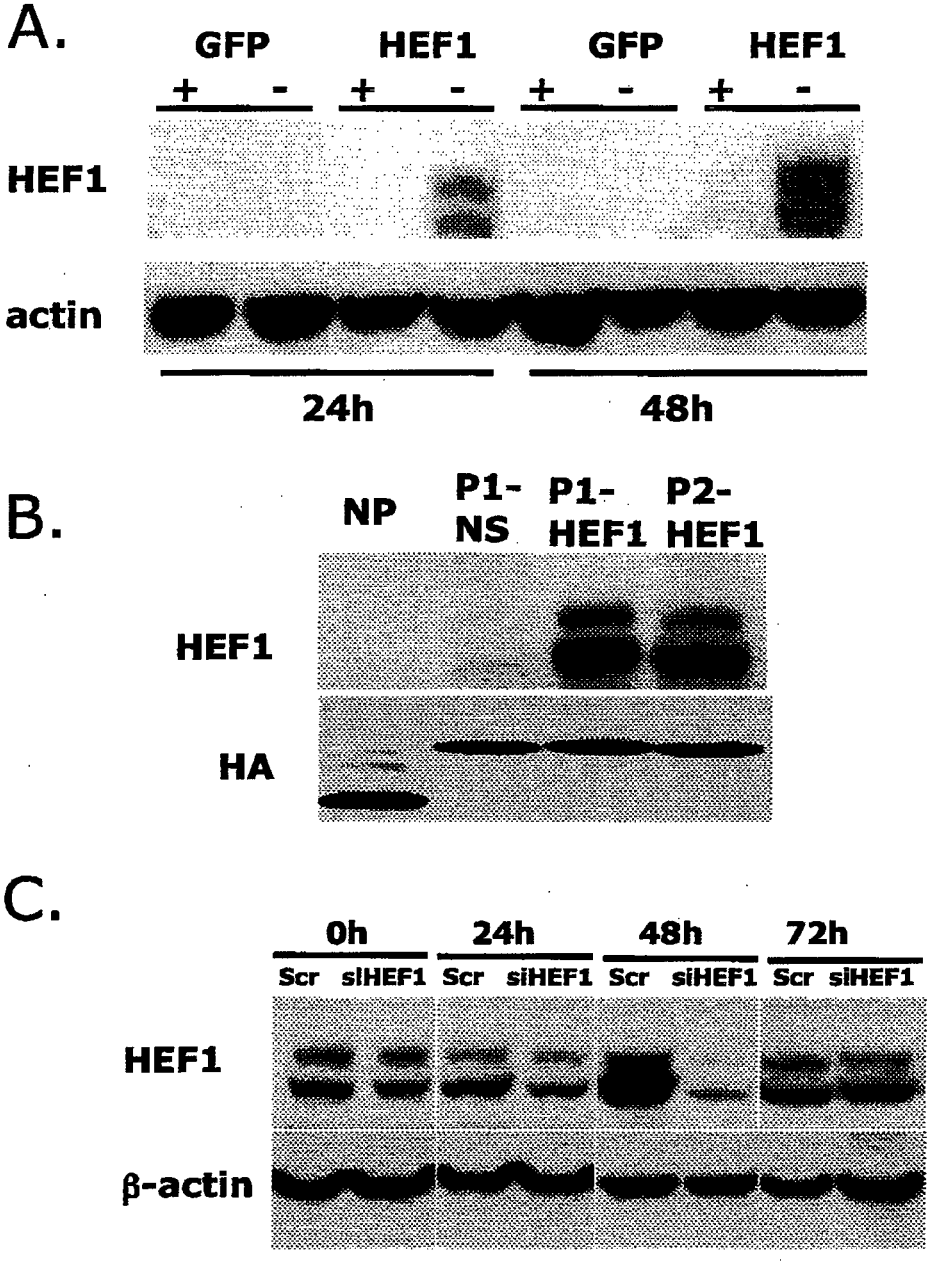
A.
GFP
HEF1
GFP
HEF1
+ - + - + - + -
HEF1
actin
24h
48h
B.
NP
P1-NS
P1-HEF1
P2-HEF1
HEF1
HA
C.
0h
24h
48h
72h
Scr siHEF1 Scr siHEF1 Scr siHEF1 Scr siHEF1
HEF1
β-actin

Figure 3

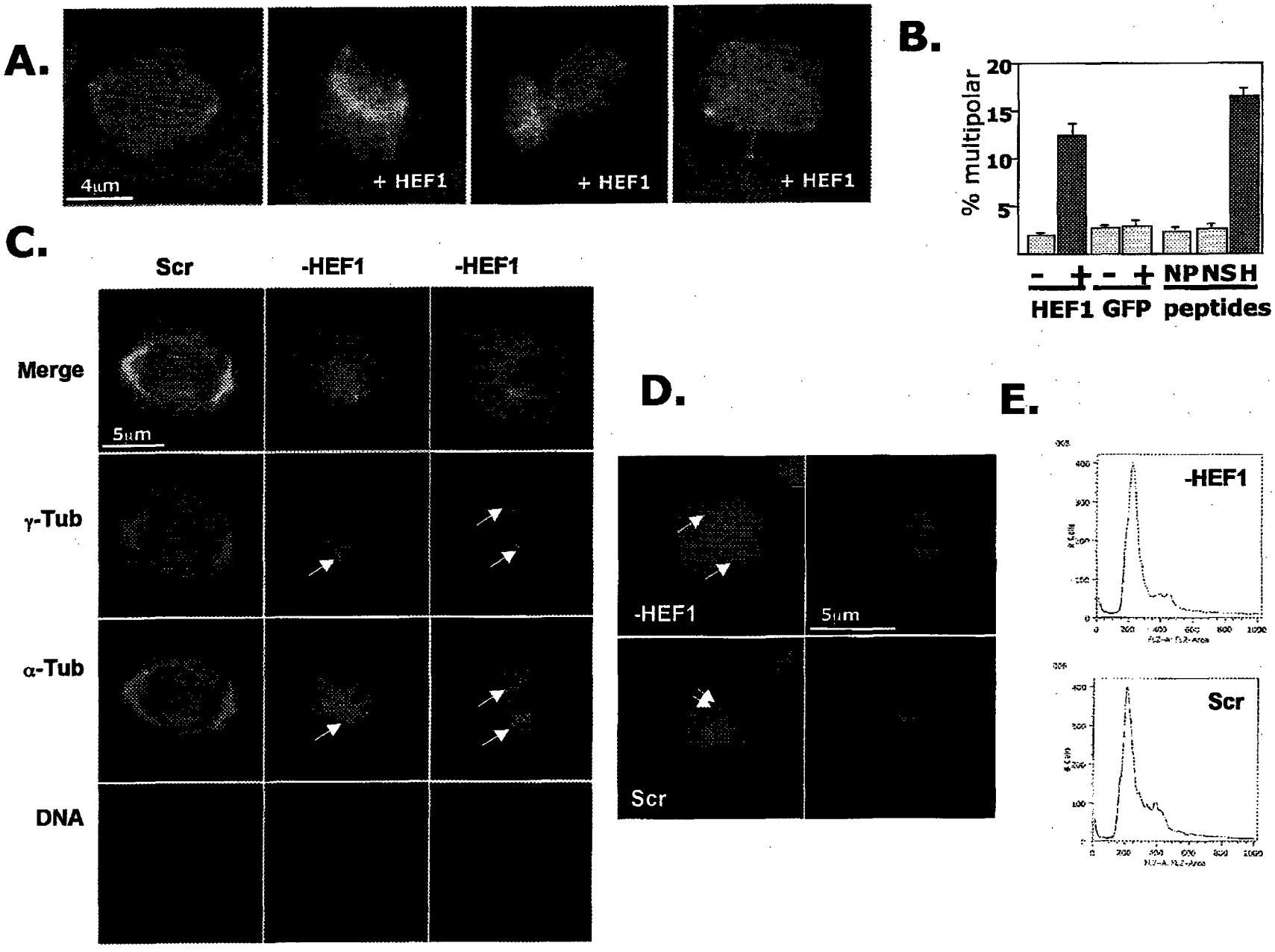
A.
4μm
+ HEF1
+ HEF1
+ HEF1
B.
% multipolar
20
15
10
5
- + - + NPNSH
HEF1 GFP peptides
C.
Scr
-HEF1
-HEF1
Merge
5μm
γ-Tub
α-Tub
DNA
D.
-HEF1
5μm
Scr
E.
-HEF1
Scr

Figure 4

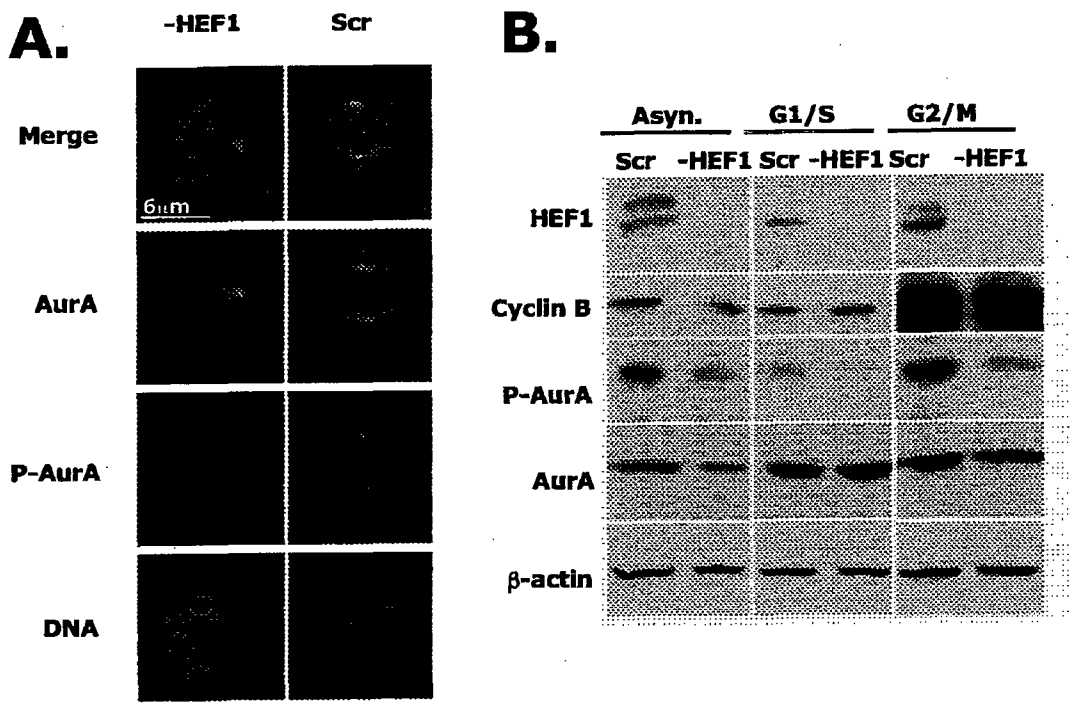
A.
-HEF1
Scr
Merge
6μm
AurA
P-AurA
DNA
B.
Asyn.
G1/S
G2/M
Scr
-HEF1
Scr
-HEF1
Scr
-HEF1
HEF1
Cyclin B
P-AurA
AurA
β-actin
C.
Asyn.
G1/S
G2/M
Scr
-HEF1
Scr
-HEF1
Scr
-HEF1
Scr
HEF1
p130Cas
P-AurA
IP:
IgG
Cas
Asyn.
G1/S
G2/M
Scr
-HEF1
Scr
-HEF1
Scr
-HEF1
Scr
HEF1
AurA
IP:
IgG
AurA

Figure 5

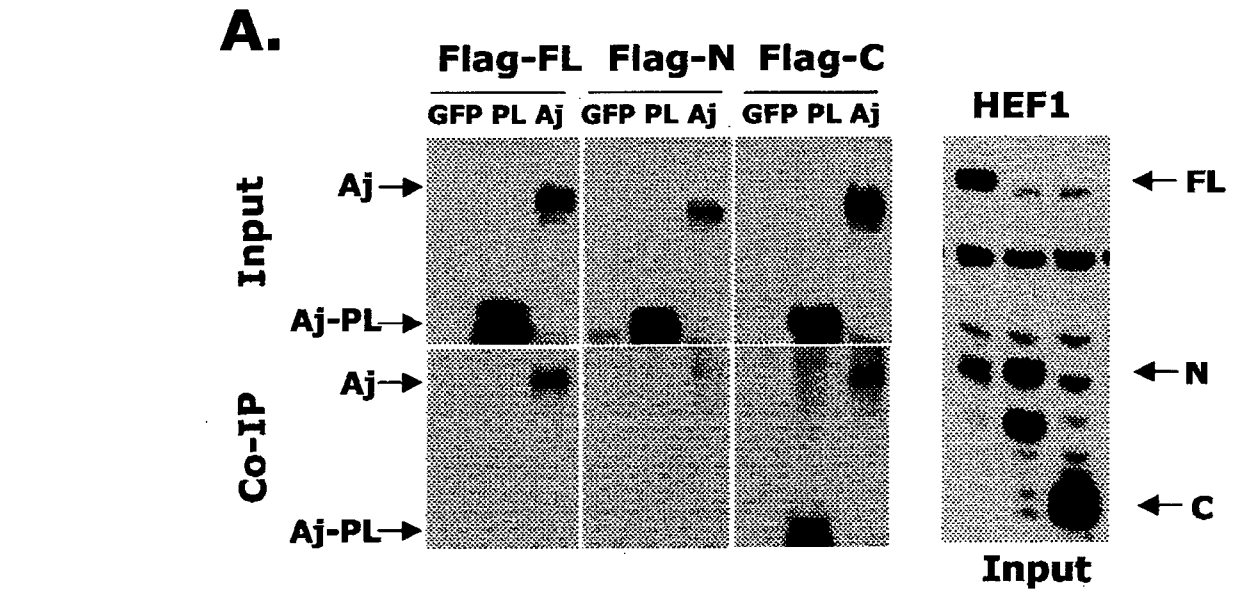
A.
Flag-FL
Flag-N
Flag-C
GFP PL Aj GFP PL Aj GFP PL Aj
Input
Co-IP
Aj
Aj-PL
Aj
Aj-PL
HEF1
FL
N
C
Input

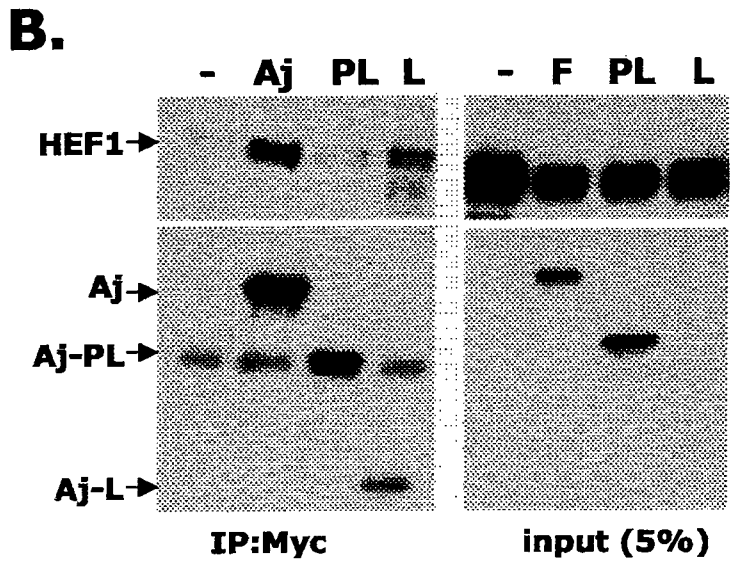
B.
- Aj PL L
- F PL L
HEF1
Aj
Aj-PL
Aj-L
IP:Myc
input (5%)

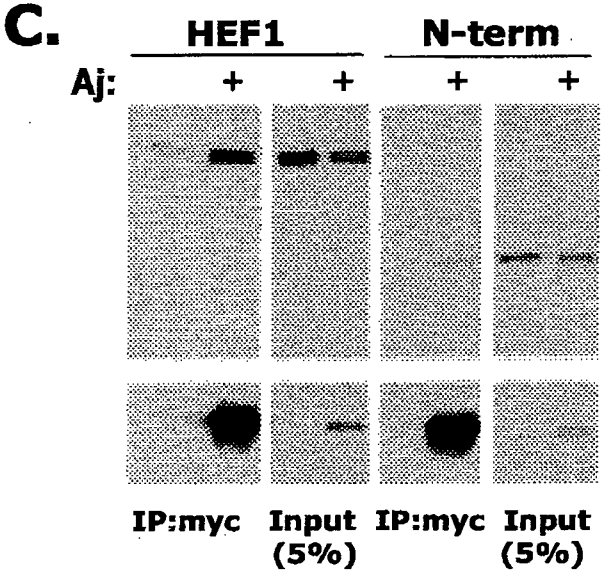
C.
HEF1
N-term
Aj:
+ + + +
IP:myc
Input (5%)
IP:myc
Input (5%)

Figure 6

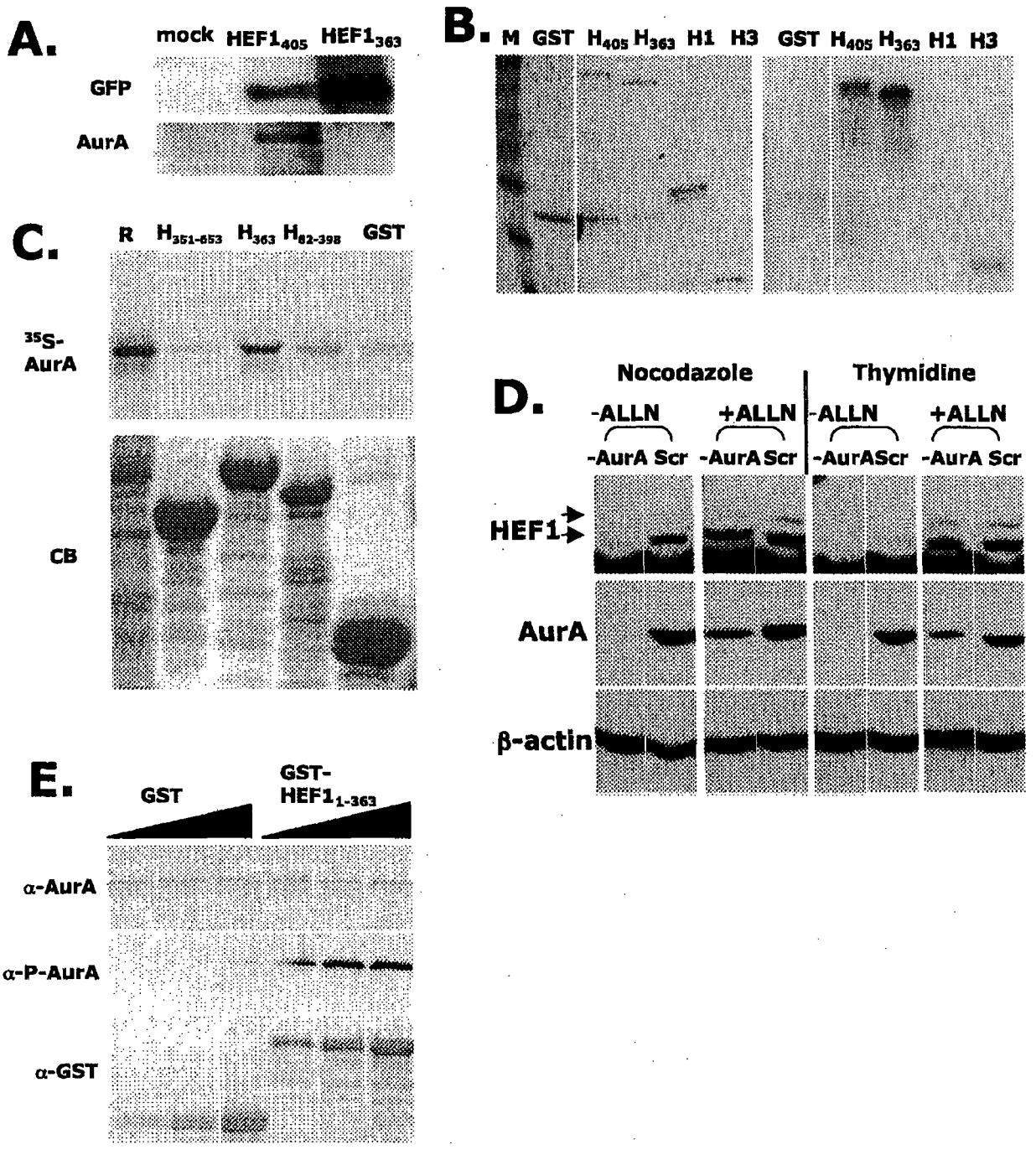
A.
mock
HEF1405
HEF1363
GFP
AurA
B.
M
GST
H405
H363
H1
H3
GST
H405
H363
H1
H3
C.
R
H351-653
H363
H82-398
GST
35S-AurA
CB
D.
Nocodazole
Thymidine
-ALLN
+ALLN
-ALLN
+ALLN
-AurA
Scr
-AurA
Scr
-AurA
Scr
-AurA
Scr
HEF1
AurA
β-actin
E.
GST
GST-HEF11-363
α-AurA
α-P-AurA
α-GST

Figure 7

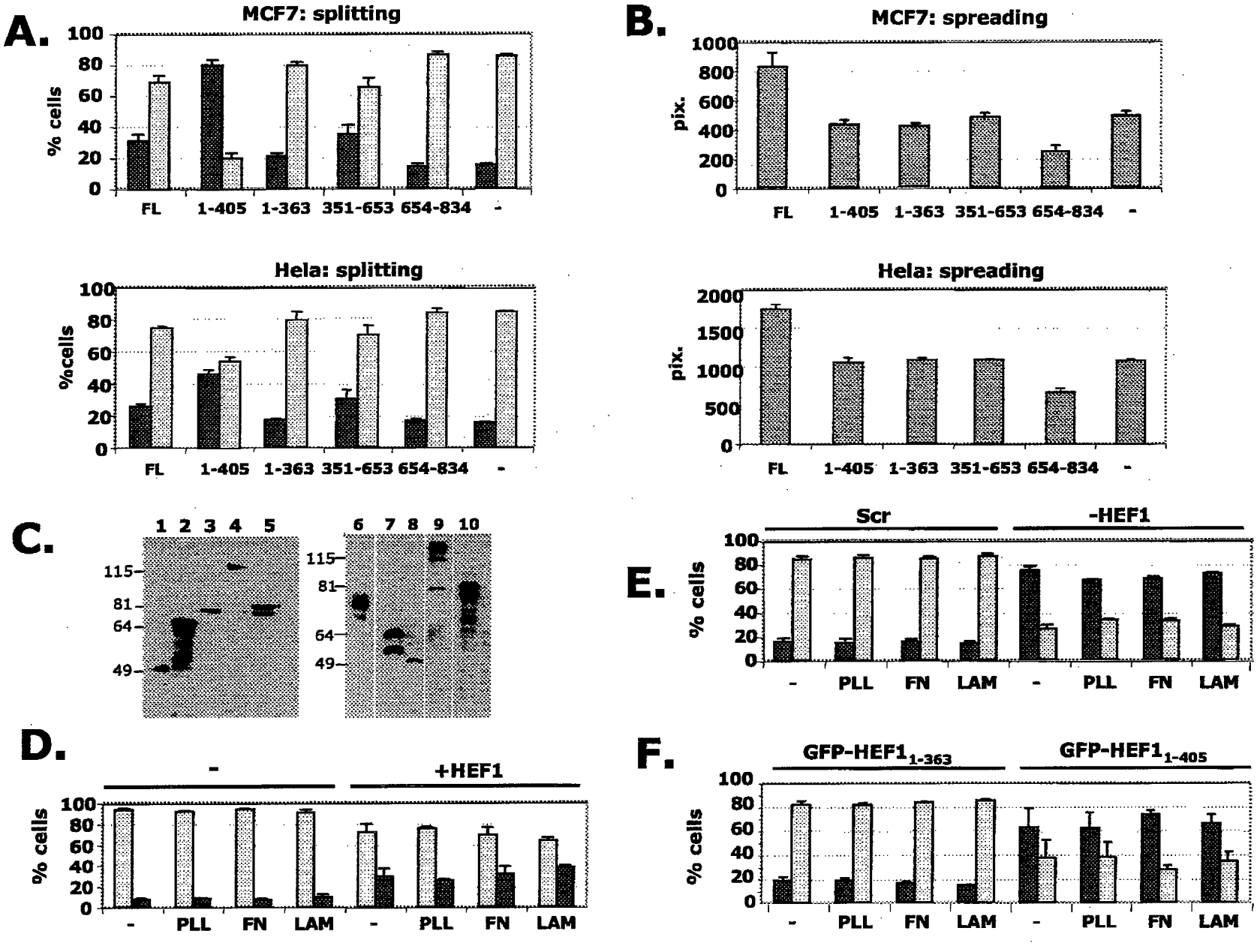
A.
MCF7: splitting
% cells
100
80
60
40
20
0
FL
1-405
1-363
351-653
654-834
-
Hela: splitting
%cells
B.
MCF7: spreading
pix.
1000
800
600
400
200
Hela: spreading
2000
1500
1000
500
C.
1 2 3 4 5
6 7 8 9 10
115
81
64
49
D.
-
+HEF1
PLL
FN
LAM
E.
Scr
-HEF1
F.
GFP-HEF1$_{1-363}$
GFP-HEF1$_{1-405}$

Figure 8

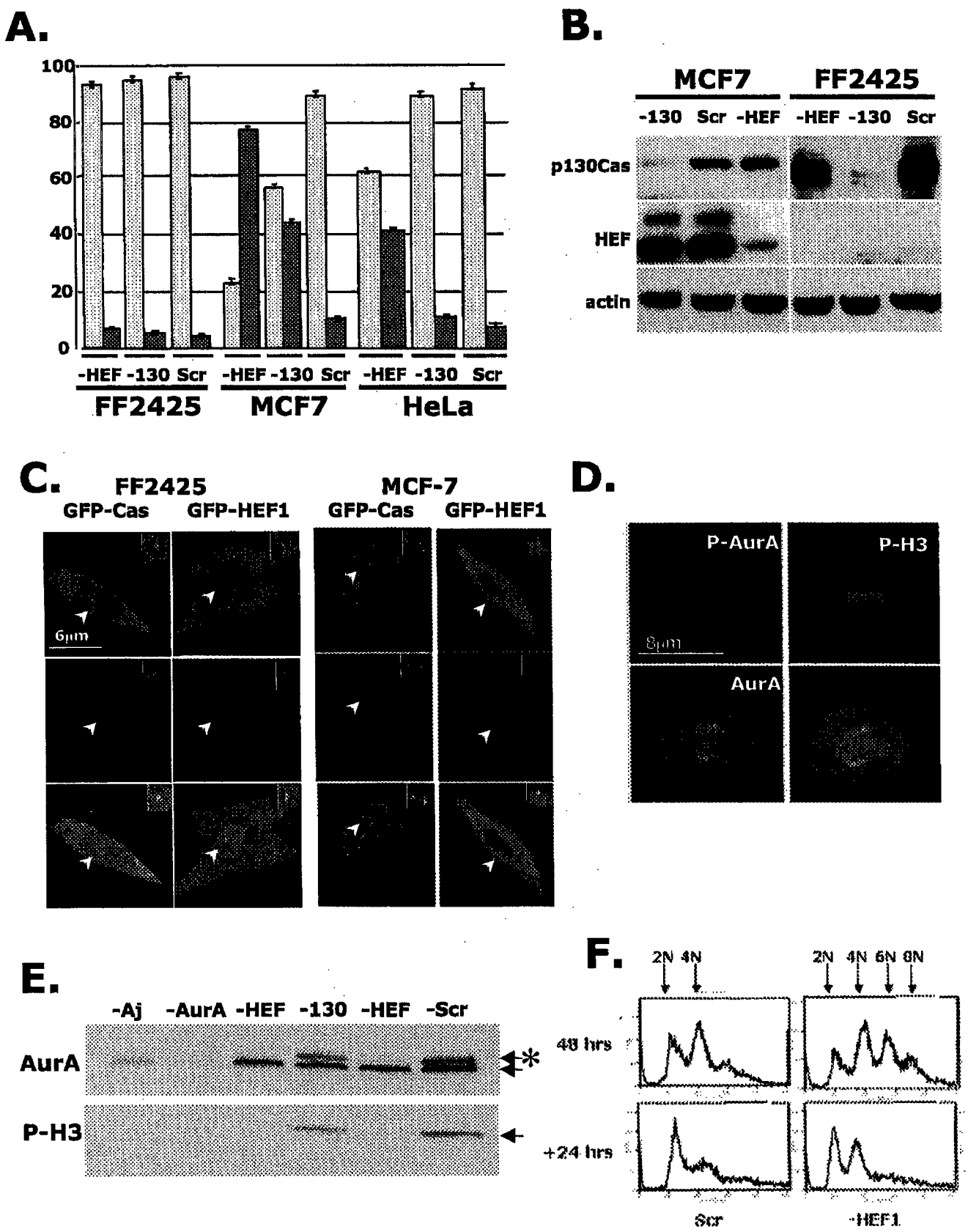
A.
100
80
60
40
20
0
-HEF -130 Scr -HEF -130 Scr -HEF -130 Scr
FF2425 MCF7 HeLa
B.
MCF7 FF2425
-130 Scr -HEF -HEF -130 Scr
p130Cas
HEF
actin
C.
FF2425 MCF-7
GFP-Cas GFP-HEF1 GFP-Cas GFP-HEF1
6μm
D.
P-AurA
P-H3
8μm
AurA
E.
-Aj -AurA -HEF -130 -HEF -Scr
AurA
P-H3
F.
2N 4N
2N 4N 6N 8N
48 hrs
+24 hrs
Scr
HEF1

* Cover Letter

6 October 2004

To the Editors,

The accompanying manuscript, "HEF1 regulates centrosomal maturation and spindle formation through control of the Aurora-A kinase", authors Pugacheva et al., was originally submitted to Cell on July 16th, 2004 (see initial cover letter, below). At that time, it was assigned the correspondence number CELL-D-04-00848, and read by Dr. Bodo Stern. Although his initial decision (7/22) was not to send out the manuscript for review, he expressed considerable interest in the findings, and stated that the manuscript would certainly be sent out for review if we would add additional experiments that addressed the relationship between the HEF1 phenotypes in centrosome maturation that we newly define therein, and the previously established role of HEF1 in cell attachment. In this modified manuscript, we have extensively addressed these points, as suggested by Dr. Stern. In a new figure 7, we have used a series of HEF1 derivative proteins to identify the domains required for centrosomal localization, thereby identifying a dominant negative element for centrosomal maturation. We have determined that this dominant negative domain is distinct from a second domain that has a dominant negative function for cell spreading. We have additionally plated cells with altered HEF1 expression on different adhesive matrices, and shown that changing the degree of cell adhesion does not impact the HEF1 affects on centrosomes. These new studies allow us to state more clearly that HEF1 possesses distinct activities in two different spheres of cell biology, and provide mechanistic insights into the protein interactions required for the execution of the novel HEF1 centrosomal activity: an exciting new merging of attachment and cell cycle signaling!

We believe that this manuscript should be of interest to researchers in diverse fields, and may accordingly benefit from being reviewed by researchers with different scientific perspectives. Scientists with appropriate expertise for the subject matter covered include Dr. Eric Nigg (Aurora A function); Drs. Greenfield Sluder, Jeffrey Salisbury, and Alexey Khodjakov (centrosome functions); Drs. Tony Hunter, Steven Frisch, Thomas Parson, and Alan Horwitz (cell attachment, with some emphasis on the Cas family): we note, we do not have close or collaborative relationships with any of these individuals. Because of possible competitive issues in the area of Ajuba studies, we would request that Dr. Hideyuki Saya not be a reviewer of the paper. We are very pleased to have the chance to have our study reviewed by your journal, and we thank you for the opportunity.

Sincerely,

Fox Chase Cancer Center
333 Cottman Ave.
Philadelphia, PA 19111 USA
(215) 728-2860 ph, -3616 fax
EA_Golemis@fccc.edu

16 July 2004

To the Editors,

We would like you to consider the accompanying manuscript, "HEF1 regulates centrosomal maturation and spindle formation through control of the Aurora-A kinase", authors Pugacheva et al., for publication in Cell. We are extremely excited by the results described in this study, and believe that they will be of general interest to the community of biologists. The main finding of this paper is the definition of the HEF1 protein as a bridge between the cell attachment and the mitotic machinery. HEF1 has a well-established biological function as a component of the focal adhesion-associated integrin signaling pathway. In this report, we show that HEF1 also functions at the centrosome, controlling the activation state of the AuroraA kinase; and that either up- or down-regulation of HEF1 protein levels results in severe defects in centrosomal maturation and mitosis. This report thus brings together two completely separate areas of study, and provides completely novel insight into the mechanism by which cell adhesion factors may regulate cell cycle progression. We thank you for your consideration.

Sincerely,

Fox Chase Cancer Center
333 Cottman Ave.
Philadelphia, PA 19111 USA
(215) 728-2860 ph, -3616 fax
EA_Golemis@fccc.edu

Editorial Manager(tm) for Cell
Manuscript Draft

Manuscript Number:

Title: HEF1 regulates centrosomal maturation and spindle formation through control of the Aurora-A kinase.

Article Type: Research Article

Section/Category:

Keywords: HEF1; centrosome; attachment; spindle; mitosis; Aurora-A; Ajuba

Corresponding Author: Dr. Erica Golemis Fox Chase Cancer Center

First Author: Elena N Pugacheva, Ph.D.

Order of Authors: Elena N Pugacheva, Ph.D.; Yungfeng Feng; Gregory D Longmore, Ph.D.; Erica Golemis, Ph.D.

Abstract: The HEF1 scaffolding protein has a well-defined role in mediating integrin-dependent attachment signaling at focal adhesions. We have previously shown that HEF1 relocalizes to the spindle asters at mitosis, but the significance of this migration was unclear. We report here that HEF1 controls mitotic spindle formation through action at centrosomes in the G2 phase of cell cycle. Increased levels of HEF1 induce supernumerary centrosomes, and multipolar spindles. Conversely, depletion of HEF1 results in premature centrosomal splitting, monoastral or asymmetric spindles, and transient appearance of >4N populations. The G2/M localization profile and overexpression phenotypes of HEF1 resemble those of the mitotic regulator Aurora A (AurA) kinase. We show that HEF1 associates with and controls activation of AurA at the centrosome, with these interactions mediated in part through HEF1 interactions with the AurA-associated protein Ajuba. These results suggest a novel mechanism for the coordination of cell attachment status with cell division in mitosis, and may provide insight into the induction of genomic instability in cancer.

THE CODON 47 POLYMORPHISM IN p53 IS FUNCTIONALLY SIGNIFICANT

Xiaoxian Li*, Patrick Dumont*, Anthony Della Pietra, Cory Shetler and Maureen E. Murphy
From the Cell and Developmental Biology Program, Fox Chase Cancer Center, Philadelphia PA 19111

Running title: Serine 47 polymorphism impairs p53 function

Address correspondence to: Maureen E. Murphy, Cell and Developmental Biology Program, Fox Chase Cancer Center, 333 Cottman Avenue, Philadelphia PA 19111, Tel. 215 728-5684; Fax. 215 728-4333; E-Mail Maureen.Murphy@FCCC.edu
*These authors contributed equally.

In addition to a common polymorphism at codon 72, the p53 tumor suppressor gene also contains a rare single nucleotide polymorphism at amino acid 47. Wild type p53 encodes proline at this residue, but in less than 5% of African Americans this amino acid is serine. Notably, phosphorylation of the adjacent serine 46 by the proline-directed kinase p38 MAPK is known to greatly enhance p53's ability to induce apoptosis. Here we show that the serine 47 polymorphic variant, which replaces the proline residue necessary for recognition by proline-directed kinases, is a markedly poorer substrate for phosphorylation on serine 46 by p38 MAPK. Consistent with this finding, we show that the serine 47 variant has up to five-fold decreased ability to induce apoptosis compared to wild type p53. Mechanistically we find that this variant has decreased ability to transactivate two p53-target genes, p53AIP1 and PUMA, but not other p53-response genes; this is the first time that phosphorylation of serine 46 has been implicated in transactivation of PUMA by p53. Down-regulation of PUMA in cells with wild type p53 using short interfering RNAs reduces apoptosis in these cells to a level comparable to that in cells containing the serine 47 variant. The combined data indicate that, like the codon 72 polymorphism, the codon 47 polymorphism of p53 is functionally significant, and may play a role in cancer risk, progression, and the efficacy of therapy.

We recently reported that a common polymorphism in p53 at codon 72 is functionally significant. Codon 72 of p53 can encode either arginine (R72) or proline (P72). We found that the R72 form of p53 has up to 15-fold increased apoptotic ability compared to the P72 form, in both inducible cell lines and in cells with endogenous p53 homozygous for each variant (1). At least part of the increased apoptotic potential of R72 is due to enhanced mitochondrial localization of this protein, where we have found that p53 can interact directly with the pro-apoptotic protein BAK, displacing Mcl-1 and allowing BAK oligomerization (2). These functional studies on the codon 72 polymorphic variants of p53 have led to a number of studies testing the impact of this polymorphism on the risk and progression of human cancer. Several of these reports indicate that the lesser apoptotic P72 form is associated with increased risk of cancer (3-5). Another report indicated that individuals in families predisposed to colon cancer who are homozygous for the P72 allele have an earlier age of onset for cancer, and tend to have increased tumor number, compared to individuals homozygous for R72 (6). Recently a polymorphism in the gene encoding MDM2, which negatively regulates p53, was shown to lead to attenuated p53 function and increased cancer risk (7). The combined data support the premise that identification of functionally significant polymorphisms in the p53 tumor suppressor gene will have an impact on our understanding of genetic determinants of cancer risk and progression.

In the present report we provide data that another polymorphism in p53, at codon 47, is also functionally significant. Codon 47 encodes proline in wild type p53, but in a small subset of individuals it can encode serine (CCG -> TCG). A single study, performed over ten years ago, was done on the serine 47 (S47) polymorphic variant. In that study, the S47 polymorphism was found in less than 5% of African Americans, and not at all in Caucasians (8). A preliminary functional analysis failed to reveal differences between S47 and wild type p53; importantly however, the

ability to induce apoptosis was not assessed (8). Additionally, it was not known at that time that phosphorylation of the adjacent residue, serine 46, was critical for p53's ability to induce apoptosis.

One of the kinases that directly catalyzes serine 46 phosphorylation is the proline-directed kinase p38 MAPK. The importance of serine 46 phosphorylation to apoptosis induction by p53 is epitomized by the findings that mutation of serine 46 to alanine, incubation with specific chemical inhibitors of p38 MAPK, or overexpression of proteins that inhibit p38 MAPK, have all been shown to markedly inhibit p53-dependent apoptosis (9-14). Significantly, the serine 47 polymorphism in p53 replaces the proline residue necessary for phosphorylation of serine 46 by proline-directed kinases like p38 MAPK, raising the possibility that the S47 variant has decreased phosphorylation on serine 46, and impaired apoptotic ability.

In this report we present data indicating that the serine 47 polymorphic variant is a poorer substrate for phosphorylation by p38 MAPK. Consistent with this we show that in multiple clones of stably transfected cells containing equivalent levels of p53, the S47 variant has up to 5-fold decreased ability to induce programmed cell death, compared to wild type p53. This decreased ability to induce programmed cell death is accompanied by a decreased ability to transactivate p53AIP1 and the pro-apoptotic p53 target gene PUMA, but not other p53 target genes. PUMA (p53-upregulated mediator of apoptosis) is known to be a critical mediator of p53-dependent apoptosis. Down-regulation of PUMA using short interfering RNAs reduces the ability of wild type p53 to induce apoptosis, to levels roughly equivalent to the S47 variant. The combined data indicate that the codon 47 polymorphism in p53 is functionally significant, and suggest that the influence of this polymorphism on altered cancer risk in African Americans should be assessed.

Materials and Methods

Human studies, genotyping analysis - All human subjects were collected with the approval of the Fox Chase Cancer Center Institutional Review Board. DNA was isolated from peripheral blood collected from 200 African Americans from the Biosample Repository at Fox Chase Cancer Center. PCR amplification of a 241 bp fragment of p53 exon 4 was carried out in a 25 µl reaction containing 20 ng genomic DNA and 0.2 µM primers (forward-5'CAC CCA TCT ACA GTC C and reverse-5' ACC GTA GCT GCC CTG GTA G) with JumpStart RedTaq Readymix (Sigma). The reverse primer was biotinylated to facilitate single-strand DNA template preparation for pyrosequencing. Primers were synthesized and HPLC-purified by Thermo Hybaid Interactiva Division (Ulm, Germany). Cycle conditions were as follows: 95°C for 5 min followed by 35 cycles of 95°C for 30 sec, 50°C for 30 sec and 72°C for 45 sec. Amplicon size and purity was verified on a 2% agarose gel containing 0.5 ug/ml ethidium bromide (Life Technologies; Rockville, MD). Single-stranded DNA template preparation was performed in a 96-well plate. The biotinylated strand was immobilized onto streptavidin-coated Sepharose beads (Amersham Pharmacia Biotech) and processed using the PSQ 96 Sample Preparation Kit (Pyrosequencing AB) according to manufacturer's instructions. The template was incubated with a sequencing primer specific for codon 47 (5'GGA TGA TTT GAT GCT GTC) and automatically analyzed on a PSQ 96 Instrument (Pyrosequencing AB) using the PSQ 96 SNP Reagent Kit (Pyrosequencing AB). Genotyping and quality assessment of the raw data was performed using PSQ 96 SNP Software (Pyrosequencing AB).

Plasmid Construction - The human p53 cDNA construct encoding temperature sensitive p53 (valine 138, ref. 15) and the GST-p53 (1-92) construct (1) were modified by site-directed mutagenesis using Stratagene's Quick-Change Kit. The A46 p53 mutant was made by introducing alanine at codon 46 using primers: 5'-GATTTGATGCTGGCCCCGGACGATATTG-3' and 5'-CAATATCGTCCGGGGCCAGCATCAAATC-3'. The S47 p53 polymorphic variant was made using primers: 5'-GATTTGATGCTGTCCTCGGACGATATTGAA C-3' and 5'-GTTCAATATCGTCCGAGGACAGCATCAAA TC-3'. The serine 33 to alanine GST-p53 (1-92) was mutated using primers: 5'-AACAACGTTCTGGCCCCCTTGCCGTCC-3' and 5'-

GGACGGCAAGGGGGCCAGAACGTTGTT-3′. These mutations were confirmed by DNA sequencing. All p53 constructs have proline at codon 72.

Cell culture, p53 induction - H1299 and Saos2 cell lines containing temperature-sensitive p53 were generated by stable transfection with CMV promoter-driven human p53 cDNA containing the temperature-sensitive Valine 138 mutation. These H1299 and Saos2 cells were maintained at 39°C in Dulbecco's Modified Eagle medium (DMEM) supplemented with 10% fetal bovine serum (FBS), 100 U/mL penicillin and streptomycin, and 400μg/mL (Saos2) or 800μg/mL (H1299) G418 in a 5% CO_2 humidified atmosphere. For temperature shift and p53 induction, cells were plated at $2x10^6$ cells per 100-mm plate and either shifted to 32°C (active p53) or maintained at 39°C (mutant conformation p53). For experiments with the p38 kinase inhibitor, cells were incubated with SB-203580 (Upstate Biotechnology) to a final concentration of 40 uM, or vehicle alone (DMSO) for 30 minutes prior to temperature shift or irradiation. Cells were irradiated with 7.5 J/m2 of UV with a Spectroline X series UV lamp, and output was measured with a traceable UV light meter (Fisher Scientific).

Western and Northern analysis - Western analysis was performed as described (1). Antisera for p53 (Ab-6, Calbiochem), phosphorylated p53 (Cell Signalling), PUMA (Oncogene Sciences), MDM2 (Oncogene Sciences) and p21/waf1 (Oncogene Sciences) were used at 1:1000 dilution, and antisera for cleaved PARP (p85PARP, Promega) was used at 1:400 dilution. For analysis of RNA, cells were harvested 24 hrs after temperature shift and total RNA was prepared using Trizol (Invitrogen) or via cesium chloride gradients, as described (16). Polyadenylated RNA was purified from cesium gradient total RNA using Poly A Quick columns, as per the manufacturer (Stratagene). Eight micrograms of total RNA, or two micrograms polyA RNA were resolved by denaturing agarose gel electrophoresis, transferred onto a nylon membrane, hybridized with probes and exposed to an X-ray film as described, as described (16).

Preparation of GST fusion proteins, p38 MAPK and HIPK2 kinase assays - GST fusion proteins were generated exactly as described (1, 2). The GST-p53 proteins were concentrated using Microcon columns as per the manufacturer (Millipore). For the *in vitro* p38 MAPK kinase reactions, the indicated amounts of purified GST-p53 (wt, S47 or A46) or myelin basic protein (MBP, Sigma) were mixed with 10μL ADBI buffer (20mM Tris, pH 7.4, 20mM β-glycerol phosphate, 5mM EGTA, 1mM Na_3VO_4, 1mM DTT and 20mM $MgCl_2$), 0.6 mM cold ATP, 20 μCi [γ-^{32}P] ATP (NEN), and 100 ng active p38β2 (Upstate Biotechnology). After a 15 min incubation at 30°C, the reaction was stopped by adding Lithium Dodecyl Sulfate and boiling for 10 min. The samples were loaded on a Nupage Novex 10% Bis-Tris gel (Invitrogen), and the gel was dried and exposed to X-ray film. For the HIPK2 kinase assays, the cDNA encoding flag-tagged HIPK2 or a kinase-dead version of this enzyme (kindly provided by Ettore Appella, National Institutes of Health) were transfected into H1299 cells using FuGene (Roche). After 24 hours cells were harvested and HIPK2 was immunoprecipitated from 400 ug of lysate with anti-flag antibody (M2, Sigma). These immunoprecipitates were washed and incubated as described (17) with 20 ug of GST-p53 (1-92) or GST-S47.

Apoptosis assays, siRNA studies - Temperature-sensitive H1299 clones were seeded onto 6-well plates at a density of 50,000 cells per well. Saos2 cells were plated at 1 x 10^6 cells/100-mm plate. Cells were shifted to 32°C and harvested at the times indicated after temperature shift. Control cells were maintained at 39°C. TUNEL and multi-caspase assays were conducted using the Guava Personal Cytometer (Guava Technologies) using protocols provided by the manufacturer (Guava Technologies). For the siRNA studies, equal number of H1299 cells with temperature sensitive wt p53 were seeded onto a 10-cm plate; after 24 hours 25 uL of siRNA for PUMA (20 uM BBC3 SmartPool oligos, Dharmacon) or control RNA (20 uM, Dharmacon) were transfected using Oligofectamine as per the manufacturer (Invitrogen). After 24 hours of temperature shift cells were harvested and subjected to Western analysis as described above.

Results

A previous study by Harris and colleagues first described the existence of a coding region polymorphism in the p53 gene at codon 47. This codon encodes proline in wt p53, but these researchers found it encodes serine in less than 5% of African Americans (8). Codon 47 occurs in exon 4 of p53, where we have shown another functionally significant polymorphism, at codon 72, also exists. Before testing the hypothesis that the S47 and wild type p53 proteins might have altered apoptotic function, it was necessary to determine the frequency with which this polymorphism was linked to either codon 72 variant (P72 or R72). Toward this end, we analyzed both the codon 47 and the codon 72 polymorphisms in genomic DNA isolated from 200 African Americans from the Fox Chase Cancer Center Biosample Repository. We identified four DNA samples that were heterozygous for the S47 variant, for an allele frequency of 1% (4/400 alleles); this is somewhat less than the previous study, although that study had considerably smaller sample size. Sequence analysis revealed that in all four cases the S47 allele occurred in *cis* with the proline 72 polymorphism (P72). This suggests that the S47 and P72 polymorphisms may be linked. Therefore, for this study we focused on the S47 allele in *cis* with P72 (which we designate S47), and we compare it to the P72 protein, which we designate as wild type (wt) p53.

p38 MAPK is a proline-directed kinase, and requires a proline residue adjacent to the target phosphorylation site for efficient recognition of that site; notably, the S47 polymorphism replaces this proline with serine (Fig. 1A). In order to test the hypothesis that the S47 polymorphism alters serine 46 phosphorylation by p38 MAPK, we created GST fusion proteins representing amino acids 1-92 of wt p53 (wt) and the S47 variant (S47). As a control for these studies we generated a p53 construct in which serine 46 was mutated to alanine (A46). Because serine 33 is also phosphorylated by p38 MAPK (Fig. 1A), initially these constructs were generated with an alanine substitution at amino acid 33; this replacement has no effect on phosphorylation of serine 46 (17 and our unpublished results). Increasing amounts of GST-p53 and GST-S47 were incubated with a constant amount of purified active p38 MAPK (Upstate Biotechnology) and γ^{32}P-ATP, using kinase conditions previously described (9). Phosphorylated p53 was then resolved by SDS-PAGE and autoradiography. As depicted in Figure 1, wt p53 was efficiently phosphorylated by p38 MAPK. In contrast, the S47 variant protein was phosphorylated markedly less well (Fig. 1B). As expected, neither GST alone nor the A46 mutant was detectably phosphorylated under these conditions (Fig. 1B). Coomassie staining of the input proteins confirmed equal loading and purity of the wt, S47 and A46 substrates (Fig. 1C). Notably, decreased phosphorylation of the S47 variant by p38 MAPK was also evident using GST fusion proteins that retained serine at amino acid 33, except that the background level of phosphorylation was higher (Supplementary Fig. 1).

The Michaelis Menton model was fit to the averaged data from three independent p38 MAPK kinase experiments performed using S47 and wt p53 as substrates. This modeling revealed a three-fold decrease in the K_m, and an eight-fold decrease in the V_{max}, for S47 compared to wt p53 (Fig. 1D). These data suggest that the S47 protein binds reasonably well to p38 MAPK, but that the ability of this enzyme to phosphorylate serine 46 is markedly reduced. To control against the possibility that the S47 protein was denatured or misfolded, we tested the ability of another kinase, the homeo-domain interacting protein kinase-2 (HIPK2) to phosphorylate S47 and wt p53. Like p38 MAPK, HIPK2 also phosphorylates serine 46, but it is not reported to be a proline-directed kinase (17, 19). As shown in Figure 1E, following transfection into p53 null cells, immunoprecipitated FLAG-tagged HIPK2 was able to phosphorylate S47 and wt p53 proteins identically. In contrast, a kinase dead version of HIPK2 (K221R, ref. 17) did not detectably phosphorylate either protein (Fig. 1E). These data indicate that the S47 variant of p53 is impaired for phosphorylation on serine 46 by the proline-directed kinase p38 MAPK.

We next determined whether the S47 polymorphism alters p53 apoptotic function *in vivo*. We generated stably-transfected cell lines containing inducible versions of wild type p53 (wt) and the S47 variant, as well as the A46 mutant. These p53 variants were generated using

the temperature sensitive version of p53 encoding valine at amino acid 138. This temperature-sensitive form p53 is well characterized; the p53 protein is denatured and inactive when cells are cultured at 39 degrees. Temperature shift of cells to 32 degrees results in wild type p53 conformation and apoptosis induction (15, 20). Twenty independent clones for each variant (wt, S47 and A46) were generated in the human lung adenocarcinoma cell line H1299 (p53-/-), which was chosen because it contains high levels of active p38 MAPK, as determined by western blotting using antisera specific for the active enzyme (Supplementary Fig. 2). Two clones for each variant were selected for further analysis based upon western analysis indicating comparable levels of p53 protein (Fig. 2A, inset western). These six clones were analyzed for apoptosis induction following temperature shift using TUNEL assay (terminal dUTP nick end labeling); additionally, three of these clones (wt-clone 4, S47-clone 8 and A46-clone 8) were further analyzed using an assay that measures multi-caspase activation. As depicted in Figure 2, TUNEL analysis following temperature shift indicated that the S47 variant consistently had between 2 to 5-fold decreased ability to induce apoptosis, relative to wt p53, while the A46 variant was almost completely compromised for apoptosis induction (Fig. 2A). Consistent with this, analysis of multi-caspase activation indicated that the S47 variant had significantly decreased ability to activate caspases, relative to wt p53 ($p<0.001$). The ability of A46 to induce apoptosis was more compromised than S47 (Fig. 2B), possibly due to residual phosphorylation of S47 by p38 MAPK or HIPK2.

To confirm these findings in another cell background, we generated stably-transfected wt and S47 cell lines in the p53-null human osteosarcoma cell line Saos2. Again, clones were selected that contained equivalent levels of p53 (Fig. 2C, inset western). For this comparison we also included a Saos2 cell line containing an inducible version of the arginine 72 (R72) polymorphic variant; in this way, all three polymorphic variants of p53 could be compared for apoptosis induction (S47, P72 and R72). As shown in Figure 2C, TUNEL analysis following temperature shift in these cell lines indicated there was an over 2-fold decrease in apoptosis in the S47 cell line compared to wild type p53 (P72, $p = 0.01$), and a 7-fold decreased ability when compared to R72 ($p<0.001$).

We extended these analyses to include a time course of apoptosis in the inducible wt, S47 and A46 cell lines following exposure to gamma radiation (clones wt-4, S47-8 and A46-8 from Figure 2, which were analyzed for the remainder of this study). In this experiment, apoptosis was measured as the appearance of the 85 kDa caspase cleavage product of Poly (ADP) ribose polymerase (PARP), using an antibody specific for this caspase cleavage product (p85 PARP). Decreased abundance of p85 PARP following induction of S47 compared to wt p53 could be seen at all time points, although at later time points the difference was more marked (2-fold difference at 6 hours, and 10-fold difference at 24 hours, see Fig. 3A). Similar findings were made following treatment with doxorubicin as the source of DNA damage (not shown). We next examined the phosphorylation pattern of p53 in these inducible cell lines following temperature shift, using antisera specific for p53 phosphorylated at serines 15, 46 or 392. These analyses revealed no difference in the phosphorylation pattern on serines 15 or 392 between the wt, S47 and A46 proteins (Fig. 3B). As expected there was a marked decrease in reactivity of the S47 variant for the serine 46 phospho-specific antibody, although we cannot rule out the possibility that the proline-to-serine change in the S47 variant interferes with recognition by this antibody. Interestingly, despite clear differences in apoptosis induction, we saw no evidence of a gross difference in the transactivation potential of these proteins. The ability of the S47 and A46 variants to transactivate the p53-response genes MDM2 and p21/waf1 was indistinguishable from wt p53 in a time course following radiation (MDM2, see Fig. 3A) or following temperature shift (p21 and MDM2, Fig. 3B).

The combined data support the hypothesis that the S47 variant has impaired apoptotic ability relative to wt p53, due in part to decreased phosphorylation on serine 46 by p38 MAPK. To solidify these findings, we made use of a well-characterized inhibitor of p38 MAPK, SB-203580 (9). Specifically, we temperature-shifted our inducible H1299 clones in the presence of SB-203580 or dilution vehicle, and apoptosis

induction and the phosphorylation pattern of p53 were assessed. As depicted in Figure 4, western analysis using an antibody specific for phosphorylated serine 46 confirmed that the p38 MAPK inhibitor effectively inhibited phosphorylation on this residue. Prior to temperature shift wt p53 was already phosphorylated on serine 46 (Fig. 4A, lane 1, S-46), and following temperature shift this phosphorylation of p53 increased approximately 2-fold (lane 4, S-46). In contrast, temperature shift in the presence of SB-203580 reduced serine 46 phosphorylation to starting levels (lane 7, S-46). As expected, this decrease in serine 46 phosphorylation was accompanied by a marked decrease in apoptosis (compare p85 PARP, lanes 4 and 7). Notably, incubation with SB-203580 brought the levels of the p85 PARP caspase cleavage product and TUNEL positive cells to levels comparable to the untreated S47 variant (Figs. 4A and 4B, respectively), indicating that the different apoptotic potential of the S47 and wt p53 proteins reflects altered serine 46 phosphorylation. SB-203580 also marginally inhibited apoptosis induced by the S47 variant, possibly due to residual phosphorylation of serine 46, or to phosphorylation of serine 33 by p38 MAPK, which can also play a role in apoptosis induction (9). Consistent with these data, we found that the SB-203580 inhibitor also effectively inhibited phosphorylation of serine 46, and apoptosis (p85 PARP appearance), in MCF-7 cells (wt p53) treated with ultra-violet light (Fig. 4C).

It has been reported previously that serine 46 phosphorylation is not required for the ability of p53 to transactivate the majority of target genes. However, at least one, the pro-apoptotic target gene p53AIP1, requires this phosphorylation event for efficient transactivation (10). In line with this, we analyzed poly-adenylated RNA isolated from our inducible H1299 cell lines, and found that while there was a modest induction of p53AIP1 in cells containing wt p53, there was no evidence for induction in lines containing the S47 or A46 variants (Fig. 5A). Unfortunately we have been unable to detect p53AIP1 protein using commercially available antibodies, possibly because the level of p53AIP1 in the cell types employed in this study (H1299, Saos2 and MCF-7) is extremely low following p53 induction. The low level of p53AIP1 in these cells prompted us to broaden this analysis to include other p53-target genes. Northern analysis of total RNA for the level of other p53 response genes revealed no difference in the ability of S47, A46 and wt p53 proteins to transactivate the p53-induced genes *Killer/DR5*, *Gadd45*, *p21/waf1*, *Mdm2* or *bax*, or to repress the genes encoding *survivin* or *cyclin B1*, either in a time course (not shown) or following 24 hours of temperature shift (Fig. 5B) Interestingly, however, there was a consistent decrease in the ability of the S47 and A46 variants to transactivate the p53 response gene PUMA. Western analysis confirmed that the S47 variant had a decreased ability to induce PUMA (2-fold decrease compared to wt p53 at 8 hours, 7-fold decrease at 24 hours, see Fig. 5C), but not the p53 target gene MDM2. Decreased PUMA levels correlated with decreased apoptosis, as measured by the appearance of p85 PARP (Fig. 5C). These data suggest that PUMA transactivation is sensitive to serine 46 phosphorylation. In support of this premise, we found that the p38 MAPK inhibitor SB-203580 efficiently inhibited PUMA transactivation in MCF-7 cells following treatment with ultra-violet light (Supplementary Fig. 3).

In order to confirm the significance of decreased PUMA transactivation to the reduced apoptotic potential of the S47 polymorphic variant, we used transfection of short interfering RNA oligonucleotides specific for the PUMA transcript to reduce its level in cells with inducible wt p53. Apoptosis in these cells was measured as the appearance of the caspase cleavage product p85 PARP. As depicted in Figure 6, western analysis of cells treated with siRNA specific for PUMA (SmartPool RNA, Dharmacon), or control scrambled RNA, indicated that the PUMA siRNA efficiently reduced the levels of this transcript, while the control siRNA had no effect. Exposure to siRNA for PUMA, or control oligos, had no effect on the ability of p53 to transactivate MDM2 (Fig. 6). Significantly, reduction of PUMA in cells with wt p53 reduced the level of apoptosis in these cells to a level equivalent to cells containing the inducible S47 variant (Fig. 6). These data support the premise that impaired transactivation of PUMA underlies at least part of the apoptotic defect of the S47 variant of p53.

Discussion

Our data indicate that the S47 variant of p53 has decreased ability to serve as a substrate for phosphorylation by p38 MAPK, as well as 2 to 5-fold decreased ability to induce apoptosis *in vivo*. Underlying this apoptotic defect we have found that the S47 variant exhibits decreased ability to transactivate the p53 response genes p53AIP1 and PUMA. In contrast, we have seen no differences in the ability of S47 to bind to DNA, induce G1 arrest, or to localize to mitochondria, compared to wt p53 (X. Li and M. Murphy, unpublished observations). These data are the first to suggest that the serine 47 polymorphism is functionally significant, and to implicate serine 46 phosphorylation in the transactivation of the p53 target gene PUMA. While the changes in PUMA transactivation by S47 appear to range only from 2- to 7-fold, transactivation of PUMA is known to be particularly critical for apoptosis induction by p53 (21-23). For example, even the heterozygous PUMA knock-out mouse (Puma +/-), with 2-3 fold reduction in PUMA levels, has a marked defect in apoptosis of irradiated thymocytes, compared to wild type mice (23).

Our data indicate that there are two polymorphisms in p53 that are functionally significant, at codons 47 and 72. It remains to be determined if the S47 polymorphism has an impact on cancer risk. In support of this possibility, missense mutations of amino acid 47 (proline to leucine) are reported in the p53 mutation data base (24).

It remains to be determined why functionally significant polymorphic variants in a tumor suppressor gene that decrease its function would persist in the human population. It is of note that both of the polymorphic variants of p53 that are associated with decreased apoptotic potential (P72 and S47) are more prevalent in populations whose origin is near the equator (Africa). This suggests that the selection for these variants may have occurred as a response to high exposure to ultraviolet light. We speculate that the decreased apoptotic potential of p53 may have been selected for in environments of high UV exposure in order to enable cells to more efficiently repair DNA, and perhaps also to accumulate the pigmentation necessary to inhibit excessive fixation of vitamin D, which can be toxic in such environments. In contrast, the higher apoptotic potential of the R72 variant, which is associated with skin of lighter pigmentation (25), would be selected for in environments where UV exposure was limited, and the increased absorption of UV rays afforded by lighter pigmentation would enhance vitamin D fixation. These hypotheses remain to be tested. The combined data suggest that a careful epidemiological analysis of the impact of the S47 polymorphism on cancer risk, progression, and the efficacy of chemotherapy and radiation therapy is warranted. Additionally, it will be important to determine if the ethnic bias of this polymorphism explains some of the differences in cancer incidence between Caucasian and African American populations

References

1. Dumont P, Leu JI, Della Pietra AC, George DL, Murphy M. (2003) *Nat Genet.* **33**:357-65.
2. Leu JI, Dumont P, Hafey M, Murphy ME, George DL. (2004) *Nature Cell Biology*, **6**:443-50.
3. Hishida A, Matsuo K, Tajima K, Ogura M et al. (2004) *Leuk Lymphoma* **45**:957-64.
4. Xi YG, Ding KY, Su XL, Chen DF, You WC, Shen Y, Ke Y (2004) *Carcinogenesis* **25**:2201-6.
5. Granja F, Morari J, Morari EC, Correa LA, Assumpcao LV, Ward LS. (2004) *Cancer Lett* **210**:151-7.
6. Jones JS, Chi X, Gu X, Lynch PM, Amos CI, Frazier ML. (2004) *Clin Cancer Res* **10**:5845-9.
7. Bond GL, Hu W, Bond EE, Robins H et al. (2004) *Cell* **119**:591-602.
8. Felley-Bosco E, Weston A, Cawley HM, Bennett WP, Harris CC (1993) *Am J Hum Genet.* **53**:752-9.
9. Bulavin DV, Saito S, Hollander MC, Sakaguchi K, Anderson CW, Appella E, Fornace AJ Jr. (1999) *EMBO J.***18**:6845-54 .
10. Oda K, Arakawa H, Tanaka T, Matsuda K et al. (2000) *Cell* **102**:849-62 .
11. Sanchez-Prieto R, Rojas JM, Taya Y, and Gutkind JS. (2000) *Cancer Res* **60**:2462-72.
12. Takekawa M, Adachi M, Nakahata A, Nakayama I, Itoh F, Tsukuda H, Taya Y, Imai K. (2000) *EMBO J.* **19**:6517-26 .
13. Bulavin DV, Demidov ON, Saito S, Kauraniemi P et al. (2002) *Nat Genet* **31**:210-215.
14. Okamura S, Arakawa H, Tanaka T, Nakanishi H, Ng CC, Taya Y, Monden M, and Y Nakamura. (2001) *Mol Cell* **8**:85-94.
15. Pochampally R, Li C, Lu W, Chen L, Luftig R, Lin J and Chen J. (2000) *Biochem Biophys Res Commun* **279**:1001-1010.
16. Murphy M, Ahn J, Walker KK, Hoffman WH, Evans RE, Levine AJ and George DL. (1999) *Genes & Dev* **13**:2490-2501.
17. D'Orazi G, Cecchinelli B, Bruno T, Manni I, et al. (2002) *Nat Cell Biol.* **4**:11-19.
18. Saito S, Yamaguchi H, Higashimoto Y, Chao C, Xu Y, Fornace AJ, Appella E and CW Anderson. (2003) *J Biol Chem* **278**:37536-37544.
19. Hofmann TG, Moller A, Sirma H, Zentgraf H, Taya Y, Droge W, Will H, and Schmitz ML. (2002) *Nat Cell Biol* **4**:1-10.
20. Martinez J, Georgoff I, Martinez J, Levine AJ. (1991) *Genes Dev.* **5**:151-9.
21. Yu J, Zhang L, Hwang PM, Kinzler KW, Vogelstein B. (2001) *Mol Cell* **7**:673-82.
22. Villunger A, Michalak EM, Coultas L, Mullauer F, Bock G, Ausserlechner MJ, Adams JM, Strasser A. (2003) *Science* **302**:1036-8.
23. Jeffers JR, Parganas E, Lee Y, Yang C, et al. (2003) *Cancer Cell* **4**:321-8.
24. Olivier M, Eeles R, Hollstein M, Khan MA, Harris CC, Hainaut P. (2002) *Hum Mutat.* **19**:607-14. (Database version R9, July 2004).
25. McGregor JM, Harwood CA, Brooks L, Fisher SA et al. (2002) *J Invest Dermatol.* **119**:84-90.

Figure Legends

Figure 1. The S47 polymorphic variant of p53 is impaired for phosphorylation by p38 MAP kinase.
A. Amino acid sequence of residues 30-57 of human wt p53, with the p38 MAPK phosphorylation sites underlined, and the site of the serine 47 polymorphism marked with an asterisk.
B. (Left panel) Kinase assay using purified p38 MAPK (Upstate Biotechnology) and the indicated concentration of purified GST-p53 and GST-S47 (both containing amino acids 1-92, with serine 33 replaced by alanine). (Right panel) p38 MAPK assay using myelin basic protein (MBP) as a positive control, and as a negative control, GST alone and GST (1-92) with serines 33 and 46 replaced with alanine (A46), 10 ug of substrate per reaction.
C. Coomassie stained gel verifying the loading and purity of GST fusion proteins used in A; Bovine serum albumin (BSA) is included as a standard.
D. The Michaelis Menton model was fit to the averaged data from three independent experiments performed in A, using GraphPad Prism v. 3.0a (GraphPad Software, San Diego CA). The K_m for wt p53 and S47 are indicated; the V_{max} for p38 MAPK for wt p53 is estimated to be eight-fold greater than for S47. Rate is indicated on the y axis as the densitometry units of phosphorylation per minute per microgram of enzyme.
E. Flag-tagged HIPK2, or a kinase-dead version of this enzyme, were immunoprecipitated with anti-flag antibody following transient transfection of H1299 cells and incubated with myelin basic protein (MBP), GST alone, GST-p53 or GST-S47 (the latter two encode amino acids1-92 of human p53, with alanine at amino acid 33).

Figure 2. The S47 variant has impaired ability to induce apoptosis, relative to wt p53.
A. TUNEL assay results from individual clones of cells stably transfected with inducible versions of p53, as indicated. Western analysis for total p53 in each clone is indicated in the inset. Values of TUNEL positive cells are given at 39 degrees (mutant p53) and 32 degrees (wild type p53 conformation) following twenty-four hours of temperature shift. Values given are the mean +/- standard error of measurement from three independent experiments. p values reflect comparison of indicated clones to clone wt-4.
B. Multi-caspase activity assay in clones wt-4, S47-8 and AP-8 from A, following twenty-four hours of temperature shift. Levels of caspase activity in uninduced samples (39 degrees, mutant conformation p53) were set to 1, and the fold increase is depicted. The values shown are the averaged results from three independent experiments, with standard error of measurement. The p value indicated is relative to clone wt-4 at 32 degrees.
C. TUNEL analysis of clones of Saos2 cells stably transfected with each p53 polymorphic variant (R72, P72 and S47), analyzed by western analysis for p53 level (see inset) and for TUNEL positive cells after twenty-four hours of temperature shift. Values are expressed as the mean +/- standard error of measurement. p values are given for each cell line (R72 and S47) compared to wt p53 (P72) at 32 degrees.

Figure 3. The S47 variant has reduced apoptotic ability, but apparently normal transactivation of MDM2 and p21/waf1.
A. Western analysis of apoptosis induction (appearance of the caspase-cleaved form of poly (ADP) ribose polymerase, p85-PARP) in cells harvested at the indicated timepoints after temperature shift. Just prior to temperature shift, cells were exposed to 6 Gy of radiation. The clones depicted are the same as those in Figure 2B. 39 degrees is mutant (inactive) p53, and 32 degrees is wild type conformation and activity. Levels of β-actin are included as a loading control.
B. Western analysis for p53 level, apoptosis (p85-PARP) and phosphorylated serines 46, 15 and 392, using phospho-specific antisera (Cell Signaling), as well as induction of the p53 target genes MDM2 and p21/waf1. Cells were temperature shifted for 24 hours. Levels of β-actin are included as a loading control.

Figure 4. The p38 MAPK inhibitor SB-203580 inhibits phosphorylation of p53 serine 46 and abrogates p53-dependent apoptosis.

A. Western analysis for the proteins indicated of H1299 clones containing the indicated inducible proteins (wt, S47 and A46) treated with the p38 inhibitor SB-203580 or vehicle alone (dimethyl sulfoxide, DMSO) 30 minutes prior to temperature-shift to 32 degrees to induce wild type p53 conformation. The data depicted are representative of three independent experiments. Levels of β-actin are included as a loading control.

B. Quantitation of apoptosis using TUNEL assay on the inducible H1299 clones indicated, following 24 hours of temperature shift; cells were pre-treated for 30 minutes prior to temperature shift with p38 MAPK kinase inhibitor (SB-203580) or vehicle alone (DMSO). Apoptosis was quantitated on a Guava Personal Cell Analysis machine (Guava Technologies).

C. Western analysis of asynchronously growing MCF-7 breast carcinoma cells treated with ultra-violet light (7.5 J/m2) and harvested after the times indicated. Cells were pre-treated for 30 minutes with SB-203580 to a final concentration of 40 uM, or vehicle alone (DMSO), before harvesting and western analysis using antisera to the proteins indicated.

Figure 5. The S47 variant has impaired ability to transactivate the p53-response genes p53AIP1 and PUMA.

A. Northern analysis of 2 ug of polyadenylated RNA isolated from the inducible H1299 clones indicated probed with cDNA specific for p53AIP1 and gapdh (glyceraldehyde 3 phosphate dehydrogenase). Temperature shift is for 24 hours.

B. Northern analysis of total RNA isolated from the H1299 clones indicated, following 24 hours of temperature shift. Results are representative of 3 independent experiments. Densitometry indicates a consistent 3 to 4-fold decrease in PUMA level in S47 and A46, relative to wt p53. Gapdh is included as a control for loading and integrity.

C. Western analysis of a time course of p53 induction in the H1299 clones indicated for p53 level, apoptosis (p85-PARP) and PUMA level. Levels of β-actin are included as a loading control.

Figure 6. Decreased ability to induce PUMA underlies in part the decreased apoptotic potential of the S47 variant.

H1299 cells containing the inducible versions of p53 indicated were temperature shifted for 24 hours; 24 hours prior to temperature shift cells were transfected with siRNA specific for PUMA, or control scrambled oligonucleotide. Western analysis was performed using the antisera indicated, and levels of β-actin are included as a loading control.

LI *et al.*, Fig. 1

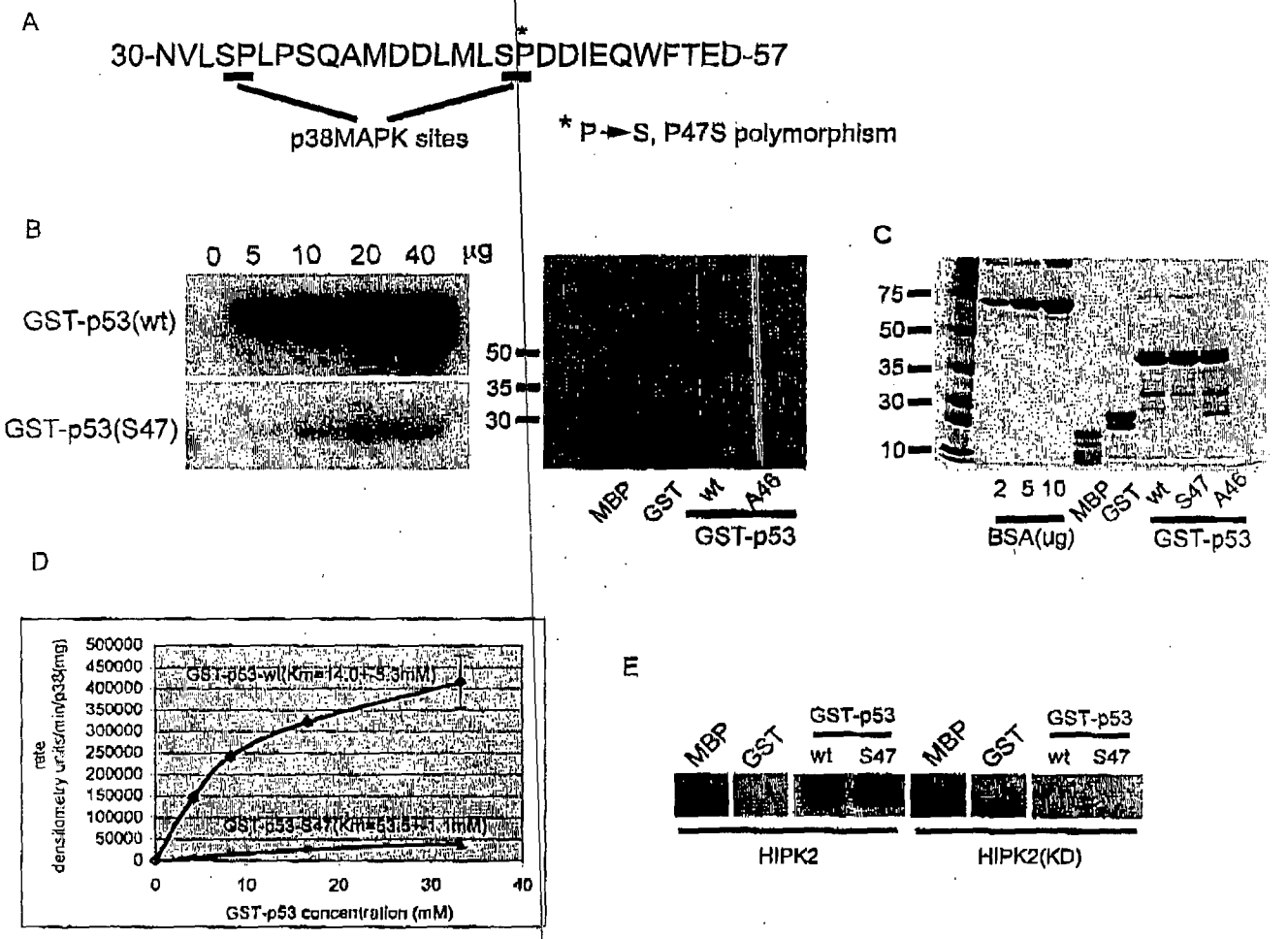
A
30-NVLSPLPSQAMDDLMLSPDDIEQWFTED-57
p38MAPK sites
* P→S, P47S polymorphism
B
0 5 10 20 40 μg
GST-p53(wt)
GST-p53(S47)
50
35
30
MBP
GST
wt
A46
GST-p53
C
75
50
35
30
10
2 5 10
MBP
GST
wt
S47
A46
BSA(ug)
GST-p53
D
rate
densitometry units/min/p38(mg)
500000
450000
400000
350000
300000
250000
200000
150000
100000
50000
0
GST-p53-wt(Km=14.0+-5.3mM)
GST-p53-S47(Km=53.5+-1.1mM)
0
10
20
30
40
GST-p53 concentration (mM)
E
MBP
GST
GST-p53
wt
S47
MBP
GST
GST-p53
wt
S47
HIPK2
HIPK2(KD)

Li *et al.*, Fig. 2

A

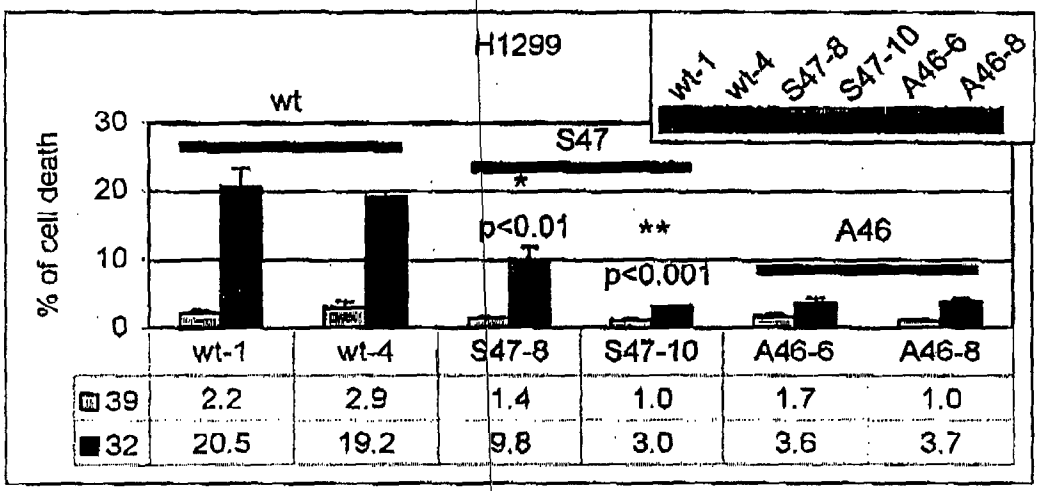

	wt-1	wt-4	S47-8	S47-10	A46-6	A46-8
39	2.2	2.9	1.4	1.0	1.7	1.0
32	20.5	19.2	9.8	3.0	3.6	3.7

B

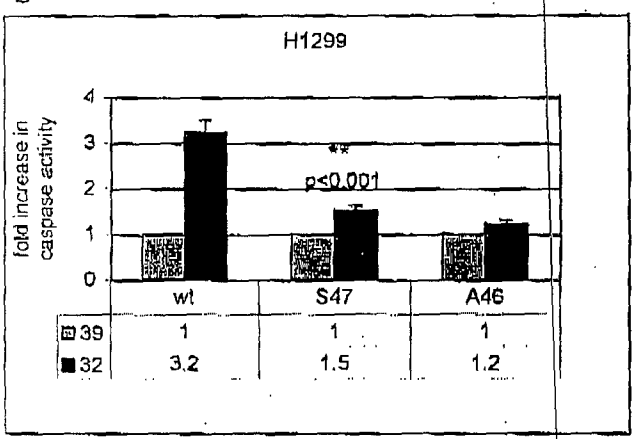

	wt	S47	A46
39	1	1	1
32	3.2	1.5	1.2

C

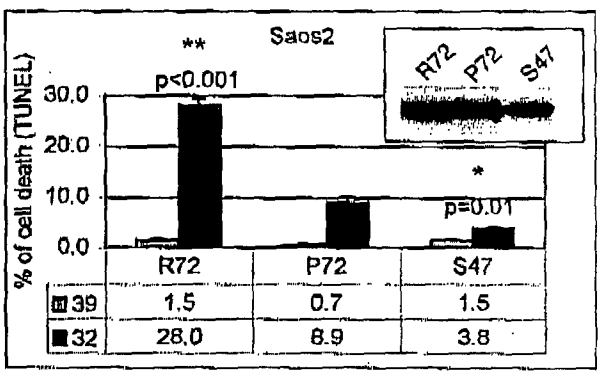

	R72	P72	S47
39	1.5	0.7	1.5
32	28.0	8.9	3.8

Li *et al.*, Fig. 3

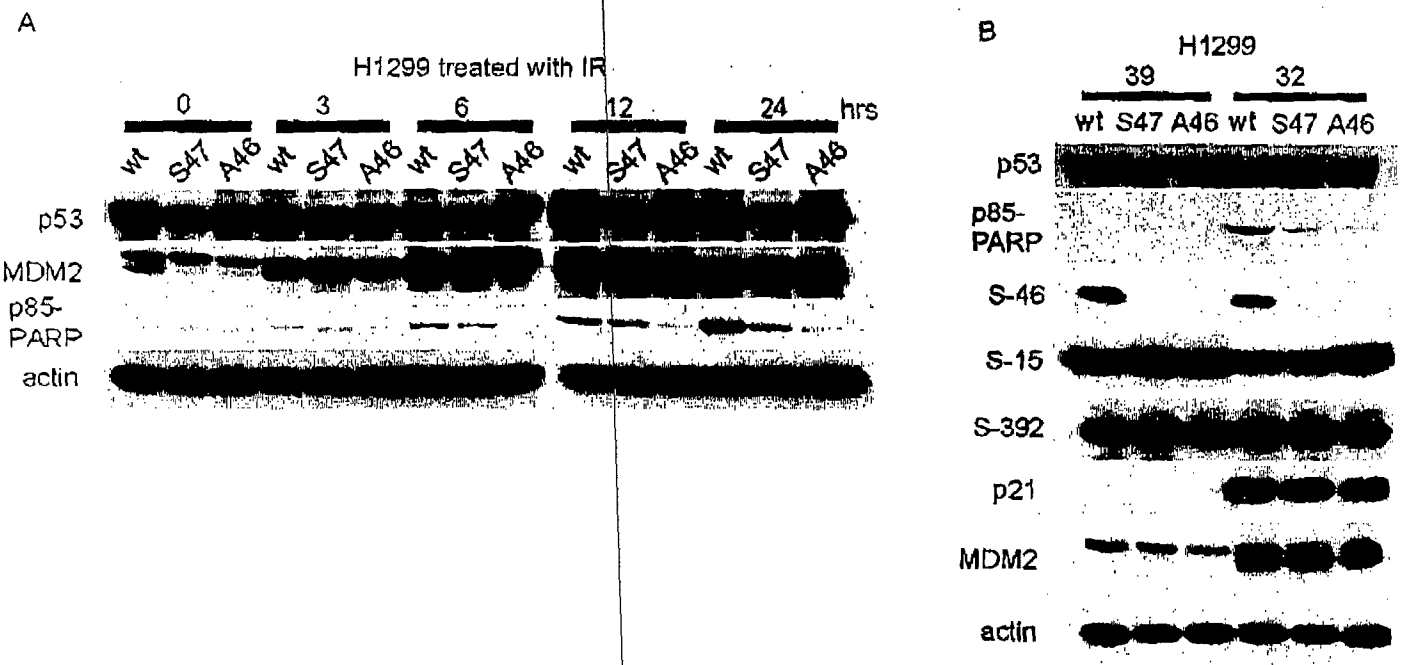
A
H1299 treated with IR
0
3
6
12
24
hrs
wt
S47
A46
p53
MDM2
p85-PARP
actin
B
H1299
39
32
wt S47 A46 wt S47 A46
p53
p85-PARP
S-46
S-15
S-392
p21
MDM2
actin

Li et al., Fig. 4

A
H1299
32/DMSO
32/DMSO
32/SB-203580
wt B47 A46 wt B47 A46 wt B47 A46
p53
p21
MDM2
p85-PARP
S-46
S-15
actin
1 2 3 4 5 6 7 8 9
B
H1299
32/DMSO
32/DMSO
32/SB-203580
% of cell death (TUNEL)
wt
B47
A46
C
MCF7 treated with UV (7.5J/m2)
0
6
12
24
hr
SB-203580
p53
S-46
p85-PARP
actin

Li *et al.*, Fig. 5

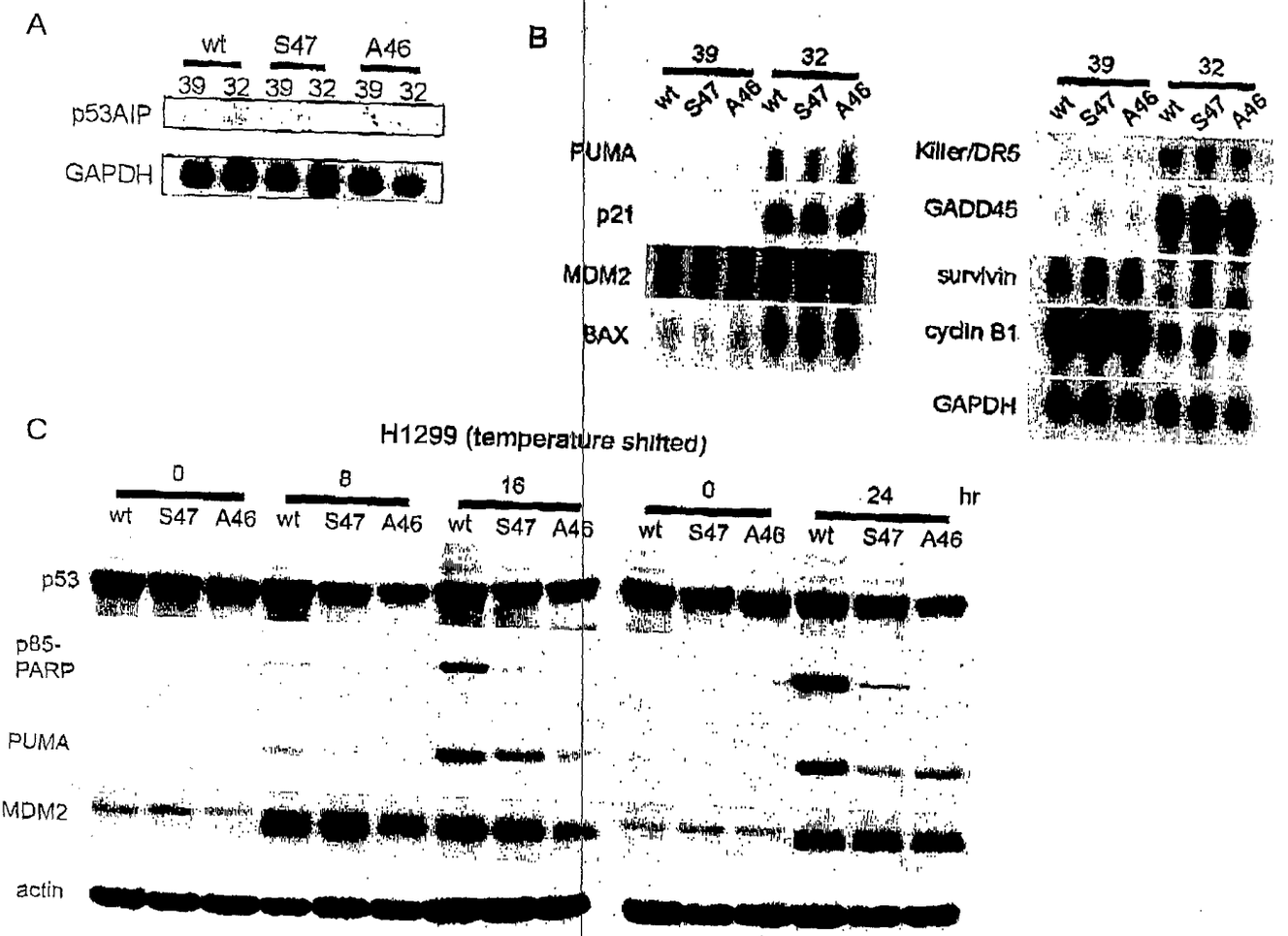
A
wt
S47
A46
39 32 39 32 39 32
p53AIP
GAPDH
B
39
32
wt S47 A46 wt S47 A46
PUMA
p21
MDM2
BAX
Killer/DR5
GADD45
survivin
cyclin B1
GAPDH
C
H1299 (temperature shifted)
0
8
16
0
24
hr
wt S47 A46 wt S47 A46 wt S47 A46 wt S47 A46 wt S47 A46
p53
p85-PARP
PUMA
MDM2
actin

Li *et al.*, Fig. 6

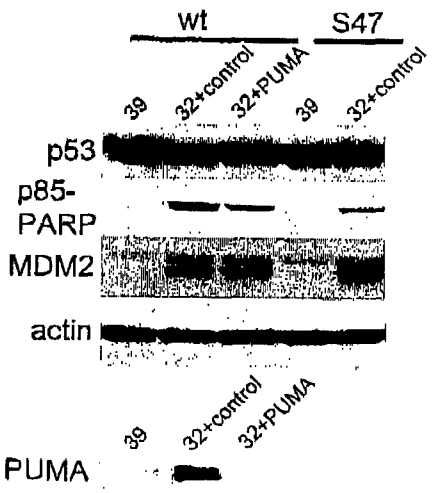
wt
S47
39
32+control
32+PUMA
39
32+control
p53
p85-
PARP
MDM2
actin
39
32+control
32+PUMA
PUMA